Investigating the Effect of Size on Gait Using a Bipedal Robot

Nazir A Karbanee

Submitted to the Faculty of Health Sciences at the
University of Cape Town
in Partial Fulfilment of the Requirements for the
Degree of Master of Science in Biomedical Engineering

December 2004

Declaration

Investigating the Effect of Size on Gait Using a Bipedal Robot

I, Nazir A Karbanee, hereby declare:

(i) This thesis of the above title is my own unaided work, and that apart from the normal guidance from my supervisor, I have received no assistance except as stated;

(ii) Where indicated to the contrary, neither the substance nor any part of this thesis of the above title has been submitted in the past, or is to be submitted for a degree in this university or any other university.

This thesis has been submitted by the author for examination for the degree of Master of Science in Medicine in Biomedical Engineering at the University of Cape Town.

Signed by candidate

Signature of Author

7th December 2004

Date

i Abstract

Observation of the readiness with which children master walking, a naturally unstable form of locomotion, suggests an inherently simple yet effective underlying mechanical strategy that requires minimal neuro-muscular contribution. This passive trait of walking coupled with the high efficiency, where over 70% of energy is recycled at optimal velocities, is attributed to the pendulum-based mechanics of the lower limbs. The emphasis of this study was to facilitate the understanding of the fundamental mechanics of human locomotion by physical replication and mathematical simulation of pendulum-based robotic motion.

A two-dimensional passive dynamic walker was designed, manufactured and tested to allow insight into the practical nature of the bipedal system's ability (and subsequent difficulties) to produce stable anthropomorphic gait. The robot consisted of two pairs of kneed legs that shared a common lateral hip, with the inner and outer leg pairs swinging forward independently of each other, when descending an incline with a slope between 3° and 8°. Comparable to a person using crutches, lateral motion was eliminated and overall balance simplified at the expense of reduced hip elevation, which in turn amplified the ever-present obstacle of foot interference at mid-swing.

Despite adjusting the mass distribution and accompanying parameters, foot scuffing in the physical model was not adequately overcome, with the most promising set-up requiring a small amount of manual delay at the hip during mid-swing. However, the evolutionary nature of the trials allowed several relationships between performance and parameter selection to be confirmed. The most influential being the distance at which the thigh centre of mass is offset from the hip, C_t. Increasing this distance amplified the swing period of the inverted pendulum motion of the stance leg, thus affording the swing leg more time to pass forwards and extend the knee.

Second, a published mathematical model, implemented in MATLAB code, was utilised to investigate the effect of size by means of the Froude number. Historically a nautical value, this parameter represents the ratio of inertial and gravitational forces in the bipedal system thus permitting the comparison of gait regardless of size, provided the gait relies significantly on pendulum mechanics. The versatility of the simulated model offered a diverse range of

otherwise physically challenging sizes and parameter variations to be explored. From these several trends were established.

First, there was a decrease in dimensionless velocity with increasing size, which implied a sacrifice of speed for stability. This phenomenon was explained by an unsustainable expenditure of energy at knee-strike that increased disproportionately in comparison to the potential energy available. This stability-related size limit of passive dynamic locomotion is overcome in growing children by maturing levels of neural control. This is thought to retain the usefulness of pendulum mechanics at larger, otherwise unstable sizes and speeds, until such time as it is energetically or otherwise not feasible.

Second, there was a linear increase of dimensionless velocity with relative stride length across size and slope which agreed well with human and animal data, illustrating the role of pendulum-based mechanics in natural legged locomotion. Although the model for passive gait was less efficient overall, stable gaits were found to exist at much lower speeds, at a Froude number of less than 0.49. This was ascribed to the inherent elastic tendon forces present in the musculo-skeletal frames of living creatures, which may hamper the pendular recycling of energy at low speeds but playing a facilitating role at higher speeds.

These findings may, with further refinements and expansion, contribute to the application of engineering in improving the efficiency of robotic gait, understanding the formation of gait in young children, or explaining the gait of amputees.

ii Acknowledgements

I would like to thank firstly the Almighty for granting me the opportunity and resources to undertake this study and for providing me with people of great character, students and lecturers alike, without whose help this project would not have reached fruition, of which the most influential have been:

First and foremost I thank Professor Kit Vaughan for serving as my supervisor, providing guidance, motivation and setting a high standard at all times.

The skilled craftsmen of the Mechanical Engineering and Health Sciences workshops, namely Mr Harry Hall, Mr Glen Newins and Mr Charles Harris who's attention to detail, innovative ideas and enthusiasm have made an invaluable contribution.

Dr Mariano Garcia for not only allowing and providing the use of his simulation but for his encouragement and advice over many issues.

My fellow students, whose friendship and concern have made the last few years truly enjoyable and a growing experience.

My parents and sisters for their unwavering support, guidance, encouragement and prayers throughout the course of these studies.

Nazir A Karbanee

December 2004
University of Cape Town

iii Table of Contents

iv List of Symbols and Nomenclature

Centre of Mass	COM
Dynamic Equivalence	DE
Thigh Length	L_t
Shank Length	L_s
Thigh Centre of Mass Distance	C_t
Shank Centre of Mass Distance	C_s
Thigh Centre of Mass Offset	W_t
Shank Centre of Mass Offset	W_s
Thigh Mass	M_t
Shank Mass	M_s
Thigh Radius of Gyration	r_t
Shank Radius of Gyration	r_s
Foot Radius	R
Foot Centre Offset	ξ_t
Ground Slope	γ
Gravity	g
McGeer's "stride function"	$f({}^iq^+, p)$.
Initial Conditions Vector	${}^iq^+$
Inertial and Geometric Factors Vector	p
"Jump Condition"	h
Joint Angle of Link *i*	θ_i
Angular Velocity of Link *i*	$\dot{\theta}_i$
Angular Acceleration of Link *i*	$\ddot{\theta}_i$
McGeer Stance Leg Angle	θ_{st}
McGeer Shank Leg Angle	θ_{sh}
McGeer Swing Leg Angle	θ_{th}

Angular Velocity of Link *i*	$\dot{\omega}_i$
Angular Acceleration of Link *i*	$\ddot{\omega}_i$
Linear Velocity of COM	V^c
Linear Velocity of Frame	V
Joint Forces	${}^i f_i$
Joint Torques	${}^i n_i$
Inertial Forces	F
Torques	N
Joint Torque Vector, (n x 1)	τ
Mass Matrix of Linkages, (n x n)	$M(\theta)$
Angles, Rates, Accelerations, (n x 1)	$\ddot{\theta}$
Artificial Gravity, (n x 1)	$G(\theta)$
Centrifugal and Coriolus Terms, (n x 1)	$V(\theta,\dot{\theta})$

v List of Figures

Figure **Page**

Figure **Page**

vi List of Tables

Chapter 1

Introduction

Every day most of us move with ease from one side of the room to another, up stairs, down slopes, turning, stopping and starting at will. Walking is taken for granted. However, looking at the first steps of a toddler we realise there lies considerable skill in achieving those first few steps. How we learn to move so effortlessly lies in the incredible design of the bipedal system, both at the mechanical and neuro-muscular control level.

Normal human gait is the end product of a complex collaboration between the neuromuscular and musculo-skeletal systems of the body. The high degree of uniformity of gait across all races, genders and body sizes lends itself well to serve as a diagnostic tool. The proficiency and ease with which a person walks thus allows insight into the status and function of several systems in the body at once.

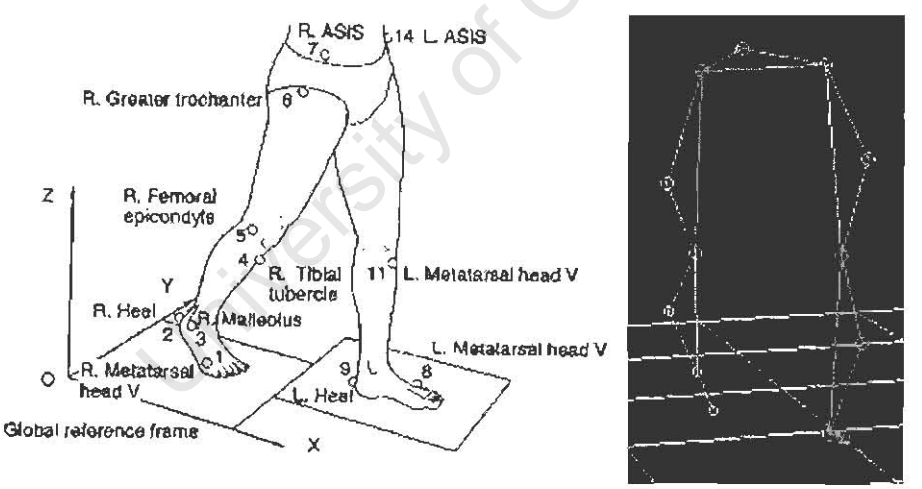

Figure 1.1 (a) A typical placement of reflective markers used in video capture analysis and (b) the corresponding 3D "stick figure" used in analysis. [Illustration from www.univie.ac.at/ cga/faq/sets/]

In deriving the maximum diagnostic benefit, gait analysis has progressed from subjective observation to precise descriptive techniques including electromyography (EMG), video capture and force plate analysis with capture rates of 1000 Hz and spatial resolution of the order of 0.5mm. One such technique that now forms the backbone of modern day gait analysis is video based motion capture. This utilises a set of reflective markers placed at strategic

landmarks on a patient (Figure 1.1a), which, once captured and processed, produces a "stick-figure" computer animation, (Figure 1.1b) whose motion is accurately quantified.

The resulting wealth and range of information takes many forms, including: temporal and spatial (stride time, length and velocity); kinematics (angles in the sagittal, frontal and transverse planes); external kinetics (ground reaction forces and moments); and internal kinetics (joint forces, moments and power). A typical product of such an analysis is shown in the plot of Figure 1.2 where the degree of flexion and extension of the left and right hip joints is plotted against time. The description of the mechanical apparatus of human locomotion has thus over the past century progressed to a detailed and accurate science.

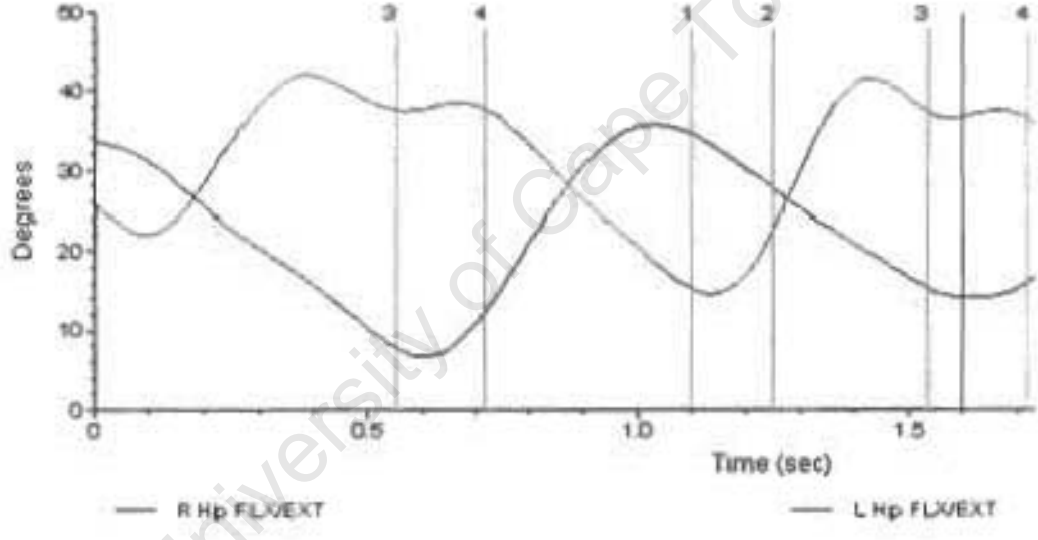

Figure 1.2 An example of gait analysis results. Shown are the change in left and right hip flexion /extension in degrees over time in seconds during a single stride. [Illustration from the Motion Analysis Lab http://www.outreach.engr.mun.ca/ biomed/gait.htm]

This range of descriptive parameters distinguishes each individual as having their own unique variation of legged locomotion, but essentially bound by the same over-riding laws. Zatsiorky *et al.* (1994) observed that tall people display longer stride lengths, and slower cadences, while Roebuck (1975) showed that larger body segments lead to larger segment moments of inertia and moment arms. In essence, each person's walk appears to be a similar version of each other, only scaled up or down according to size.

These seemingly simple variations complicate the effectiveness of gait analysis. When distinguishing between normal and pathological gait data, an individual must be compared to a reference population. Ideally this should be constituted from subjects who are identical to the patient but displaying normal gait.

In reality, inter-subject variations are unavoidable. In an effort to minimise these, several methods of scaling (normalising) gait data according to subject mass and height have been employed. One such method, dimensionless parameters, popularised by Hof (1996), involves dividing the fundamental dimension of a quantity (*e.g.* Force = mlt^{-2}) by a characteristic quantity of mass (m), length (l) and time (t). Within the realms of gait analysis, total body mass and limb length are commonly used to normalise mass and height.

The early years of a child's life see the mastery of bipedal motion, the period being marked also by the growth of the central nervous system (CNS) and the musculo-skeletal system. The works of Vaughan *et al.* (2002) and Ivanenko *et al.* (2004) show that concurrent variations in the primary gait variables of growing children imply that both the pattern and underlying dynamics of a child's gait differ from normal adults during this time.

The works of Garcia *et al.* (1998) propose that the chief energetic cost of gait is of mechanical origin rather than within the realms of neural control. In Figure 1.3, Okamoto *et al.* (2003) showed how the practical manifestation of this theory is displayed in the decreasing EMG activity of major muscle groups associated with a growing child's gait. The primary aim of these changes hints at a directive to improve the mechanical efficiency of the legs first by optimising their physical parameters, rather than employing increasingly complex neural

control of musculature. To determine if this is the case, passive robotic gait may be compared to the gait of children using dynamic similarity as illustrated by Vaughan and O'Malley (2004).

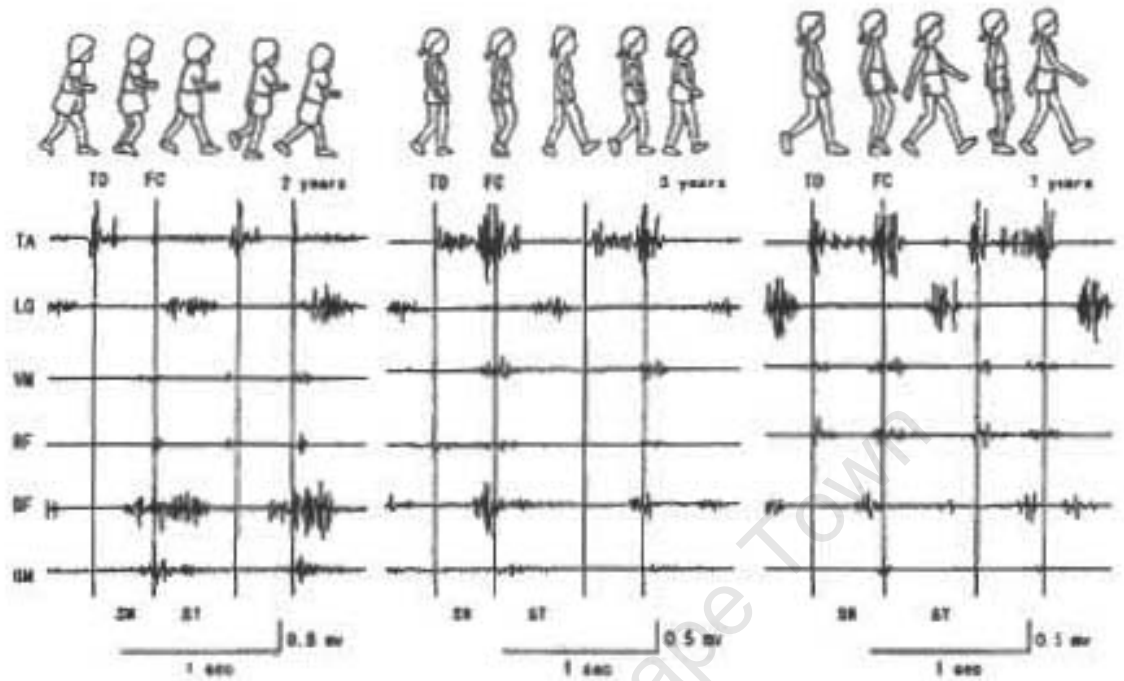

Figure 1.3 EMG trace showing the learning process of a child walking with maturity, (left: 2 years; Centre: 3years; Right: 7years) TA- Tibialus anterior; LG-Lateral head of gastrocnemius; VM-Vastus medialus; RF-Rectus femoris; BF-Bicep femoris; GM-Gluteus maximus,[Illustration from Okamoto *et al.* (2003)].

The degree to which CNS or musculo-skeletal growth is responsible for these disparities is subject to the appropriate normalisation of musculo-skeletal growth. Presently, many clinicians regard walking speed scaled to body size, termed the Froude number, as a true reflection of a child's locomotor function. As Vaughan (2002) reported initially, and demonstrated more recently by Bullimore *et al.* (2004), it is unclear whether such scaling allows for accurate comparison between normal and pathological gaits.

Introduced to the life sciences by D'Arcy Wentworth Thompson (1917) and popularised by the research of the zoologist Alexander (1976), the dimensionless Froude number has been used throughout the life sciences to normalise gait not only between subjects but between entire species, be they bipeds or quadrupeds. This ability to group such seemingly diverse forms of locomotion stems from the substantial reliance of all legged motion on inertial and gravitational forces, the ratio of which is represented by the Froude number. Similar to a pair of coupled

pendulums, passive gait shows little need for muscular contribution, but is rather an outcome of mechanical advantage inherent to legged species.

This theory corresponds well with the EMG data of human gait collected by Basmajian (1980), Inman *et al.* (1994) and Okamoto *et al.* (2003) who showed minimal muscular activity confined mostly to the beginning and end of each stride. The Froude number, though a simple ratio of inertial and gravitational forces, indicates the dynamic similarity of gaits. This means that two people, or animals for that matter, of differing heights walking at different speeds but with the same Froude Numbers, have dynamically equivalent gaits. As a consequence, gait researchers may confidently compare the gait of any patient with the normal population regardless of natural differences in size and stature.

The expanding roles of robots have forced recent automaton design to incorporate locomotion. At first glance wheeled support would seem the more appropriate locomotive mechanism, providing both speed and manoeuvrability. However, both these attributes rely on the provision of a hard, relatively flat ground surface, without which such wheeled robots are severely hampered. Nature's solution – bipedal and quadrupedal locomotion – has no such dependence and provides rapid gait over widely variable terrain, including cities and their buildings.

The great advantage of the Froude number to predict and evaluate the dynamic similarity of legged gait has in recent years found appeal and importance in the ever-expanding field of robotics with McGeer (1990), Garcia *et al.* (1998), Vaughan *et al.* (2002 and 2004) and Collins *et al.*(2001) utilising it to varying degrees. The ongoing quest to design anthropomorphic humanoid robots that display a fluid, stable and efficient gait makes the comparison between them and humans vital. This enables researches to track the progress and trends of gait with parameter variation and also to investigate the ability of differing strategies in replicating legged locomotion.

Clinically, this evolutionary approach to the design of efficient bipedal robots will facilitate an increased understanding of the biomechanics and neuromuscular control of normal human gait. Such understanding could facilitate the improved design of prosthetic limbs, artificial joints and overall rehabilitation of amputees as per the investigation of Sellers *et al.* (2004) into the effect

of prosthetic mass properties on gait. Furthermore, an improved understanding of gait, derived by duplication, can be applied to both child and adult pathologies, such as cerebral palsy, giving insight into their specific cause and hence treatment. A simulated model employing this approach is illustrated by Hurmulza (1993).

A primary direction of such research is to provide stable yet fluid motion, at minimum energy expenditure, to a system that is naturally unsteady. In this regard, passive bipedal robotics is the ideal foundation to begin understanding the inherent natural dynamics of human motion, which consequently expands to the role and advantage of neuro-muscular function. The physical manifestation of this is a minimalist design, borne from an understanding of the underlying principles of the system. However, as Atkins (2004) has emphasised, the principle must not be merely a simple idea, but must also be applicable throughout observable science as well.

It has been widely believed and substantiated by Alexander (1982) and Minetti *et al.* (1994), amongst others, that the essence of human locomotion, namely the system of bipedal gait, is based on and governed by the underlying principle of pendulum motion, which is applicable regardless of the height, gender, race or age of an individual.

The extent to which the human frame relies on such passive dynamics to reproduce efficient and stable gait was the focus of this investigation. Specifically, the aim of this project was to investigate the characteristics of passive gait by physical construction of a bipedal robot based on the mathematical model pioneered by McGeer (1990) of the Massachusetts Institute of Technology (MIT). In addition the computer simulation of this model developed by Garcia (1997) was used to investigate the role of size on passive dynamic gait, using the Froude number as an indication of dynamic similarity.

Chapter 2
Literature Review

2.1 Robotics and Gait

2.1.1 Bipedal Gait

Legged locomotion comes at a high price. Bipedal systems, being inherently unstable, require complex neuro-muscular interaction and control in order to maintain stability. In aiming to understand and implement such control, several classes of robotic gait have been described, based on their mode of stability.

Static Gait: is whereby a robot is in equilibrium at every point in its walking cycle. Practically, this translates to a robot that may pause at any position without losing balance. Much like a stalking cat, the inertial forces are minimized by low velocities and allow greater control. This stability requires large feet coupled with control software to ensure the centre of mass is always supported, and strong ankle joints. The Adaptive Suspension Vehicle of Russell (1983) and Odex and Waldron (1986) produced early examples of the effectiveness of such robots.

Dynamic Gait: requires the subject to be in motion in order to maintain balance. A telling sign is the deviation of the centre of mass from the support base during a walking cycle. McGeer (1990) has compared this to, and subsequently modelled it as, a rimless, spoked wheel rolling down a slope. If stationary it would topple over, but when in motion stability is achieved.

Quasi-Dynamic Gait: appears when part of the walking cycle is in static equilibrium and the remainder in dynamic equilibrium. Human walking and several animal gaits display this mixture of stability, shown schematically in Figure 2.1. During the swing phase, the stance leg supports the entire weight of the subject and before heel strike the centre of mass moves away from the support. Heel strike itself provides stability by its dissipating effect, as shown by the model of Coleman *et al.* (1997).

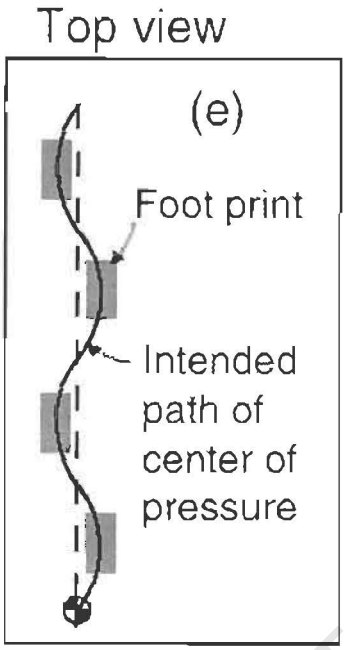

Figure 2.1 Path of a bodies centre of mass when walking with quasi-dynamic stability. [Illustration from Collins *et al.* (2001)]

Ballistic Walking: is a specific gait that requires no (or a minimum number of) actuators, yet exists at a natural frequency. Mochon and McMahon (1980) found they could describe this passive gait as a pair of coupled pendulums. The stance leg behaves as an inverted pendulum pivoting about the ground contact, while the swing leg behaves as a compound pendulum about the hip. As with all pendulum motion, most energy is recycled between intervening stages of kinetic and potential energy. The resulting energetic advantage and natural motion are ideal for use in autonomous robots. Furthermore, the deduction by Mochon and McMahon (1980) that normal human gait is largely ballistic has been supported by Inman *et al.* (1981) in their EMG study of gait. Their findings show that all intrinsic leg muscles exhibit phasic activity at the initiation and completion of a stride but are otherwise non-active. Hence the majority of walking gait may be more a result of the inherent dynamics, rather than forced actuation, of the legs.

2.1.2 Passive Dynamic Walking

Normal human gait is the product of a balanced combination of advanced neuro-muscular control and muscular-skeletal mechanics. The fact that young children can master bipedal gait while possessing limited co-ordination points to an underlining mechanical advantage built into human limbs. The degree to which the human form, its mass balance, inertia and joint friction contribute towards stable gait has been the subject of several studies (namely Garcia, 1997, 1998; McGeer, 1990, 1993; and Hurmuzlu, 1987, 1993) amongst others. Mostly this research has involved the duplication of such passive gait in robots, relying only on gravity for their propulsive force.

Motivation

Inspired by the wobbling gait of small gravity-powered toys of Mochon and McMahon (1980), McGeer (1990) showed how a simple planar mechanism could sustain a stable gait without the use of actuators. McGeer`s motivation for ignoring the role of control and actuation revolved around the philosophy "simplicity promotes understanding".

Drawing analogy with the evolution of powered flight, McGeer reasoned that the Wright Brother's careful study of the aerodynamics of gliders provided them with a firm foundation of understanding. Such problems as drag, lift and stability were confidently resolved by focusing on their role in natural flight. Thus, once secure in their initial design, adding a power source was of little consequence. In the same manner a designer would seek to firstly understand the basic governing fundamentals of passive gait. Adding actuators and control to overcome upward slopes or steps would then be a minor modification, as argued by McGeer (1988).

Furthermore, compared to classical mechanics, the realm of neurological control is mostly uncharted. The feedback loops and control algorithms used by the brain an spinal cord to maintain gait are not fully understood. Any attempts to duplicate their

function without a full understanding would further complicate robotic design unnecessarily.

Moreover, McGeer's passive dynamic walker concurred well with the human-inspired *ballistic model* of Mochon and McMahon (1980) and the EMG-based evidence of Basmajian and Tuttle (1973) as well as Inman *et al.* (1981). The latter found that at the preferred walking speed, muscular activity in human gait is confined to initiation and cessation of the step-cycle. Such a passive swing phase implies a greater role for pendulum mechanics in the control and propagation of gait.

Subsequently, McGeer (1990) formulated the design philosophy which Garcia (1998) adopted whereby bipedal robots and prosthetics may be better realized by improving the mechanics of a system, taking advantage of the natural dynamics available, rather than imposing complex control algorithms and arbitrary amounts of actuation.

Models

A simple derivation of passive gait was first shown by McGeer's (1990) *rimless wheel*. This consisted of a hip-centred mass, curved feet and weighted spokes serving as knee-less legs. In converting to bipedal gait the number of spokes was reduced to two and connected at the hip by a frictionless pin joint. If placed on a shallow slope, the free foot swings forward to synthesize a continuous rim. Support is then transferred from trailing to leading foot and stable periodic gait ensues.

Foot clearance, ignored in the model, was dealt with in two ways in the physical representation. The swing foot would flap upward at the lowest point of its swing using hinged, motored ankle joints and lead screws. A simpler passive solution preserved the walker and rather adjusted the terrain to accommodate foot clearance, producing a "checker-board" surface of differing elevation.

Subsequent models sought better understanding of parameter dependence by simplification of the compass biped. Alexander's (1995) *Minimal Biped* and the *Simplest Walking Model* by Garcia *et al.* (1998) both described a point foot walker

with two rigid, mass-less legs linked at the hip. The mass distribution of Garcia *et al* (1998) differed by the inclusion of infinitesimal point-masses at the feet but as with McGeer's (1990) model, foot scuffing was ignored. This allowed further simplification of the mathematics and mechanics. By rendering the governing equations non-dimensional, Garcia *et al.* (1998) reduced their model to a single free parameter, the ground slope. This simplification allowed for the discovery of a chaotic gait as well as a limp and stagger motion. Additionally the walking speed was seen as proportional to stance angle, which in turn was proportional to the cube root of the ground slope.

The results by McGeer (1990, 1991, 2001), Garcia *et al.* (1997, 1998), Goswami *et al.* (1996) and McMahon (1984) thus tend to support the idea of natural, passive or quasi-passive human gait with minimal control. However, the fundamental physical challenge of ground interference still exists. Observation of natural gait points towards several solutions, including a combination of tilting at the hip and bending of knees. Both solutions may be implemented successfully either in tandem or separately.

Lateral Motion

The walking toys of Fallis (1888), McMahon (1984) and Coleman and Ruina`s (1997) *Tinker-Toy* all performed three-dimensional (3-D) passive gait. The elusive problem of ground interference during mid swing was overcome by an inherent lateral motion or leaning. Conversely McGeer`s (1991) 3D model, which incorporated roll and yaw, was intrinsically unstable. More recently, investigating the stability of lateral motion, Kuo (1999) used a similar 3D model but excluded yaw. He offered five possible schemes of direct and indirect control that preserved much of the passive character of ballistic gait.

The direct control strategies influenced roll motion by applying torque in the frontal plane. These took the form of:

1. Ankle torque at the swing leg;

2. Applying torque to a pelvis mounted reaction wheel which changes the balance of angular momentum in the system; and
3. Swinging a levered mass about a hinge at the pelvis, the equivalent of shifting the torso from left to right.

Indirect control was performed in two ways. The first utilized a torsion spring mounted at the hip. This produced equal and opposite torques on the swing and stance legs. However, the gains in controllability were outweighed by the considerable energy cost. The second, more efficient and simpler strategy exploited changes in lateral step width. A quasi-static application allowed small incremental changes over any time period. Such step-width control neither adjusts trajectory nor ground contact time.

Kneed Motion

Following Mochan and McMahon's (1980) idea that kneed motion is passive, McGeer (1990) implemented kneed walking with his rimless wheel. The resultant model displayed uncontrolled periodic motion of human-like form. Substantial loss of kinetic energy during knee lock consequently decreased efficiency. Minimization of this loss necessitates smaller swing-leg kinetic energy when compared to the entire system. Such a ratio implies concentrating most of the mass at the hip. Despite this dissipation of energy, McGeer (1990) found this method less costly at 0.2 J, than the addition of active, motorized foot retraction where the energy requirements increased to 3 J.

The physical model shown in Figure 2.3 of Garcia *et al.* (1998), as well as that of Coelmann and Ruina (1997) displayed similar patterns of natural kneed gait. In particular, the strobe photographic data of the Garcia *et al.* (1997) model compared to that of normal human gait data from Winter (1987) in Figure 2.4, we see a surprisingly high degree of similarity.

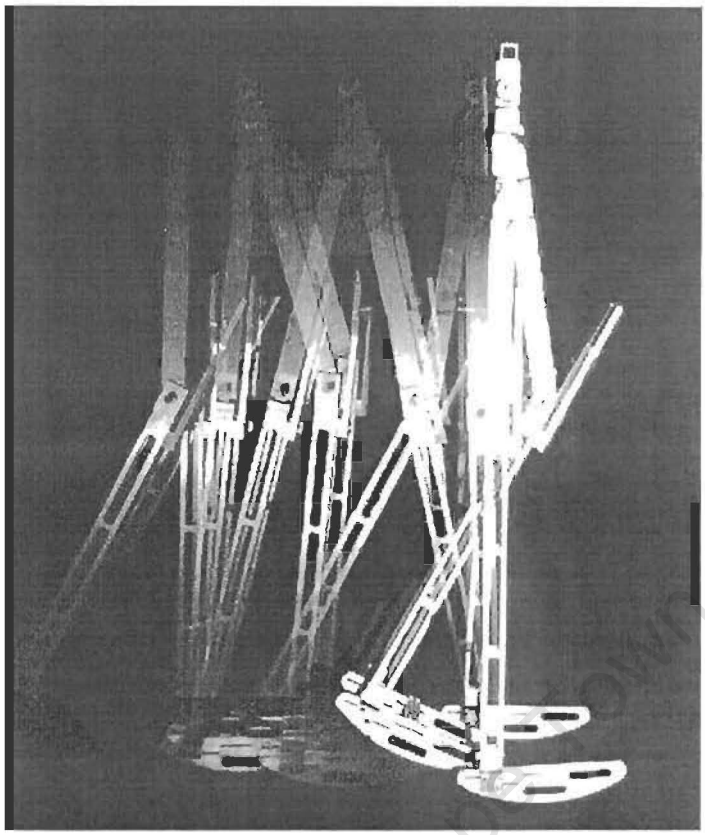

Figure 2.2: Strobe photograph of the physical model designed and simulated by Garcia *et al.* (1998), (Illustration from Garcia *et al.* 1998).

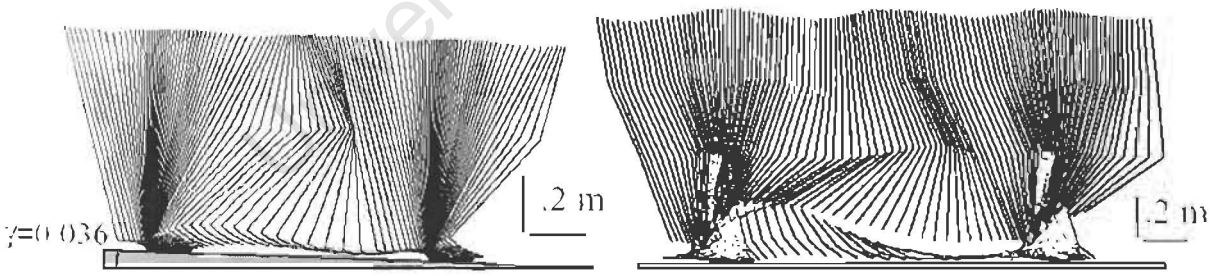

Figure 2.3: Strobe -like simulation data (left) of the Garcia *et al.*(1998) walker on a slope of γ=0.036, compared to that of normal human gait, from Winter (1987). The similarity exists despite the lack of an ankle joint, and trunk in the model. (Illustration from Garcia *et al.* 1998).

2.2 The Froude Number

The early centuries of English shipbuilding had been more guesswork and rule of thumb than design. Several efforts to enhance ship design through research and experiment, although diverse, were overshadowed by the groundbreaking work on hull design by William Froude and his son Robert. Froude senior began with resistance experiments of scale model ships in the river Dart. Prompted by a particularly expensive mistake, the 1860`s saw Froude construct his own private testing tank. As Vaughan and O`Malley (2004) explain, the mistake arose during the design and construction of the period's largest ship *The Great Eastern*. Despite paddle wheels, a screw propeller and sails, the propulsive power failed to drive the ship at a viable speed. Having been involved in the ship's design, Froude realized the relevance and magnitude of wave resistance to ship design.

Vaughan and O'Malley (2004) explain that subsequent hydrodynamic research allowed Froude to make several observations, the most pertinent being that geometrically similar hull shapes of all sizes produced different wave patterns if towed at higher speeds. However, at certain individual speeds each hull produced identical patterns. Developed further, Froude theorized that geometrically similar hull shapes displayed dynamically similar wave patterns at a particular ratio of speed (V) to the height of the bow wave (H) and gravity (g). This ratio, later known as the Froude Number, took the form:

$$Fr = \frac{V^2}{gH} \qquad 2.1$$

Fr = Froude number

H = Bow wave height

V = Speed

g = Gravity

This dimensionless number describes the ratio of inertial to gravitational forces per unit volume. Since its introduction, it has proved invaluable to nautical engineers in predicting the wave-induced drag of hulls before setting sail.

2.2.1 Introduction to Animal Locomotion

Since its arrival, the Froude number has proved to be an extraordinarily powerful tool within modern zoology. D'Arcy Wentworth Thompson first commented in his book *On Growth and Form* that despite obvious differences in size and musculature of species they shared a surprisingly common pattern of locomotion. It was thus proposed that this effect of physical similarity exists due to a common mechanical strategy, which Thompson showed could be determined using the nautical expression we know as the Froude number.

It has since expanded its role, allowing the comparison of animal gait across a spectrum of parameters spanning size, speed and even number of legs, as pioneered by Alexander (1984). However, this is only part of its diverse range of applications.

Using the fossilized tracks of dinosaurs and early hominids, Alexander (1976, 1984, 1991) first used the Froude number to uncover the myths of dinosaur gait as well as predicting the walking speeds of Man's ancestors by application of the theory of dynamic similarity. The same dimensionless number has more recently helped Kubat (2000) and Minetti (2001), understand the reliance on gravity in determining the preferred gait of astronauts on other planets. On a more terrestrial application Minetti *et al.* (1994) have explored the dynamic nature and metabolic efficiency of Pygmy gait, while Chang *et al.* (2000) have used the same principle to analyse the similarity of Gibbon brachaiction to bipedal walking. Even the common speed reduction felt by athletes running around an Olympic track has been quantified and explained by Greene (1985) by using a "Radial Froude Number".

Detailed observation of animal gait was made possible by the introduction of an accurate, sequential photographic compilation of several species in motion by

Muybridge in 1887. Thus, beginning with the observation and analysis of animals in motion, Alexander (1976) showed that certain binding principles were evident. This new tool allowed Alexander to confidently calculate several defining parameters of the various gaits. Initially these included the speed (V), stride length (L) and hip-height (H) of each animal. After plotting normalized stride length (L/H) against a normalized speed (V^2/gH), he noticed a surprisingly linear relationship (Figure 2.4). Alexander reasoned that such conformity must stem from a common underlying mechanical principle that seemed to govern, to varying degrees, all forms of legged locomotion.

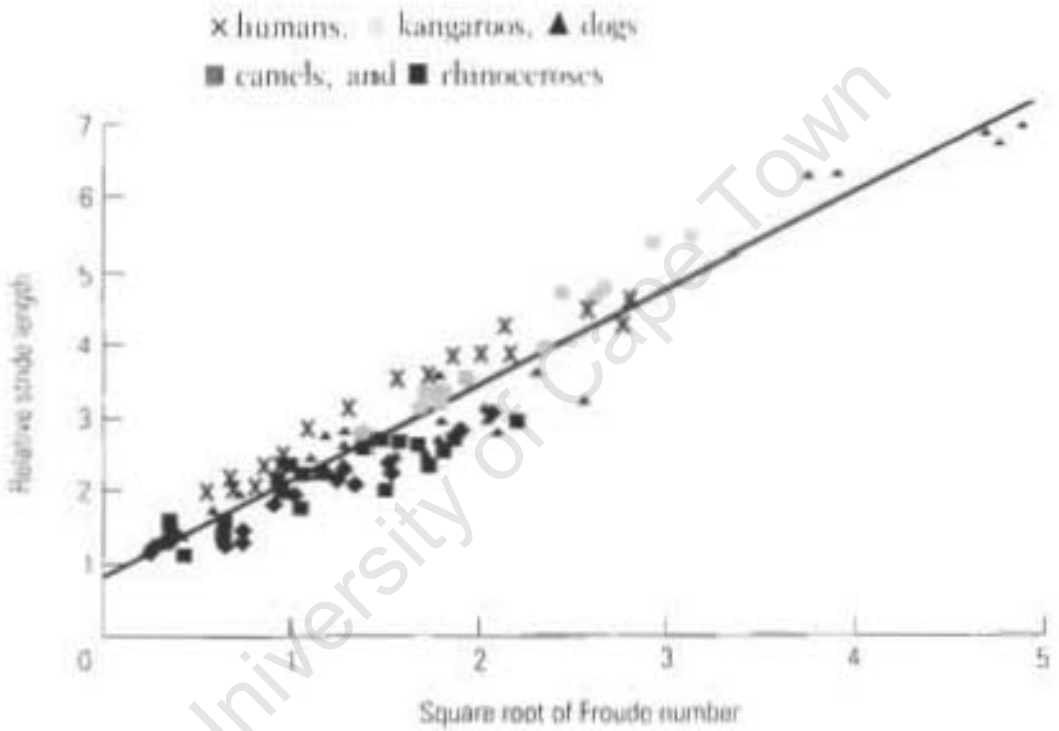

Figure 2.4 Alexander's (1976) results show a high degree of dynamic similarity between several species of different sizes and at different dimensionless velocities which implies a common reliance on a binding principle of legged motion [Illustration from Alexander (1976)].

2.2.2 Dynamic Similarity

Alexander's unique justification for this trend introduced the theory of physical or dynamic similarity. He explained that the underlying element linking animals of different sizes and walking at different speeds but having identical Froude Numbers

was described as the dynamic similarity of motion. The notion of dynamic similarity broadens the more familiar concept of geometric similarity. Two shapes are geometrically similar if all the linear dimensions of one are a constant multiple of the other. Duncan (1953) explained that two such objects in motion, say two pendulums, are not inevitably dynamically similar. However, if their linear dimensions are multiples of one constant, their time intervals by another and forces by a third, only then is dynamic similarity possible.

By virtue of Newton's Laws, the forces acting on a body govern its subsequent motion. If the ratio of forces between two bodies is equal, the motions are similar. In the case of simple pendulum motion, the governing forces are gravity and centripetal force. The ratio of these two forces was known to Alexander as the dimensionless speed, but later, for historical consistency as the Froude Number.

$$Fr = \frac{mv^2}{r} \times \frac{1}{mg} = \frac{v^2}{gr} \qquad 2.2$$

Where v is the velocity, g is the acceleration due to gravity and r is the radius of the pendulum or leg length.

Conditions for Dynamic Similarity

Alexander and Jayes (1983) defined the five requirements for dynamically similar locomotion:

1. *Same phase relationships:* characterize the motion of the limbs relative to each other. In symmetrical bipedal gait, each foot always contacts the ground 180 degrees out of phase with the other. This applies to both walking and running.

2. *Equal duty factors*: refers to the fraction of stride time that a foot is in contact with the ground. In bipedal motion this ratio is always greater than 0.5 as one foot always maintains contact with the ground.

3. *Equal relative stride lengths:* signifies the length between each foot in a normal stride, divided by the subject's leg length.

4. *Corresponding feet* must exert equal multiples of body weight at corresponding points in the stride.

5. *Mechanical power outputs* must be proportional to body weight multiplied by speed, (i.e. equal metabolic costs of transports).

The Froude number's utility as a key parameter in describing dynamically similar gait is attributed to the pendulum-like mechanics of gait, which shows a similar dependence on gravity and inertial forces. As is illustrated below, the Cavagna *et al.* (1977) pendulum model of walking, and thus the Froude number, applies well to walking but does not fully describe the mechanics of running, indicating one or more additional sources of energy.

2.2.3 Human Walking and Running

Alexander (1984), Cavagna *et al.* (1977) and Mochan and McMahon (1980) have modelled walking gait as two coupled pendulums (Figure 2.6) This passive model has been confirmed by the EMG recordings of Rose and Gamble (1994), Machon and McMahon (1980), and Okamoto *et al.* (2003) who found muscular activity confined to the beginning and end of a stride. More recently, further support for the pendulum based model of human locomotion was found by Minetti *et al.* (1993). In their work with Pygmies they found that shorter leg lengths increase stride frequency in accordance with the equation for pendulum frequency [$f = \sqrt{(2\pi/r)}$].

Further confirmation by means of force platforms and kinematic measurements by Cavagna *et al.* (1977) and illustrated by Farley *et al.* (1998) show that up to 70% of the mechanical energy required to move the centre of mass from step-to-step is conserved at optimal walking speeds. This again suggests a substantial reliance on pendulum mechanics.

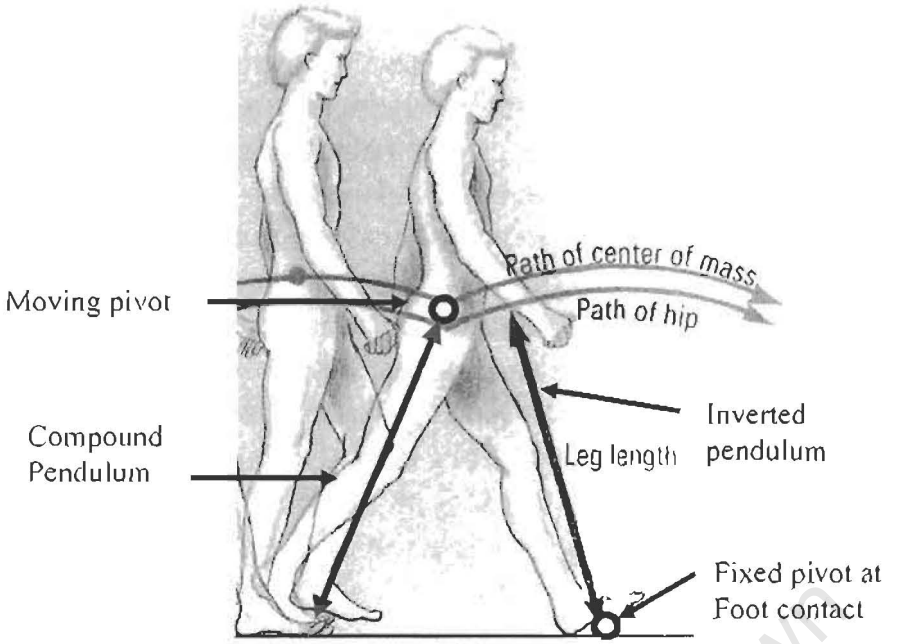

Figure 2.5 The inverted pendular behaviour of the stance leg lends itself well to describing walking gait. High percentage of kinetic and potential energy recycled from one form to the other is thought to be responsible for the high gains in efficiency an inherent characteristic of pendular motion. [Illustration adapted from Alexander (1992)]

Despite the immense value of this energy efficient system, with increasing speed the pendulum motion of walking is less effective at conserving mechanical energy and must be supplemented by muscular exertion. At a certain walk-run transition speed, the pendulum motion of walking is replaced by the elastic spring mechanism of running. Farley *et al.* (1993) confirmed such an analogy with a simulated model, and showed that running gait, unlike walking, is governed not only by inertial and gravitational forces but also by the elastic properties of the limbs with energy stored in the tendons.

A vital, energy-based distinction between walking and running thus emerges. As seen in Figure 2.6, walking has a steady state energy level where potential and kinetic energy are approximately 180° out of phase. The sum total energy is thus held for the most part constant. Conversely, Figure 2.7 shows that in running the kinetic and potential energies are in phase and coupled with spring energy from muscles and tendons alike. The resultant total energy is not constant and changes with each stride.

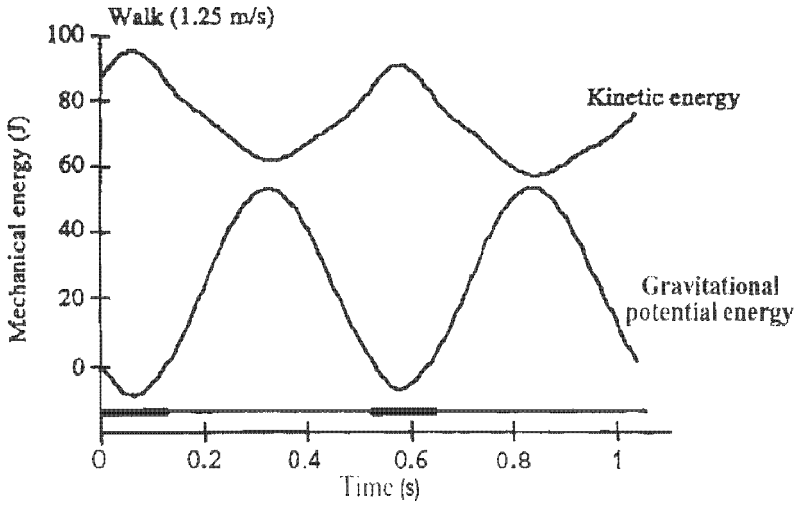

Figure 2.6 The variation of potential and kinetic energy of the centre of mass during walking at a speed of 1.25ms^{-1}. The thick horizontal line indicates doubles support while the thin portion represents swing phase. [Illustration from Farley *et al.* (1998)]

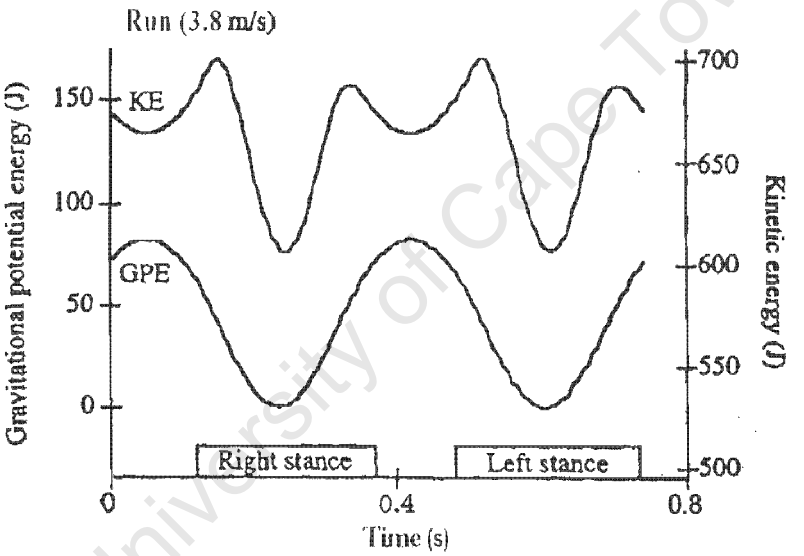

Figure 2.7 Energy changes of the centre of mass during running at 3.8ms^{-1}.[Illustration from Farley *et al.* (1998)]

The ratio of the kinetic to potential energy is again reducible to the Froude number. It is thus appropriate for the Froude number to accurately predict dynamically similar walking. In the case of running, however, a third energetic contribution, spring energy, is not accounted for in the Froude number, leading to lesser degree of congruity.

Preferred Transition Speed

Over the years several possible explanations for gait transition have been proposed by, amongst others, Alexander (1984) and Heglund and Taylor (1988). Each has shown a high correlation between body size and gait transition, over wide ranges of both size and species.

A further observation by Alexander (1977) in his initial analysis was a tendency for differing species to change from walking to running at different speeds but similar Froude numbers. He noted that in humans the transition occurred at a speed of 2.5 ms^{-1} and Fr = 0.8. Similar Froude numbers in the range 0.7-0.9 mark the transition of horses while Fr = 0.6 for cats.

The trigger for such a transition has been attributed to the dynamics of an inverted pendulum system by Kram *et al.* (1996). This model predicts the maximum walking speed occurring at Fr =1. At this point the centripetal force equals the gravitational force, lifting the pendulum off the ground. Several authors, including Alexander (1989), Gatesy (1991) and Hreljac (1995b), have shown the transition to occur at Fr = 0.5. This discrepancy between predictive model and observation is still unresolved, possibly signifying an incomplete description of gait. An alternate but simpler explanation may be that the swing-leg speed is double that of the overall subject progression speed (V).

2.2.4 Gravity's Role

Alexander (1976, 1984, 1989, 1991), Cavagna *et al.* (1983), Cavagna and Kram (1989), Kram *et al.* (1997) have used the Froude number to analyze the influence of gravity on normal locomotion. Donnelan and Kram (1997, 2000) and Kram *et al.* (1996) have explored the effect of reducing the magnitude of gravity to explain its role in governing the mechanics of walking and running and the transition point between the two modes of locomotion.

Using the five requirements as outlined by Alexander and Jayes (1983), Kram *et al.* (1996) found that the Froude number was able to predict human locomotion over wide ranges of size and speed, but was restricted to locomotion within normal gravity. They have shown that in reduced gravity leg swing is not a passive event, hence upsetting the ballistic pendulum model. This is supported by the studies of Roberts (1963) as well as those of Boda *et al.* (1996) who utilized differing techniques to simulate the effects of reduced gravity. These involved either suspending a subject using a sling and winch system, or the more elaborate option of parabolic flight. The former system's drawback is that it leaves the limbs subject to normal gravity, but offers easy repetition of an experiment. The latter alternative, although subjecting the entire body to reduced gravity, the limited time period available and the difficulty of repeating exact conditions constrains the extent of research.

2.3 Theory and Simulation of Passive Bipedal Gait

Inspired by the early walking toys in Figure 2.9, designed by the American inventor Fallis in the late 18th century (US Patent No. 376588), as well as the more recent work by Mochon and McMahon (1980), McGeer's (1990) pioneering efforts in passive dynamic bipedal systems established a walking model to represent the geometric and dynamic parameters of a kneed passive dynamic walker in 2D, as well as formulating the accompanying equations of motion and subsequent analysis of the produced gait. Similar setups and analytic procedures borne from McGeer's (1990) approach were implemented in modified forms by the majority of succeeding researchers, including Garcia *et al.* (1998), Coleman *et al.* (1997), Goswami *et al.* (1996), Hurmuzlu (1986, 1987,1993).

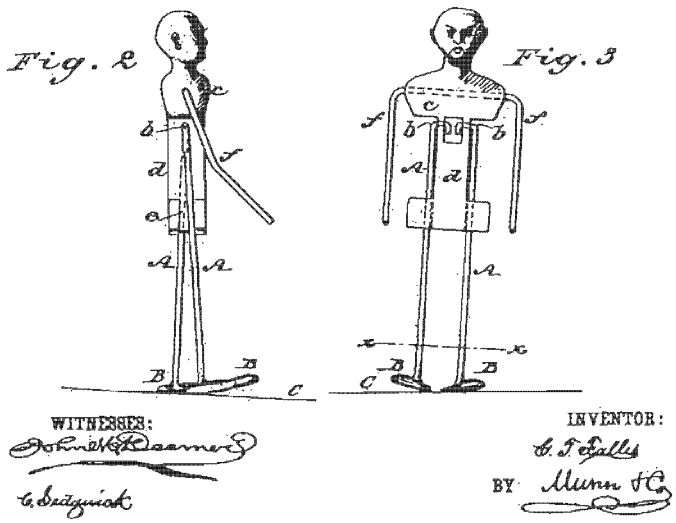

Figure 2.8 One of the earliest passive bipedal walkers designed by Fallis (1888) shows the elegant use of pendular mechanics with lateral hip motion to generate a stable quasi-dynamic gait.

The initial specification design stage of this project relies on one such mathematical interpretation of McGeer's (1990) previous work. The parameter selection of Garcia *et al.* (1998) was used as a foundation for the constructed physical model. In addition, use is made of the accompanying MATLAB simulation by Garcia (1998) to fine tune and guide the design of the constructed biped, in addition to investigating the possibility and characteristics of further stable parameter combinations. Following is an overview of the McGeer (1990) mathematical model and the Garcia (1998) version of analysis which he employed in formulating the MATLAB simulation of a generalised 2D passive dynamic biped with knees.

2.3.1. The McGeer Model

The free body diagram of Figure 2.9 consists of two rigid legs of distinct mass sharing a frictionless hinged hip joint. The identical legs constitute a thigh and a shank section, which are joined by a frictionless pin-joint knee. During a single gait cycle each leg performs the role of either a stance or a swing leg. The former has a locked knee and is in contact with the ground; conversely the swing leg is flexed and is thus off the ground.

As a subsequent version of the *rimless-wheel* it is governed by Newtonian multi-body dynamics, subject to certain ideal conditions. The equations of motion are based on perfectly non-slip and inelastic foot-ground impact at heel-strike. The knee offers no resistance to flexion of the stance leg but prevents over-extension of the swing leg when the shank meets the thigh in a plastic collision which is referred to as "knee-strike". After impact, the leg configuration remains unchanged, unlike the velocities of the feet. At all times angular momentum is conserved about the point of impact for the entire system, and only about the hip for the swing leg.

Although based on ideal conditions, the final "return map" matrix describing the interchange of foot velocities produced several modes of periodic gait on differing slopes. The model thus illustrated that on completion of a step the appropriate conditions necessary for the second step are automatically produced.

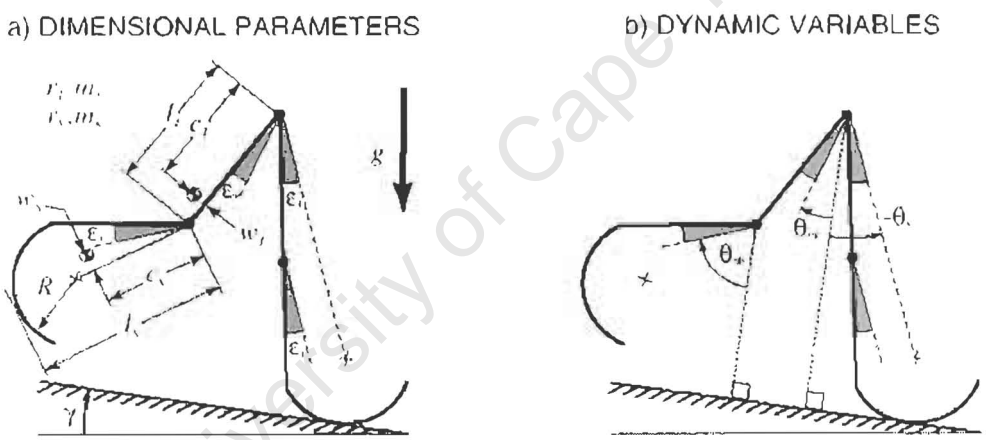

Figure 2.9: Description of the dimensional and dynamic parameters of McGeer's kneed 2D biped as interpreted by Garcia *et al.* (1998) | Illustration from Garcia *et al.* (1998)].

The notation used by Garcia *et al.* (1998) to describe the geometric and dynamic parameters is shown schematically in Figure 2.9. Contact with the ground is provided via circular feet of radius R, which allow the hip to roll forward and, to a limited degree, upward. The foot centre is offset by an angle of ε_t from the stance leg and is attached to the lower shank by a rigid ankle joint. The masses and radii of gyration of the thigh and shank are indicated by m_t, r_t and m_s, r_s respectively. The positions of the

centre of mass of the thigh and shank are denoted by the distances l_t and l_s, from the hip or knee joint as well as the offsets, w_t and w_s from the thigh centre line and the line connecting the knee and the foot centre.

The biped moves on a firm surface of slope γ; on heel-strike the swing foot meets the ground in a no-bounce, no-slip (*i.e.*inelastic) collision. After impact the leg configuration remains unchanged, although the velocities of the feet are switched over, and hence the old stance leg will now flex at the knee and progress forward as the new swing leg. A similar reversal in role occurs with the swing leg. The dynamic variables, θ_t, θ_{sh} and θ_{st} upon which the equations of motion are based, are taken between the perpendicular with the ground and the respective leg portions and offset by the angle ε_τ.

Formulating the Stride Function

The motion of the biped during a step is described by the non-linear Poincaré map, also known as McGeer's "stride function" $\mathbf{f}$, consisting of the vectors $({}^i\mathbf{q}^+, \mathbf{p})$. Here ${}^i\mathbf{q}^+$ is a vector describing the initial conditions of the system (*e.g.* θ_{sh}) and $\mathbf{p}$ is a vector of inertial and geometric factors (*e.g.* m_t).

In the interest of simplifying the derivation and analysis, several authors including McGeer (1990), Coleman (1997), Garcia *et al.*(1998) and Goswami *et al.*(1997), take $\mathbf{f}$ as formed by two simpler functions. The first, $\mathbf{d}$, maps the swing phase and is obtained by integrating the equations of motion $\boldsymbol{G}$, of gait from just after one heel-strike i, to just before the next $i+1$. The second map is a "jump condition" $\mathbf{h}$, which governs the collisions of knee-strike and heel-strike, the latter of which includes support transfer. Using the notation of Coleman (1997), this gives the relationship

$$f = h \circ d \qquad 2.3$$

Equations of Motion During Swing Phase

To describe the movement during a stride, without the collisions of knee and heel-strike, Garcia *et al.* (1998) utilise the procedure of Craige (1989) and Luh *et al.*

(1990). This algorithm is well known, robust and efficient and may be modified easily to accommodate circular feet or applied joint torques in the case of actuated or damped bipeds.

When formulating the algorithm, the first step of Garcia (1997) is to define the necessary angles and reference frames for each link. As the swing leg leaves the ground and flexes at the knee, the biped behaves as a *three-link* mechanism, and hence the number of reference frames is three. Likewise, from knee-strike onwards, the biped behaves as a *two-link,* straight-legged walker and has two reference frames.

The orientation of the reference frames is as follows; Z_i, along the joint axis of rotation; X_i, between the origins of frame *i* and i + 1; Y_i, as per the right hand rule. To convert angular references to those of McGeer (1990), the following are used:

$$\theta_{st} = -\theta_i \qquad \textbf{2.4}$$

$$\theta_t = \pi - \theta_1 - \theta_2 - \varepsilon_\tau \qquad \textbf{2.5}$$

$$\theta_{shank} = \theta_t - \theta_3 + \varepsilon_\tau \qquad \textbf{2.6}$$

To change from one reference frame to another a rotational matrix R, is employed:

$$^{i+1}p = {}^{i+1}_{i}R\ {}^{i}p \qquad \textbf{2.7}$$

Where ^{i+1}p and ^{i}p are the same vectors, only written with respect to different coordinates. Subsequently Garcia (1997) establishes the angular velocities $\dot{\omega}_i$ and accelerations ($\ddot{\omega}_i$) of each link as

$$^{i+1}\omega_i = {}^{i+1}_{i}R\ {}^{i}\omega_i + \theta_{i+1}\ Zi{+}1 \qquad \textbf{2.8}$$

$$^{i+1}\dot{\omega}_i = {}^{i+1}_{i}R\,{}^{i}\omega_i + ({}^{i+1}_{i}R\,{}^{i}\omega_i)(\theta_{x+1}\,Zi+1) + \theta_{i+1}\,Zi+1 \quad \textbf{2.9}$$

Craig (1989) and Luh *et al.* (1990) further define the inertial forces **F** and torques **N** with respect to θ_i, $\dot{\theta}_i$, $\ddot{\theta}_i$ as:

$$^{i+1}F_{i+1} = m_{i+1}\,{}^{i+1}V^{c}_{i+1} \quad \textbf{2.10}$$

Where V^c is the velocity of the link, while the inertial torques acting on a single link i+1:

$$^{i+1}N_{i+1} = ({}^{i+1}I^{c}_{i+1}\,{}^{i+1}\dot{\omega}_{i+1}) + {}^{i+1}\omega_{i+1} \times {}^{i+1}I^{c}_{i+1}\,{}^{i+1}\omega_{i+1} \quad \textbf{2.11}$$

In the same manner the joint forces ${}^{i}\mathbf{f}_i$ and torques ${}^{i}\mathbf{n}_i$ are:

$$^{i}f_i = {}_{i+1}{}^{i}R^{i+1} + {}^{i}F_i \quad \textbf{2.12}$$

$$^{i}n_i = {}^{i}N_i + {}_{i+1}{}^{i}R^{i+1}\,{}^{i}n_i + {}^{i}p_i^{c} \times {}^{i}F_i + {}^{i}p_{i+1}{}^{c} \times {}_{i+1}{}^{i}R^{i+1}\,{}^{i+1}f_{i+1} \quad \textbf{2.13}$$

Adapting the above equations to accommodate disk feet, Garcia (1998) takes two further steps: (1) change the angular momentum balance of the stance leg for a moving pivot in a different trajectory to that of a point-foot walker: and (2) change the acceleration of the stance leg centre of mass (COM) and relevant reference frames. The modified equations are reducible to describe point-foot walking by equating the foot radius (R) to zero.

$$^{0}\dot{V}_0 = [g\cos\gamma;\ R\ddot{\theta}_1 - g\sin\gamma;\ 0] \quad \textbf{2.14}$$

$$^{1}\dot{V}_1 = {}_{0}{}^{1}R^{0}\,\dot{V}_0 \quad \textbf{2.15}$$

As per Craig (1989), Garcia (1997) uses the terms *gcosγ* and *-gsinγ* to represent the artificial gravitational force simulated by accelerating the ground upwards. A further

complication of circular feet is the need to account for the impact observed at heel-strike. Once again Garcia (1998) uses the reference frame rules to his advantage by subtracting the torque about the foot centre shifted by a rotational matrix $[{}^{1}_{0}R_{0}]$ to give:

$$ {}^{1}n_1 = ({}^{1}N_1 + {}^{1}_{2}R^{2}n_2 + {}^{1}p^{c}_{1} \times {}^{1}F_1 + {}^{1}p_2 \times {}^{1}_{2}R^{2}f_2) - {}^{1}_{0}Rp_1 \times {}^{1}f_1 \qquad \textbf{2.16} $$

By applying the law of conservation of angular momentum about the contact point for the whole biped, and about the hip joint for the swing leg, the defining ordinary differential equations of motion are derived numerically. Taking into consideration the additional forces present and using the notation of Craig (1989), the general form of the final equations of motion during the swing phase as used by Hurmuzlu (1993), Coleman (1997) and Garcia (1997) is given as:

$$ \tau = M(\theta)\ \ddot{\theta} + V(\theta_i \dot{\theta}) + G(\theta) \qquad \textbf{2.17} $$

Where

τ = (nx1) joint torque vector = 0 for passive walkers

$M(\theta)$ = (n x n) mass matrix of linkages

$\ddot{\theta}$ = (n x 1) angles, angular rates, angular accelerations

$G(\theta)$ = (n x 1) *artificial* gravity

$V(\theta_i \dot{\theta})$ = (n x 1) Centrifugal and coriolus terms

Numerically inverting the mass terms, the angular acceleration can be made the subject of the formula, giving:

$$ \ddot{\theta} = M^{-1}(\theta)\ [\ \tau - V(\theta_i \dot{\theta}) - G(\theta)] \qquad \textbf{2.18} $$

In the cases of Coleman (1998) and McGeer (1990) the coriolus and centrifugal terms are neglected as the swing leg velocity is regarded as suitably small in their models. However Garcia (1998) does not make this assumption when dealing with the 2D

kneed bipedal simulation, as the knee allows the swing leg to reach greater velocities than the compass gait biped and is thus noted in this explanation.

Transition for Knee Strike and Heel Strike

The ordinary differential equations (ODE's) are integrated forward in time until knee-strike is detected. The knee-strike collision and that of heel-strike are taken to be instantaneous with zero time and no rebound. Implementing the conservation of angular momentum, firstly about the swing foot point of contact for the entire biped, and secondly about the hip joint for the new swing leg, Garcia *et al.* (1998) numerically calculate the "jump" equations for both collisions. This set of "jump equations" map the conditions an instant before knee-strike to an instant after, which act as the initial conditions for the following *two-link* , point-foot walker swing stage.

After knee-strike the stance leg maintains its inverted pendular motion, but the swing leg now behaves as a rigid-body pendulum, with both maintaining a moving fulcrum. Once more the ODE's are integrated forward in time until the heel-strike conditions are met. This is achieved when the following collision relationship, the equivalent of which is described by Garcia *et al.* (1998), is satisfied:

$$\theta_t - \theta_{st} = 0 \equiv \Phi(t) - 2\theta(t) = 0 \qquad \textbf{2. 19}$$

Moreover, the stance leg must be an ample distance past the vertical in order for true double support to occur. A second method of collision detection as implemented by Garcia *et al.* (1998) and Coleman *et al.* (1997) is a version of the Henon (1962) method.

At heel-strike an impulsive force occurs between the ground and the swing leg. The analogous force produced when the old stance leg lifts off the ground is neglected. Finally, combining the ordinary differential equations of the swing phase and the jump condition maps of knee and heel-strike, the single nonlinear Poincaré map, or "stride function", is formed.

This single matrix **f** takes the initial launch conditions, ${}^{i}\boldsymbol{\theta}$, (i.e. angles and angular rates) for a given set of parameters and plots the resulting motion for a single gait cycle, giving the final conditions ${}^{i+1}\boldsymbol{\theta}$, in a similar form:

$$ {}^{+1}\theta = f({}^{i}\theta) \qquad \textbf{2.20} $$

In order to determine whether any gait cycles indeed exist for a given set of parameters, and if they are stable, requires two analytic processes of the stride function.

Finding Stable Gait Cycles

For a gait cycle to exist, the end conditions of a stride must provide a sustainable set of initial conditions for the following step. Ideally these should be identical to the initial conditions set. Symbolically this may be written as $\mathbf{f}({}^{i}\boldsymbol{\theta}) = {}^{i+1}\boldsymbol{\theta} = {}^{i}\boldsymbol{\theta}$. Garcia *et al.* (1998) term this type of walking a *period one* gait. If the initial conditions are repeated only after every second step it is termed a *period two* gait (*i.e.* limping) and so on.

The existence of a gait cycle is determined by finding the roots (fixed points) of the stride function either analytically or numerically. Analytical location of fixed points of the stride function is identical to McGeer (1990), who employs root finding algorithms to solve $\mathbf{g}(\boldsymbol{\theta}) = \mathbf{f}(\boldsymbol{\theta}) - \boldsymbol{\theta}$. The numerical solution as per Garcia *et al.* (1998), utilises the Newton-Raphson method.

Although this entails solving n equations for n unknowns (n being the dimension of the Poincaré map), this does not guarantee a stable or an anthropometric gait. If by chance the parameter selection sets the initial conditions within the basin of attraction, as defined by Goswami *et al.* (1997), running the simulation for a number of steps will yield an immediate indication of stability, which may be gauged either by the biped's animated gait, or a plot of the McGeer angles. Analytically, stability may also be ascertained by evaluating the eigenvectors of the Jacobian of the Poincaré map. If these lie within or on the unit circle, for any fixed point on the Poincaré map, asymptotic stability is assured.

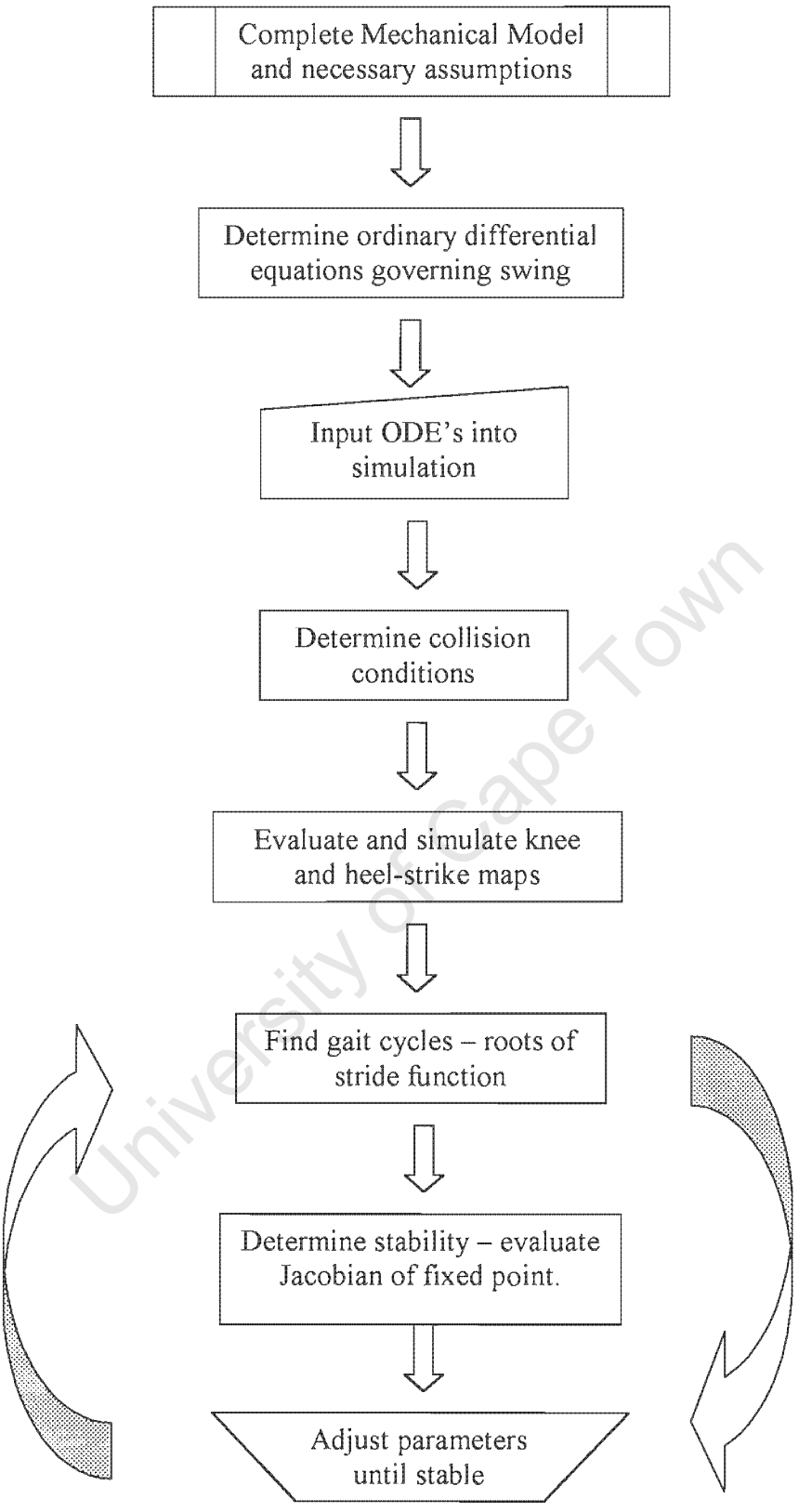

Table 2.1: An illustration of the Garcia (1997) interpretation of the McGeer (1990) "recipe" to model, simulate and analyse passive bipedal gait when restricted to two dimensions.

Chapter 3

Design of the Physical Model

3.1 Final Assembly

The final assembly shown in Figures 3.1 and 3.2 is our version of the 2D bipedal walker that was based on the parameter selection of Garcia *et al.* (1997). It comprised of four identical legs coupled at the hip such that each pair moved as one structure independent of the other.

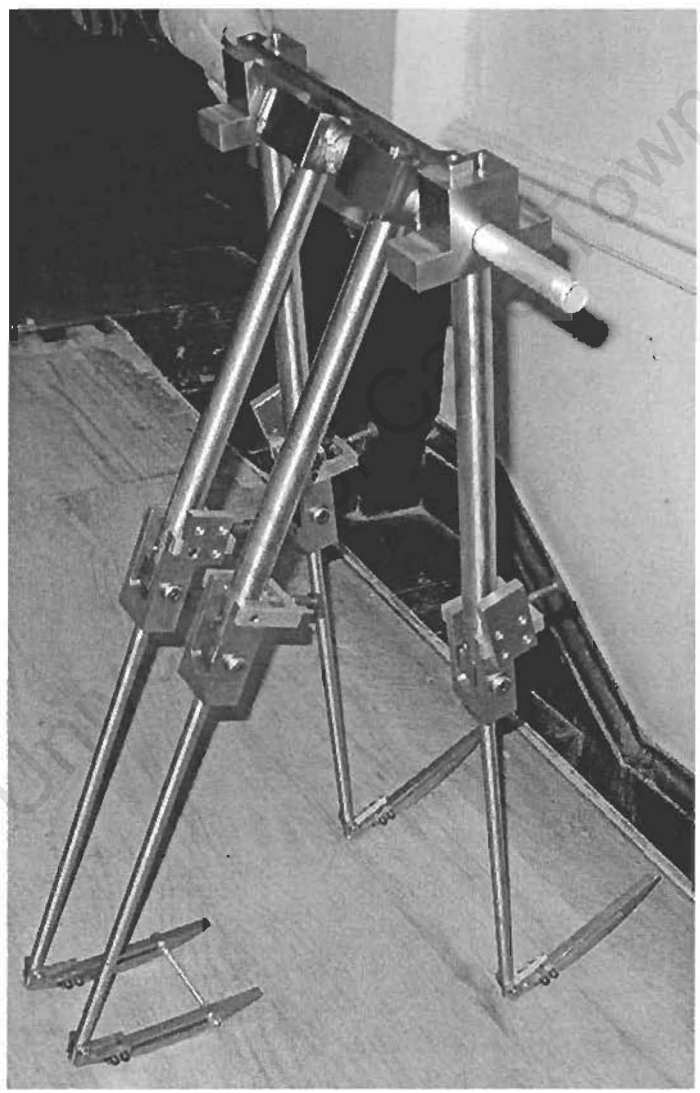

Figure 3.1 The manufactured, original physical walker set-up as tested.

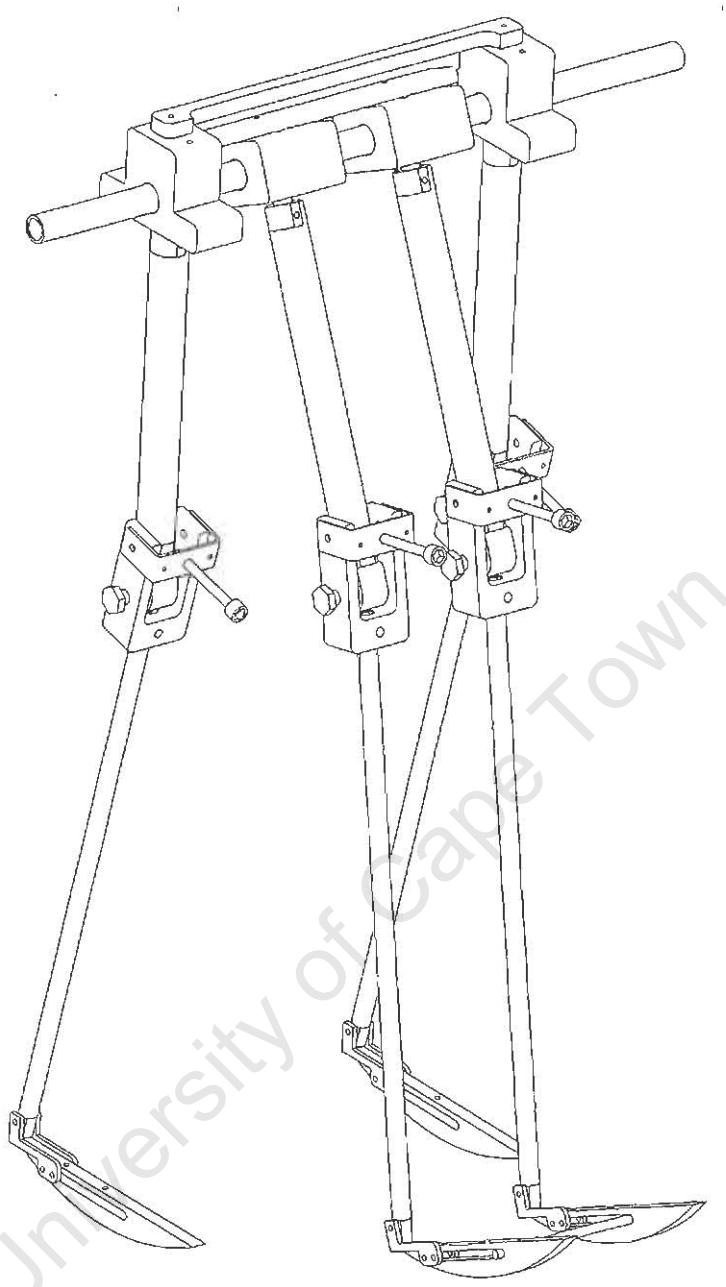

Figure 3.2 SolidWorks drawing of the assembled walker excluding the suction-cup mechanism.

Each pair of legs is identical to its neighbour and displays the parameters specified in Table 3.1.The specifications of each component were designed by a two-step procedure. Firstly, unknown lengths or positions, for example the shank leg length, were determined geometrically from the schematic of Garcia (1997) in Figure 3.4. Secondly, the centre of mass (COM) location and mass of each individual element was calculated by balance of moments about the overall COM or a the relevant joint.

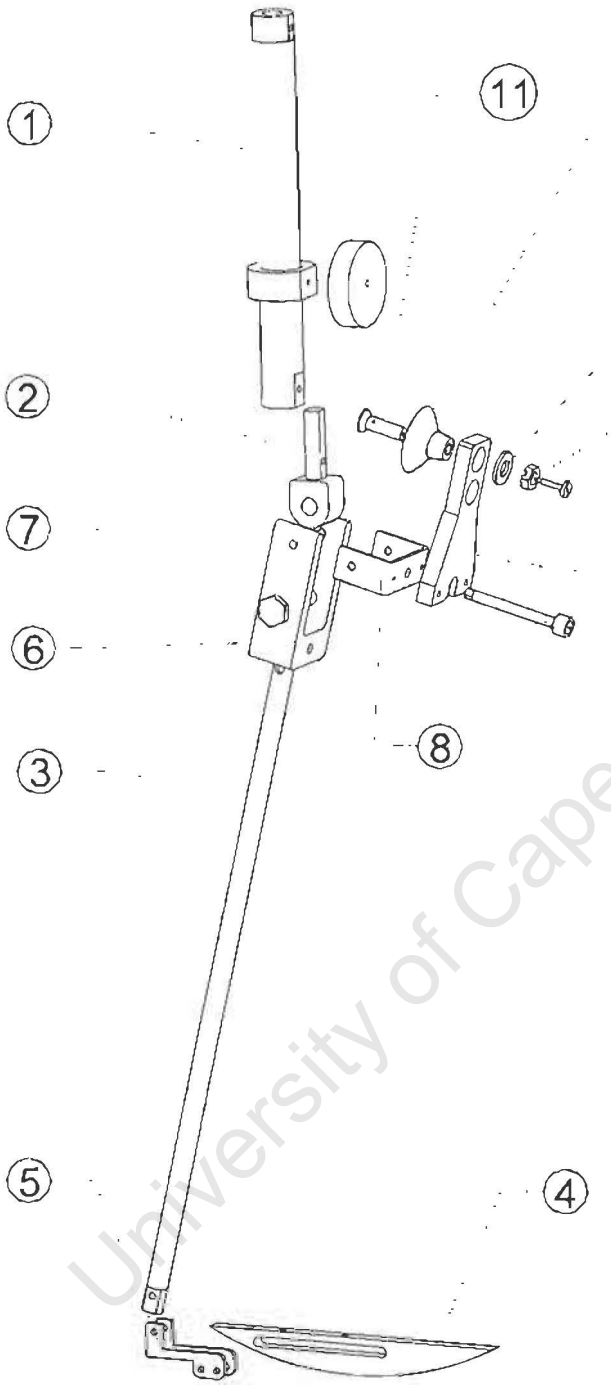

ITEM NO	QTY.	PART NO.
1	1	Thigh_2_simple
2	1	Thigh_Knee_1
3	1	Shank_1
4	1	Foot_1
5	2	Ankle_4
6	1	Knee_1
7	1	Knee_PIN
8	1	knee_stop_plate
9	1	knee_stop_pin
10	1	Suction_cup
11	1	Bolt
12	1	Nut
13	1	Needle_valve
14	1	cup_mounting
15	1	Washer
16	1	Collar
17	1	Plate

Figure 3.3 Exploded view of components used for a single leg final assembly. Shown are the thigh and shank, linked by a knee joint with accompanying suction-cup knee-stop mechanism, the circular foot and ankle joint brackets. The individual hip joint is excluded from this particular view.

At each design stage of the individual components and their subsequent assembly, the mass properties were confirmed by use of the Solid Works 2000 drawing package. In addition any design changes to the biped were first implemented virtually using this package to determine the effect on the overall weight, COM and moments of inertia. This proved useful in both confirming the geometric relationships and momentum balance equations, as well as ensuring

accurate mating of the components and avoiding unnecessary interference during their relative motions.

Before testing, the simulation was run using the new set of parameters to determine the level of stability. If instability was detected the responsible part was redesigned to have a less significant effect.

3.2 Parameter Specifications

The global dimensions used in parameter selection of the physical model were based on the constructed biped of Garcia *et al.* (1998). These geometric properties, as illustrated in Figure 3.4, were established by Garcia *et al.* (1998) via mathematical analysis, and confirmed by both simulation and physical construction to give a stable, efficient gait on a shallow slope of two degrees. The exact values of the dimensional parameters to be implemented are given in Table 3.1.

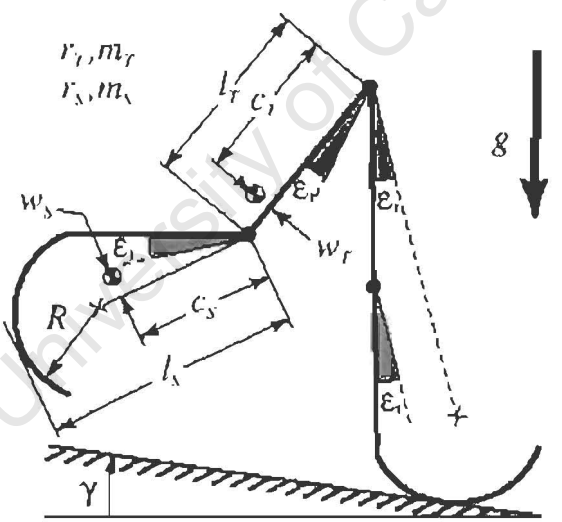

Figure 3.4 Dimensional parameters as specified by Garcia *et al.* (1998)

In addition to the global parameters of Garcia *et al.* (1998), several practical design issues were incorporated into the constructed biped. Fundamental to the design of our biped was to permit a moderate range of variation of key parameters, such as weight, COM position and leg length which may be adjusted on site, between tests without any re-machining. As a whole, the design also had to allow both ease of manufacture and assembly while maintaining the desired accuracy.

Table 3.1 Dimensional parameters and values of a single leg as determined by Garcia *et al.* (1998) and implemented in the current biped version.

Parameter	Symbol	Value
Thigh Length	L_t	0.35 m
Shank Length	L_s	0.46 m
Thigh Centre of Mass Distance	C_t	0.091 m
Shank Centre of Mass Distance	C_s	0.17 m
Thigh Centre of Mass Offset	W_t	0 m
Shank Centre of Mass Offset	W_s	0.025 m
Thigh Mass	M_t	2.354 kg
Shank Mass	M_s	1.013 kg
Thigh Radius of Gyration	r_t	0.099 m
Shank Radius of Gyration	r_s	0.197 m
Foot Radius	R	0.2 m
Foot Centre Offset	ξ_t	0.197 rad
Slope	γ	0.0349 rad
Gravity	g	9.81 ms^{-1}

With these goals in mind, the principal design approach constructs each of the four bipedal legs from discrete components, which, much like human limbs, form two distinct thigh and shank subassemblies. The former includes a rigid limb and a hip joint while the latter set comprises a similar limb connected to the knee joint at its caudal end and the circular foot, via an ankle, at its distal end. The distinct component masses, when grouped in this manner with the correct orientation, result in the overall shank and thigh COM positions as specified in Table 3.1.

Moreover, the limbs of the passive biped should accommodate a change in overall leg length of approximately 10% to facilitate fine-tuning. In the same light, a system of movable weights should be provided to allow moderate adjustment of the shank and thigh COM with ease. In order to investigate the change in Froude number with size, the ability for the limbs to be interchanged easily with a set of significantly larger or smaller leg lengths must be considered.

At an individual level, the hip joint must serve as a frictionless axis of rotation while providing a point mass of specific quantity as well as coupling the inner and outer leg pairs to form a single unit for locomotion. The motion of each of these pairs is to be synchronised such that they act as a single limb when viewed in the sagittal plane. Lastly, save for the normal transmission of forces and changes in momentum via the hip at knee and heel-strike, the inner leg dynamics had to be independent of those of the outer during the majority of the stride, with no other physical link existing between the two.

Linking the shank and thigh of each leg, a knee joint of minimal frictional resistance ensures that both limb sections are aligned in the same sagittal plane throughout the stride, as well as incorporates a knee-stop to allow an adjustable angle of extension. The knee-stop should not only provide minimal rebound at knee strike but, in the same instance, offer no hindrance to knee flexion at the beginning of a stride, or as McGeer (1990) terms it, a no-bounce no-stick knee-stop.

In the event of broadening the investigation to include compass gait, the knee joint must also allow easy conversion from a kneed walker to a straight-legged walker without resorting to refashioning of the constructed parts. The ankle joints are to be fixed during testing but allow both angular and fore-aft adjustment of the foot position as required. Moreover, allowance must be made for the simple removal of the feet in order to reduce the biped to a point-foot walker.

Lastly, the constructed biped must be sufficiently robust to allow a large number of trials over an extended period without failure of any key parts. However, if for any unforeseen reason a replacement part is required, its design must permit quick and simple machining without the need for overly specialised equipment.

3.3 Limb Profile and Extension

The selection of thigh and shank limb profile rests on several factors including the strength to weight ratio, the ease of manufacture and assembly, accommodation of additional weights and the capacity for small changes in length of approximately 10%. In Figure 3.5 some commonly used profiles to be considered are shown, namely the C-bar, solid and hollow circular shafts.

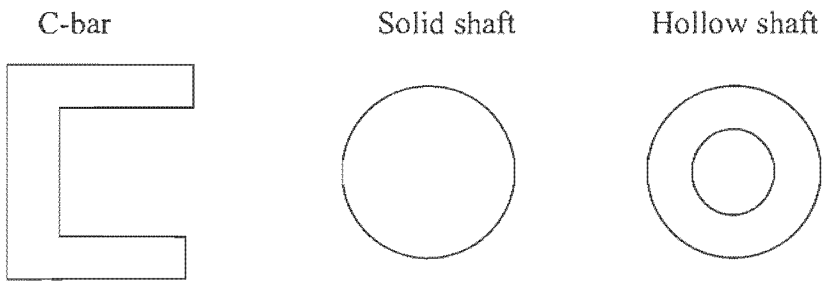

Figure 3.5 Possible "limb" profiles

In terms of their ability to accommodate a change in leg length and additional weights, the profiles may utilise three possible limb arrangements illustrated in Figure 3.6. The first two design options use a C-profile, with either a length-wise slot or alternatively a series of holes to house a support pin to fix weights on either side.

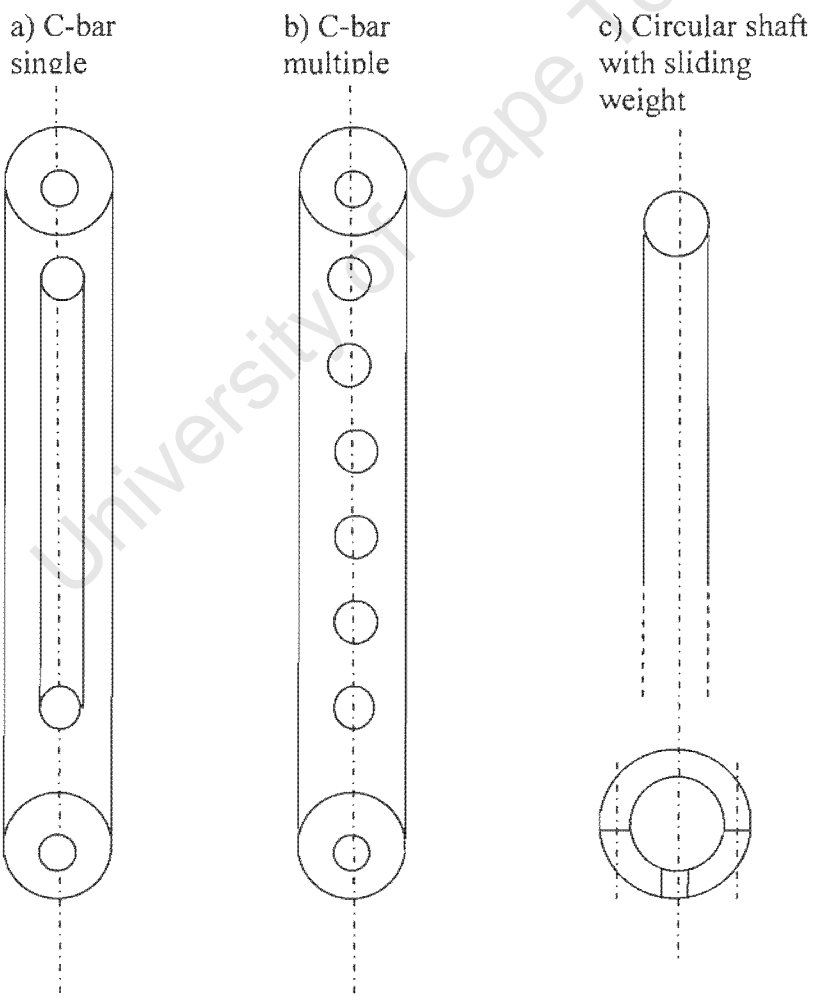

Figure 3.6 Some of the possible limb arrangements to allow for both change in leg length and the addition of weights

Leg extension maybe realised by attaching additional segments on either the outer or inner faces of the C-bar. However the attachment of these additional parts would be unnecessarily taxing both physically and with respect to time of assembly, thus impeding the versatility of the biped during testing.

On the other hand, producing leg extension with a circular shaft is a simpler task. Including short inner runners, localised to either end of the limb, would prove both simpler to implement and adjust during testing, the only provision being a groove or locating dimple to ensure correct alignment as even minor deviations can disrupt the shank motion. Additional weights in the form of collars, as in Figure 3.6, may be easily attached to slide on the outer surface, their positions adjusted quickly by fastening of a grub screw.

The collars themselves may be a single element or formed from two halves to facilitate initial attachment to the limb. In the final design, however, the single element collar was implemented as the removal of the thigh or shank section is by comparison a simpler task to that of fastening several half collars together. Furthermore, using several collars of smaller mass, as opposed to a single element of set mass, has the added advantage of permitting incremental variation. It was thus decided that the profile of choice would be of circular cross-section, ruling out the C-bar and similar flat-face shapes.

At this point either the solid or hollow shaft may be implemented, although there is a bias toward the solid shaft by virtue of its need for minimal machining. The choice also rests on the projected diameters for each cross-section. This would influence both the form and size of the attached components, specifically the hip and knee joints as well as the knee-end attachment.

The final design implemented was a combination of the hollow and solid circular shafts. Essentially the main body of the "limb" would remain solid while limb extension takes place at the end sections, which include a hollow portion to house the runner as in Figure 3.7. The joint-end segment would be equivalent in mass to the length of the limb, which it replaces.

Two design alternatives present themselves when realising the mechanism of the runner-shaft principle in Figure 3.7. The first concept employs a right-hand screw thread machined onto the inner surface of the limb and a complementary pattern to the outer face of the runner. A

similar mirrored (i.e. left-hand thread) arrangement is applied to the opposite end. By twisting of the shaft, infinitesimal adjustment of leg length may be achieved while a locknut at each end fixes the desired position. A drawback of this system is the components at the opposing ends; say the hip and knee are not guaranteed to be parallel with either each other or their complementary parts on other legs. Moreover, the free space available, especially at the knee end as shall be apparent further on, may not permit the use of a locknut or at best make adjustment with a spanner difficult and awkward.

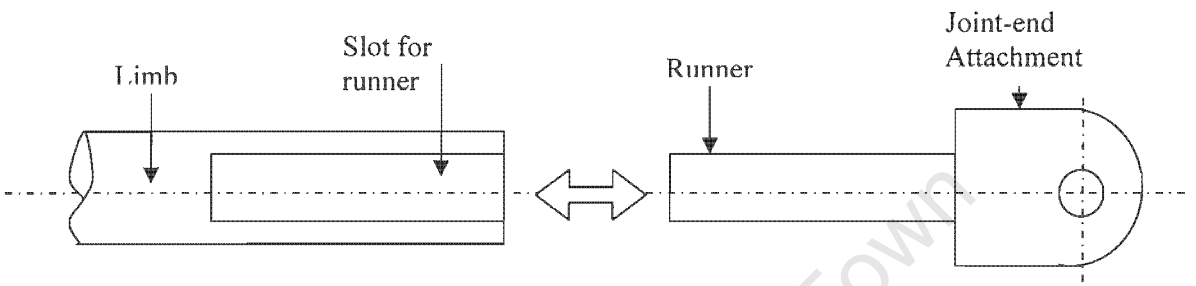

Figure 3.7 Schematic representation of the runner-shaft principle used for length-wise extension of a circular shaft.

An alternative design sidesteps these issues by dispensing with the screw thread and opting for a simple loose-fit slider shaft. A grub screw arrangement is employed to fix the shaft's position, as an Alan key is more suited to quick adjustment in limited space. Machining a locating groove on each sliding shaft, parallel to the required face, ensures correct orientation. The groove's small depression also aids traction, thus reducing the number of grub screws required. This also simplifies assembly as once the groove is located and sited along the hole, the slider shaft is inserted and the grub screw fastened.

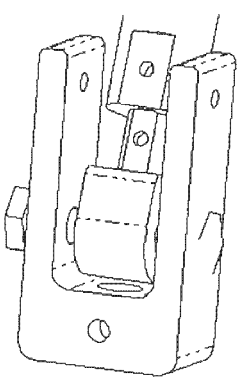

Figure 3.8 3-D view of the knee-end attachment of the thigh extension, including a locating face and dimple set at the minimum distance.

3.4 Thigh Subassembly

The critical parameters describing the thigh subassembly are the length, mass and position of the centre of mass (i.e. COM) as given in Table 3.2.

Table 3.2 Thigh subassembly parameters

Parameter	Symbol	Value
Thigh Length	L_t	0.35 m
Thigh Mass	M_t	2.345 kg
Thigh Centre of Mass Distance	C_t	0.091 m
Thigh Centre of Mass Offset	W_t	0 m
Thigh Radius of Gyration	r_t	0.099 m

The subassembly comprises of the hip joint and the thigh "limb" of mass m_{hip} and m_{leg} respectively, as illustrated in the free body diagram of Figure 3.9. To calculate the necessary distribution of mass and hence dimensions of each component a momentum balance about the centre of mass is performed.

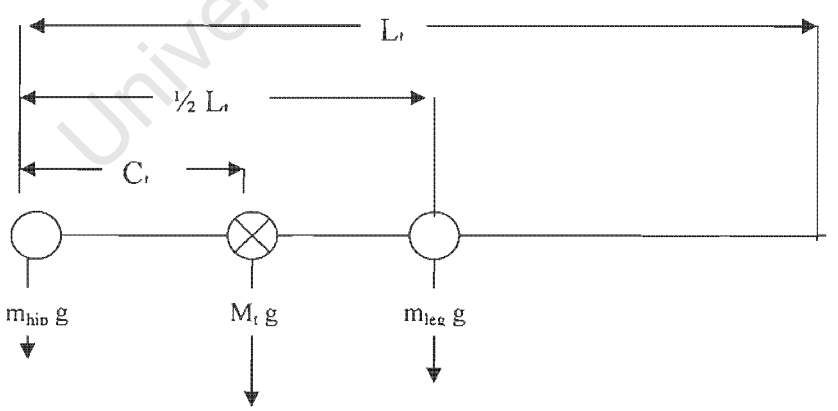

Figure 3.9 Free body diagram of thigh subassembly

Using the fact that the overall mass of the thigh $M_t = 2.345$ kg, is the summation of the hip-joint mass and the limb mass, the moment balance, shown in Appendix A, gives the masses of the hip and leg as $m_{hip} = 1.1256$ kg and $m_{leg} = 1.2194$ kg.

The size of the thigh cross section was determined by volume calculation (see Appendix A1). For a solid mild steel shaft of density ρ = 7850 kg/m^3, using a circular profile the required radius is r_t = 12 mm, while that of a hollow shaft would be r_{inner} = 5 mm, r_{outer} = 13 mm. When designing the joint-end sections, care was taken to ensure they are equivalent in mass to the length of limb, which they replace so as to preserve the limb's COM.

3.5 Shank Subassembly

The shank subassembly comprises of a knee joint attached to a straight limb at an angle of ξ_k = 12.5° from the centre line which in turn is parallel to the y-axis. A rigid ankle joint at the distal end completes the subassembly by attaching a circular foot of radius R and angle of arc β. The foot itself is centred about point O, 0.26 m below the knee along the shank centreline, with its particular centreline offset by an angle of σ. The foot COM lies along this centreline at a distance λ from point O. As illustrated in the free body diagram of Figure 3.10, the number of unknowns, given in normal font, is significantly greater than that of the thigh subassembly. The equations defining the shank subassembly, as given in Appendix A2, are initially derived from geometric principles followed by moment balance about the knee joint in the x and y-axes.

Geometrically, the majority of defining lengths and angles are known with the exception of the shank leg length L_{leg}, the angle of the foot arc β, as well as its angular offset σ. The former is determined by both geometric construction and application of the cosine rule using the triangle formed by the knee, ankle, point O and the angle ξ_k, to give a length of L_{leg}= 440 mm. The latter two parameters, β and σ, are dependent on the foot COM position and thus sought by balance of moments.

Note, in the free body diagram of Figure 3.10 the masses of the ankle and knee are not shown. In the interest of simplification the knee and leg masses are combined to form the overall limb mass, m_{leg} shown. Reducing the number of unknowns further, the ankle joint mass may be considered negligible, thus dispensing with its effect of shifting the shank COM away from the knee and the foot mass off its centreline.

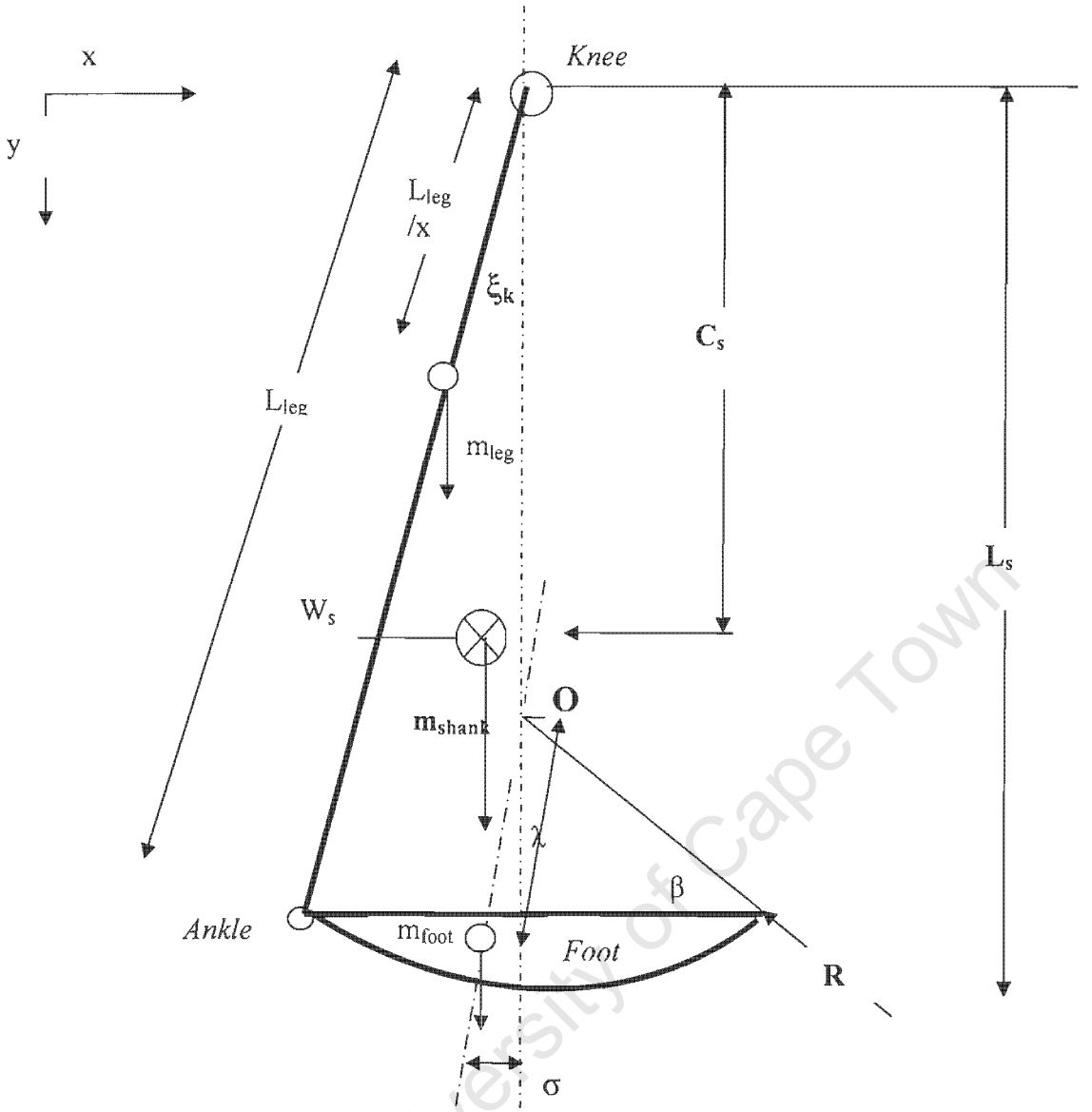

Figure 3.10 Free body diagram of shank subassembly, set parameters from Garcia et al. (1998) are bold, design specific parameters are in normal font

However, as a totally mass-less ankle is unobtainable, its contribution may be easily balanced on assembly by adding an equivalent mass to the knee end. Hence the calculations of Appendix A2 focus initially on the distribution of the foot and leg mass components (m_{leg}, m_{foot}) to generate the overall shank COM (W_s, C_s, M_s) and shank length (L_s) given in Table 3.3.

Table 3.3 Known dimensional parameters of shank subassembly

Parameter	Symbol	Value
Shank Mass	M_s	1.013 kg
Shank Length	L_s	0.46 m
Shank Centre of Mass Distance	C_s	0.17 m
Shank Centre of Mass Offset	W_s	0.025 m
Foot Radius	R	0.2 m
Foot Centre Offset	σ	0.197 rad

In the first stage of the shank COM calculations, Appendix A2, the magnitude and position of the masses m_{leg} and m_{foot} are determined. It is assumed that m_{leg} is not restricted to the mid-point of the "limb"; instead its COM is constructed in a similar manner to that of the thigh whereby the combined masses of the knee joint and the leg produce the desired location, denoted as a fraction L_L/x in Figure 3.10. A further assumption is that the centre line of the foot is offset from that of the overall shank subassembly by the angle σ. This, together with the distance λ, measured from the foot COM to its centre O, is necessary to produce the x-axis offset W_s. In turn the variables λ and σ are dependent on the foot parameters, angle β and mass m_{foot}.

Taking moments about the overall COM and then incorporating basic trigonometric relationships, equations 3.4 to 3.9 are reduced to the resulting final equation 3.11. Taking the denominator x = 4 and the angle ξ_k=14°, the equation was solved numerically in Excel; Appendix A2.

Sum of Moments about the x-axis

$$M_{shank} W_s = M_{leg} L_x + M_{foot} F_x \qquad 3.1$$

Sum of Moments about the y-axis

$$M_{shank} C_s = M_{leg} L_y + M_{foot} F_y \qquad 3.2$$

Substituting Equation 1 into Equation 2

$$W_s (F_y - L_y) - L_x F_y = C_s (F_x - L_x) - L_y F_x \quad 3.3$$

Where

$$F_y = 0.26 + \lambda \cos \sigma \quad 3.4$$

$$F_x = \lambda \sin \sigma \quad 3.5$$

$$L_x = \frac{L_l}{x} \sin \xi_\kappa \quad \text{(Where x is a variable denominator = 4)} \quad 3.6$$

$$L_y = \frac{L_l}{x} \cos \xi_\kappa \quad 3.7$$

$$\lambda = R^2 \sin^3 \alpha \left[\frac{\alpha}{\sin \alpha - \alpha \cos \alpha} \right] \quad 3.8$$

$$\xi_k = \xi_t + \xi_f = 14^\circ \quad 3.9$$

Final equation solved numerically: 3.10

$$0.0065 + 0.025 \lambda \cos(32^\circ - \alpha) - 0.025 (L_L/x) \cos(14^\circ)$$
$$0.17 \lambda \sin(32^\circ - \alpha) + 0.17 \lambda \sin(14^\circ) = - \lambda (L_L/x) \cos(32^\circ - \alpha)$$
$$\sin(\xi_k) + 0.26 (L_L/x) \sin(\xi_k) - \lambda (L_L/x) \sin(32^\circ - \alpha) \cos(\xi_k)$$

Using a mild steel shaft of circular cross-section the required diameter calculated is 12 mm. The final design parameters for the knee joint, leg and foot components of the shank subassembly are given in Table 3.4.

Table 3.4 Calculated geometric and mass parameters of the shank subassembly components

Parameter	Symbol	Value
Knee Joint Mass	m_{knee}	0.417 kg
Shank Leg Mass	m_{leg}	0.402 kg
Shank Leg Length	L_{leg}	440/405 mm
Shank Leg Diameter	R_{shank}	12.0 mm
Foot Mass	m_{foot}	0.611 kg
Foot Angle of "Sweep"	β	$= 90^\circ - 25.2^\circ$
Foot Thickness	t_{foot}	10 mm
Radius of Gyration (kgm^4)	r_s	69.62×10^{-3}

3.5.1 Foot Design

The feet of the biped have been almost fully defined by their radius R, angle of arc β, mass M_{foot} and centre of mass position along the centreline λ. The final parameter required is the foot thickness t_{foot}, which is calculated by using equations 3.11 and 3.12, which give a thickness of 6 mm.

$$t_{foot} = \frac{M_{foot}}{\rho A_{foot}} \tag{3.11}$$

$$A_{foot} = R^2\left[\frac{\alpha\pi}{180^0} - 0.5\sin 2\alpha\right] \tag{3.12}$$

By incorporating a lengthwise slot centred about the COM, the foot thickness is increased to 10 mm. However, as shown in Figure 3.12, the slot is shifted slightly to the left to accommodate the ankle joint and a foot-link spanning the inner feet, which will be discussed towards the end of this chapter. The resulting shift in COM position is marginal, with $\Delta\lambda$ = 0.5 mm and Δx = 4.7 mm and thus implemented.

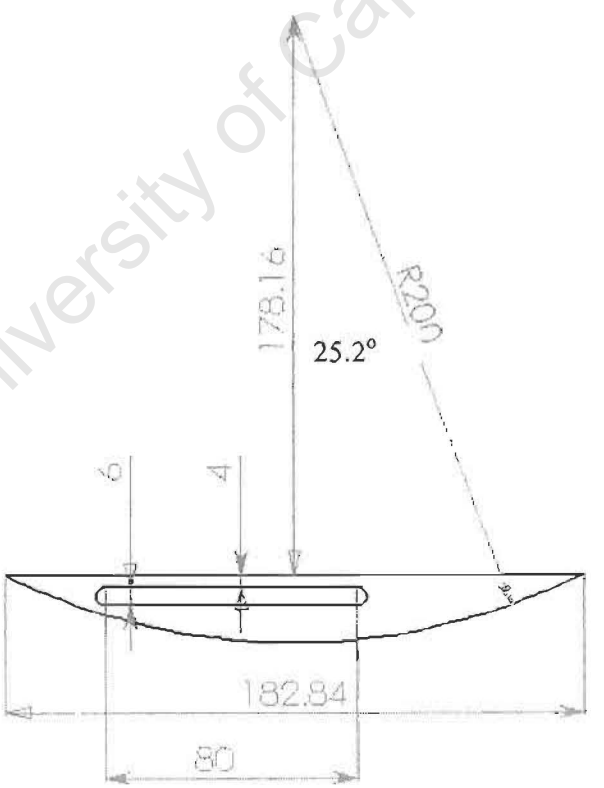

Figure 3.11 Foot profile dimensions.

3.6 Hip Joint

Although the required mass of the hip joint has been determined, it is not the only role it must play in the bipedal system. Several practical issues must be dealt with in conjunction with providing the predetermined mass.

As calculated each hip must provide a mass of M_{hip} = 0.417 kg concentrated about the common axis of rotation. During mathematical analysis and subsequent simulation, the hip joint is assumed frictionless and as McGeer (1997) states, should the friction be more than negligible it will destroy the gait cycle entirely.

The design is tackled from two perspectives: that of providing a frictionless joint with a specific mass for each leg, and that of structurally separating and synchronising the motion of the four legs as inner and outer pairs. After selecting the structural concept to be implemented, the shape of the individual hips were formulated and their sizes designed for. Furthermore the structural design must allow the attachment of extra weight to each hip pair about the axis of rotation to facilitate parameter variation during fine-tuning.

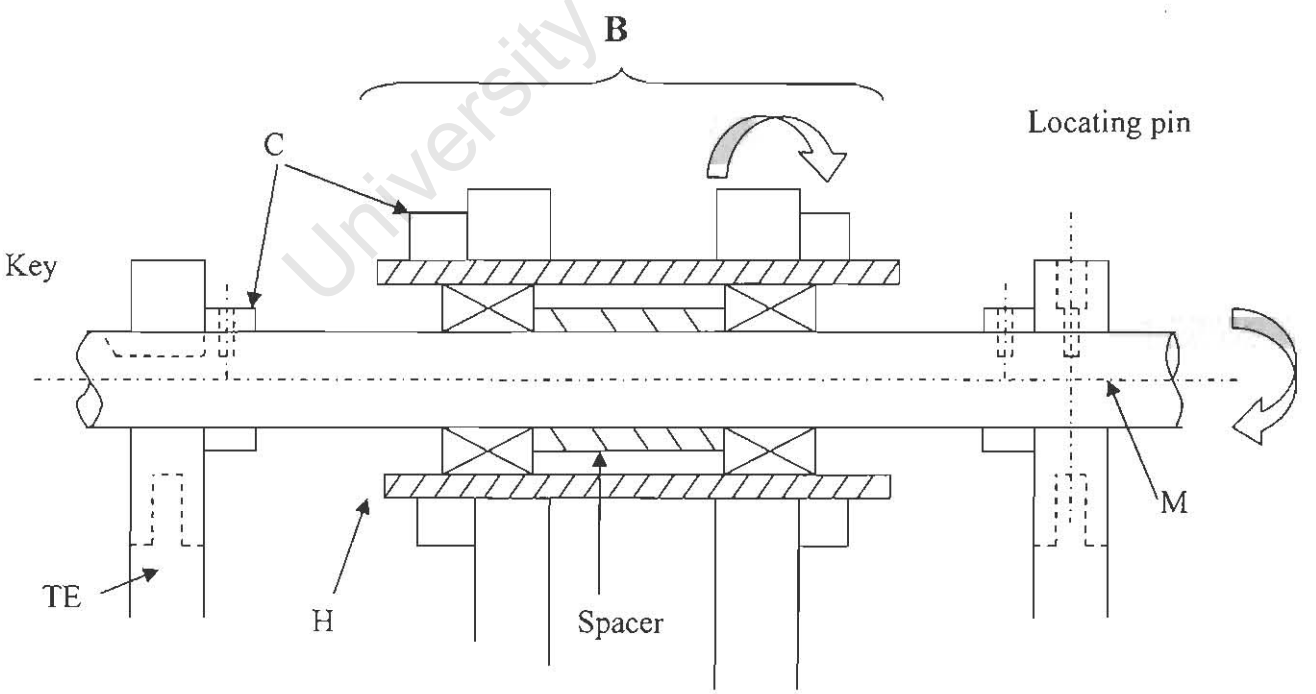

Figure 3.12 Schematic of possible structural concept for hip joint

The following two concepts were considered when attempting to fulfil the structural aspect of the requirements. In Figures 3.12 and 3.13 the outer and inner hips share a common support shaft S, although only the inner pair of hips rotate about the shaft, isolated from its rotational movement by virtue of a paired bearing arrangement B. The bearing housing H serves multiple purposes by accommodating the bearing and additional collars C, as well as ensuring the simultaneous movement of the inner legs by fusing the inner hips.

The outer hips on the other hand, are linked by virtue of the main shaft M, which they are fixed to by either a key or locating pin that passes through the upper portion of the separate thigh-end piece, TE. The main shaft provides structural support, synchronisation and contributes to the hip mass of the outer hips, hence reducing their volume. Additional weights in the form of collars C may be attached to either pair by sliding onto the housing or main shaft and fixed by means of a locating pin, thereby ensuring the extra weight is centred about the common axis of rotation and moves in synchrony with the adjacent hip. Extra length is produced at the junction between the thigh and the thigh-end piece by a slider and grub screw in a similar manner to the knee-end piece as discussed in section 3.4

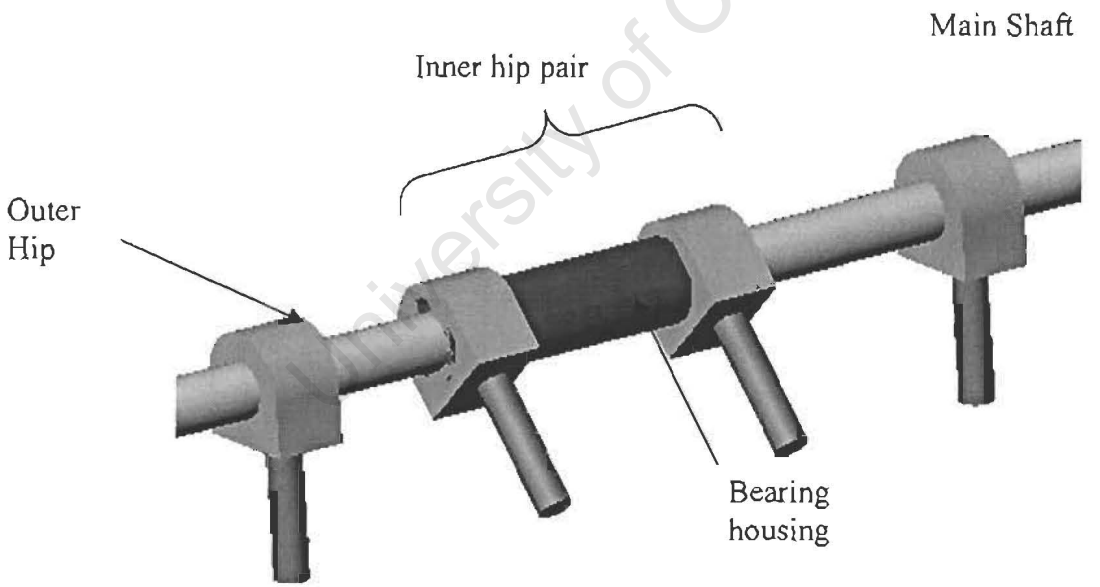

Figure 3.13 3D view of possible hip arrangement

An alternative and simpler concept is shown in Figure 3.14. This more obvious arrangement possesses a similar main shaft M; however in this case both outer and inner hips are isolated from rotational movement with a simple lubricated clearance fit or journal bearing (not shown in the diagram). Synchronisation is less elegantly achieved by overhead inner and outer links (I_L and O_L) fastened onto the top of each hip. A problem arises as the main shaft's rotation

and hence mass is not fixed to one pair of legs. However, as determined using the Garcia (1997) simulation, provided the shaft is sufficiently lightweight, its inertial contribution to either pair will be negligible and the end of step conditions are within the limits of the subsequent swing leg's required initial conditions.

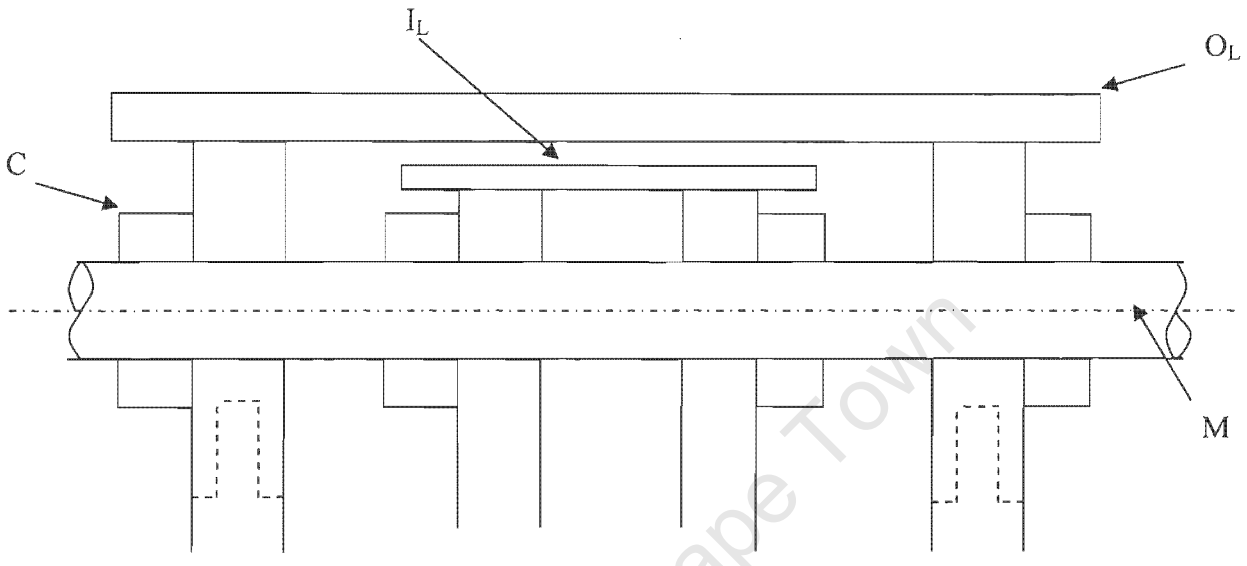

Figure 3.14 Schematic of simple hip joint with "overhead" links;
C-collars; O_L –outer link; I_L-inner link; M-main shaft

Although simpler to assemble and modify, this arrangement sacrifices the inertial and COM symmetry of the inner and outer legs. Nevertheless, as explained by Garcia (1998), this dynamic equivalence is easily restored by addition of weights at specific positions on the thighs, a trait already designed for during the selection of the limb profile. Fixing of collars C, and extending leg length, may be accomplished in a similar manner to that of the previous concept.

Considering these factors, the hip structural layout of Figure3.14, was chosen and implemented. Before completion two more design choices must be made, the securing of the links to each hip, and the shape and size of the individual hip segments.

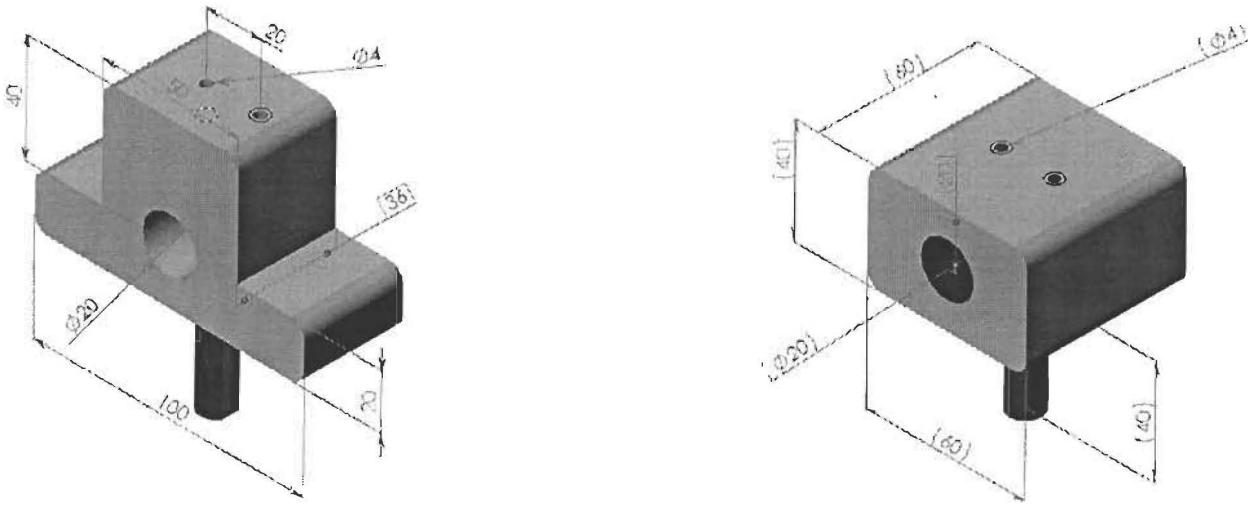

a) Outer Hip b) Inner Hip

Figure 3.15 Dimensions of implemented outer and inner hips

Each individual hip was to be of mass, m_{hip} = 1.1256 kg centred about the axis of rotation as determined in Appendix B.1. On assembly the links were to display sufficient clearance for all possible thigh angles occurring during gait to ensure no interference between the outer and inner legs. This clearance was provided by an increased elevation of the outer hips, which take on an inverted T-profile to ensure the weight was balanced symmetrically about the centre of rotation. Similarly, the inner hips assisted clearance with a shorter and narrower profile. Change in thigh length was realised by a short slider screwed into the base of the hip. This ran within a hollow at the cordate thigh end and was secured by a pair of grub screws.

The link's ability to transmit torque from one leg to another was paramount, although several additional criteria did exist. In formulating a design each set-up aimed to minimise weight while providing sufficient strength, accessibility and versatility. The latter refers to the need for change in limb separation, which from the physical trials displays a decrease in yaw and a more robust heading with the widening of the hips. Two such methods considered for fastening are shown in Figure 3.16.

The first concept had a circular rod spanning the distance between the thighs secured to the top face of each by a modified saddle clamp. A flat face machined on the bottom of the shaft ensured maximum friction and limit free rotation, while the rod itself may slide back and forth as required. A variation would involve housing the rod directly within the hip. However the limited volume of the individual hips, particularly the taller outer pair, would compromise its

strength. As a result the links are to remain "separate" from the hip, with fastening limited to the outer faces.

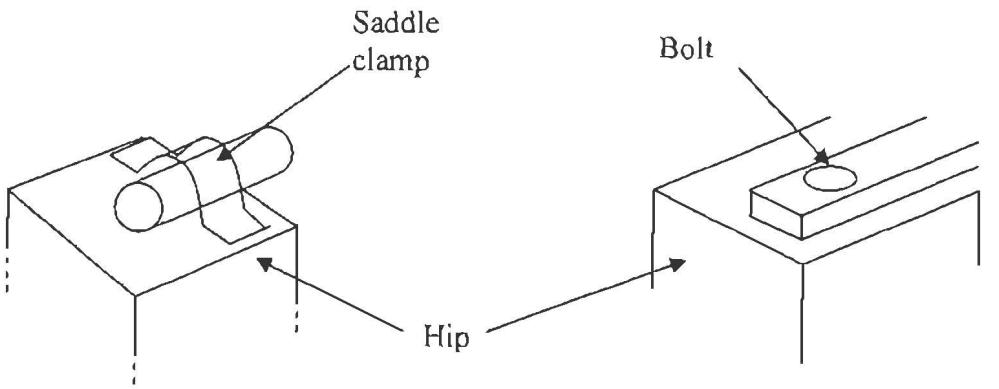

Figure 3.16 Possible fastening methods: (a) saddle clamp with circular link; (b) bolted square link

The alternative idea (b) ustelised a link of rectangular profile with pairs of equally spaced locating holes machined at each end, through which bolts attach to the top face. The larger available contact area facilitates torque transmission between hips while shifting the points of attachment between each pair of holes quickly and simply varies separation distance. In addition this lends itself well to using various links of differing mass. Ultimately the square link profile was chosen. With these criteria in mind the final outer and inner hip designs shown in Figure 3.17 were realized.

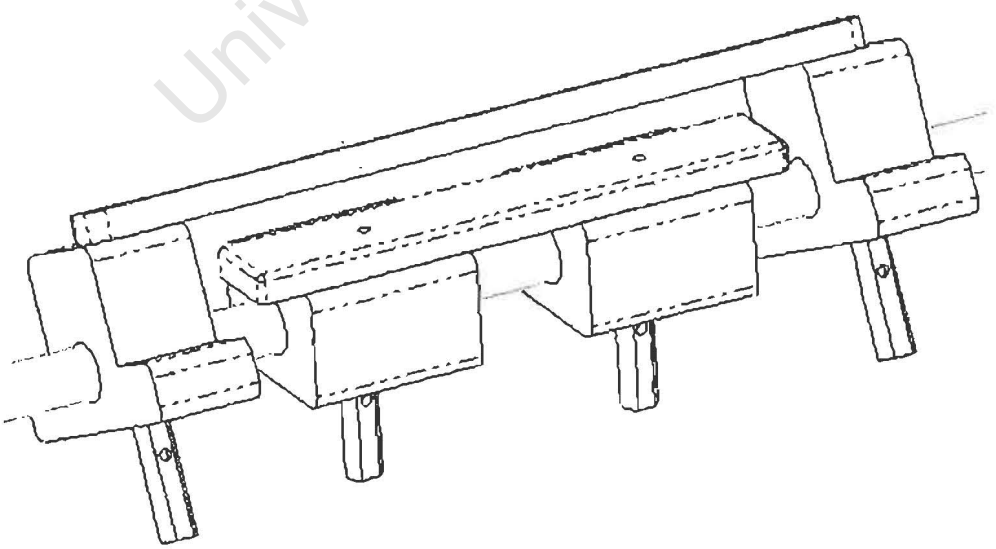

Figure 3.17 Implemented hip joint arrangement

3.7 Knee Joint

The knee joint played a double role in the formation of the bipedal system, acting as both a frictionless interface between thigh and shank as well as a point mass in the shank COM. In the latter the knee was to impart a mass of m_{knee}=0.417 kg positioned equally about the axis of rotation, while as the former the knee must house both shank and thigh sections as a frictionless hinge with limited limb extension. A knee-stop preventing over-extension in a no-bounce non-stick collision, without affecting flexion, was thus incorporated into the design of the knee. This latter function will be discussed once the final form of the knee joint has been chosen.

In view of these requirements the variations of a hinge joint shown in Figure 3.18 and 3.19 were evaluated. Considering the large difference in diameters between the thigh and shank, 24 mm and 12 mm respectively, the natural step was a pronged thigh-end with a pin spanning the gap and supporting the shank section.

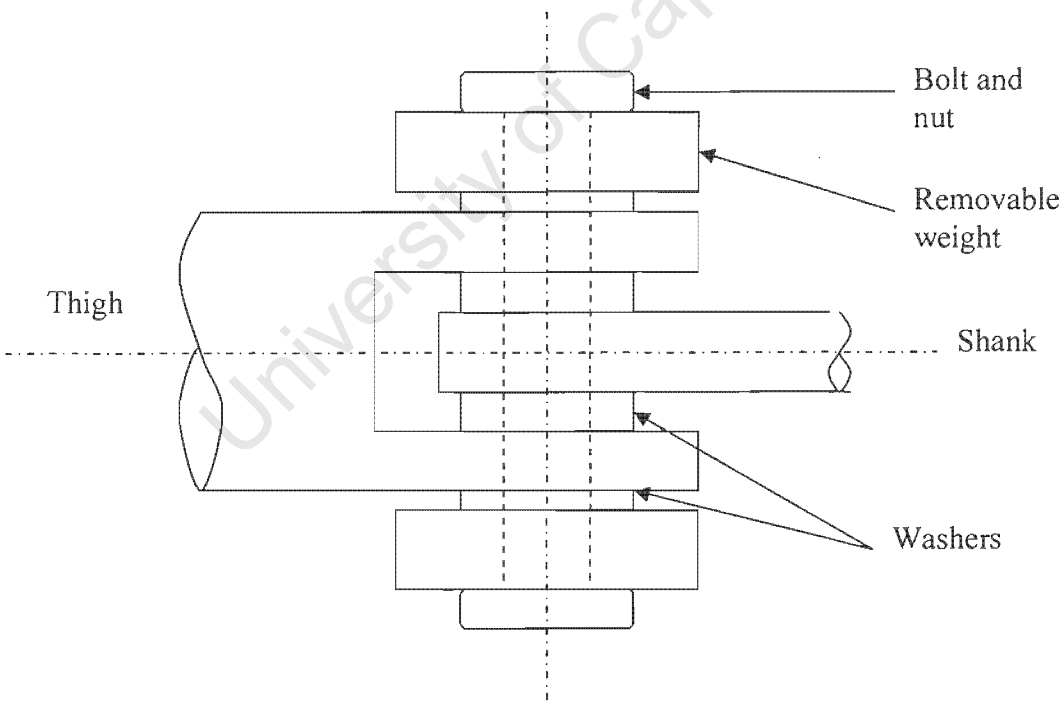

Figure 3.18 Knee joint concept (a)

To achieve the required point mass about the axis of rotation collars were fastened to each side, where grub screws ensure they rotation was synchronised with the shank section. Although side-wall friction is reduced by the simple addition of brass washers, leg extension

here required the machining of a threaded runner into the shank body which limited both the strength of the limb as well as it's versatility, as alignment of the feet allow only full turns.

The reverse condition, using a pronged shank-end shown in Figure 3.19, was achieved by the addition of a separate knee component K to the shank. This negated both the need to split shank limb and the use of collars, provided the mass was symmetrical about the axis of rotation. The shank attachment in the base was adjusted by a grub-screw, allowing a portion of length to move into or out of the knee, thus effecting length change. Alignment was guaranteed by means of a locating groove, which guides the fastening screw during assembly. The thigh too used a similar discrete interface that screwed onto the outer face, while the rounded weight-bearing extension fits in the gap G. Rounded faces ensured the separation distance between shank and thigh is minimal while multiple pivot points allowed for moderate limb length adjustment. This second idea was thus preferred for its adaptable shank-end. However, before implementation the opposing thigh piece was first refined to more efficiently permit the required movement while using the limited volume available.

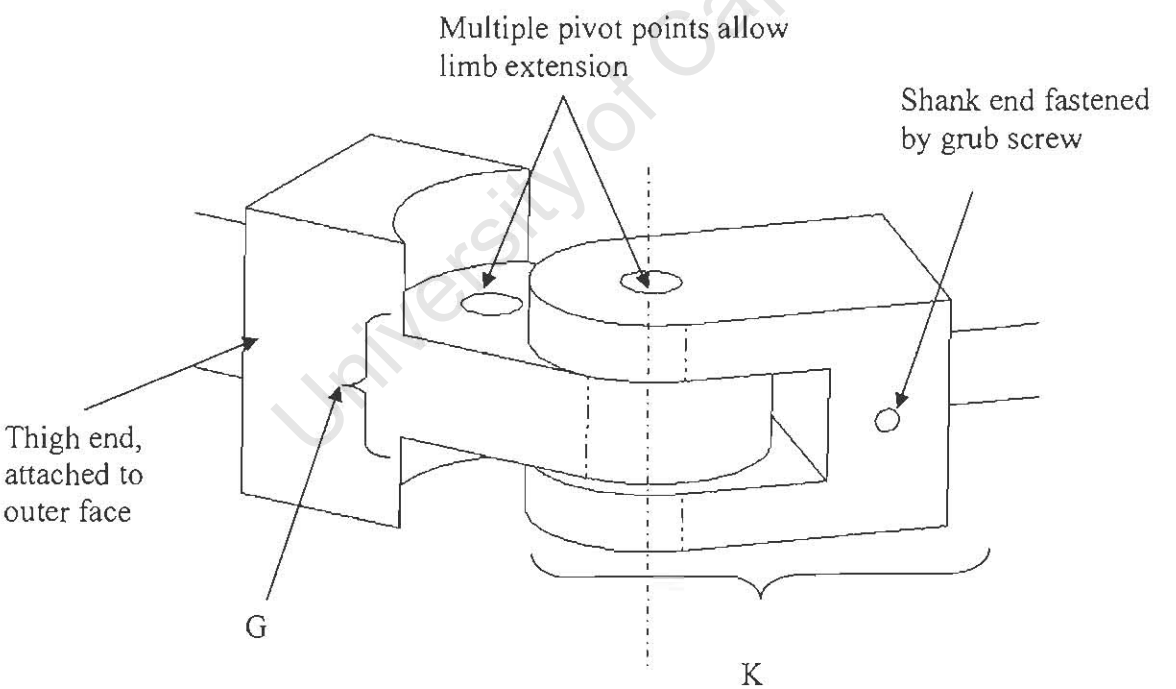

Figure 3.19 Knee joint concept (b)

The final implemented form of the knee joint, shown in Figures 3.20, 3.21 and 3.22, which used a reduced thigh–end piece T to minimise both weight and the separation distance between the limbs. During design care was taken when allocating the correct masses within the knee assembly. For example, if the pin rotates with the thigh, its mass contributes to the

thigh only. In a similar light the shank limb mass is separate to the knee, hence the "missing" mass in the base must not be added to the calculations. Moreover the effective shank length was measured from the pin centreline and not from the knee base as is natural to assume during trials.

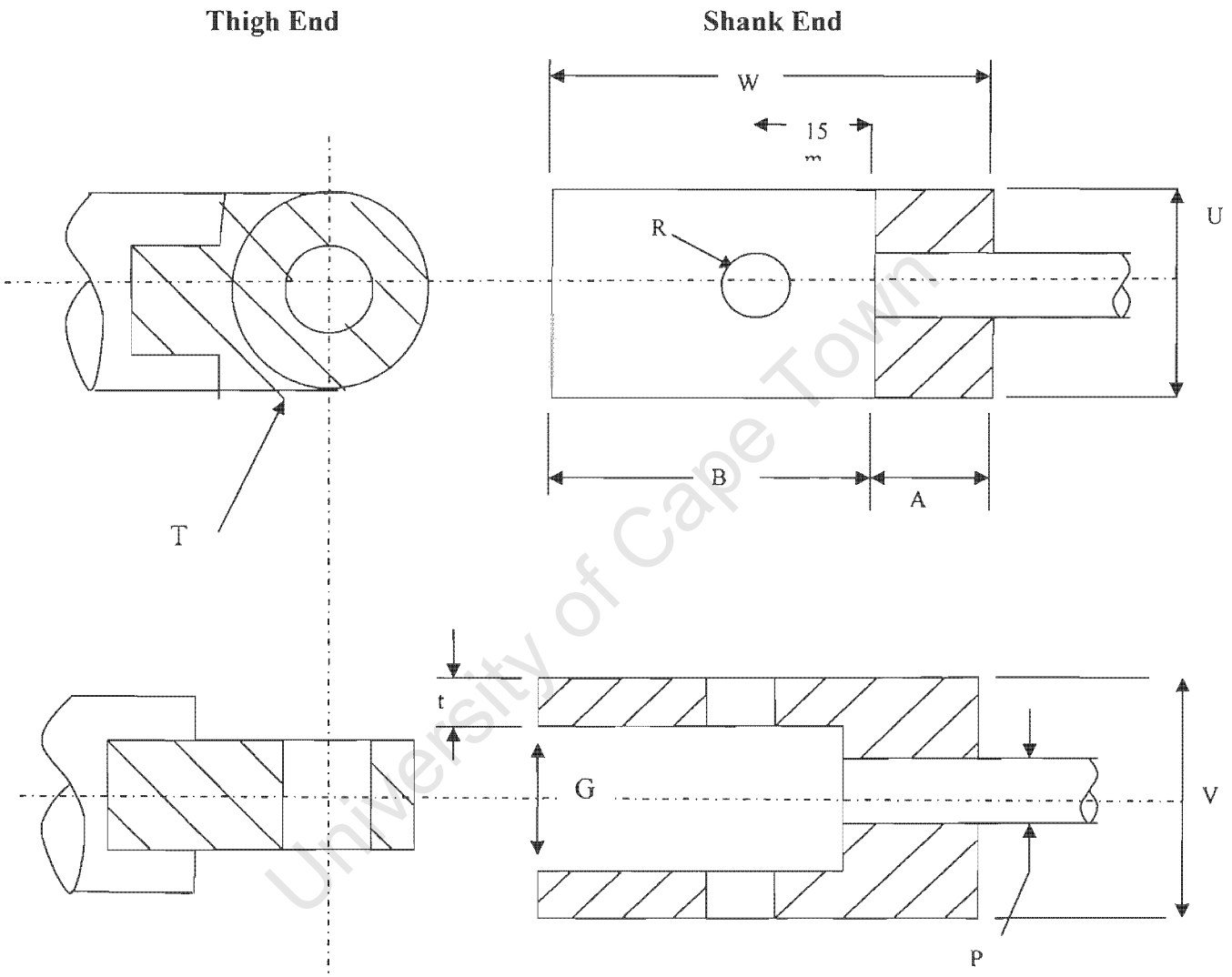

Figure 3.20 Schematic of chosen knee shape showing key dimensions to be designed

The exact dimensions shown in Figure 3.22 were calculated by balancing the area and hence mass about the axis of rotation, the final equation as derived in Appendix B.2 was solved numerically using Excel and checked with Solid Works as shown in Figure 3.21.

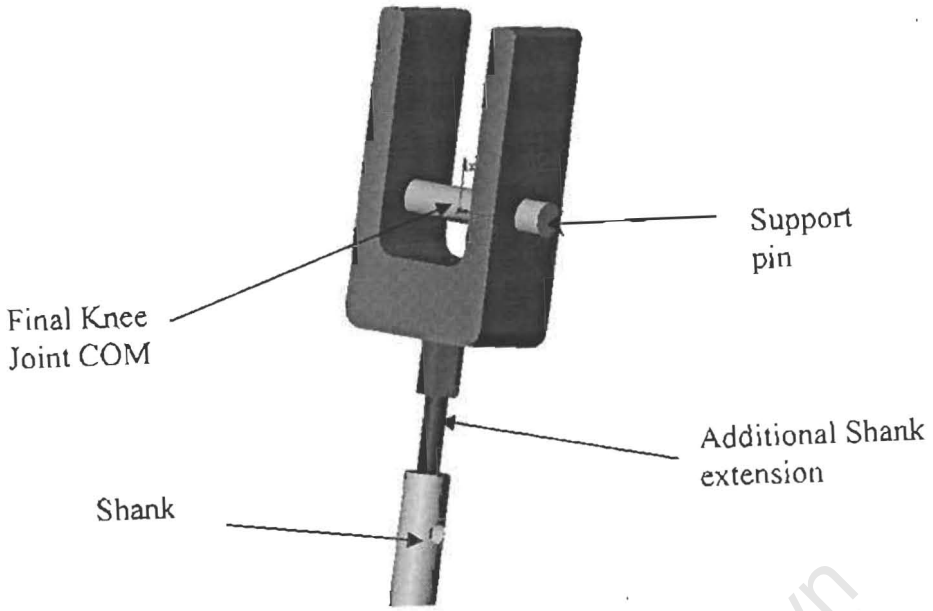

Figure 3.21 3D view of knee joint centre of mass (COM) from Solid Works

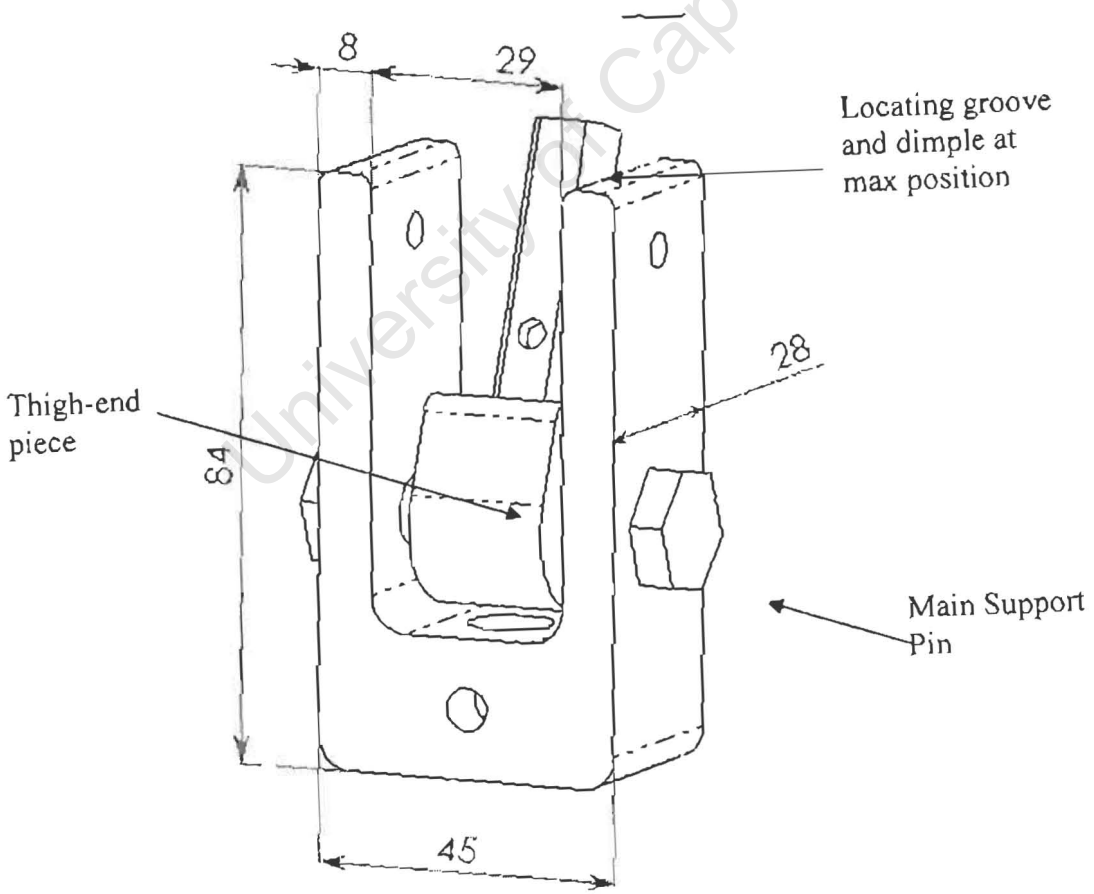

Figure 3.22 Implemented Knee joint with dimensions

3.7.1 The Knee-Stop

To complete the knee a mechanism was added to prevent the over extension of the shank in a non-bounce, non-stick (*i.e.* plastic collision) manner while being sufficiently lightweight so as to preserve the mass balance of the knee. In addition, in order to expand the range of flexible parameters the degree of knee extension permitted was designed to be easily adjusted.

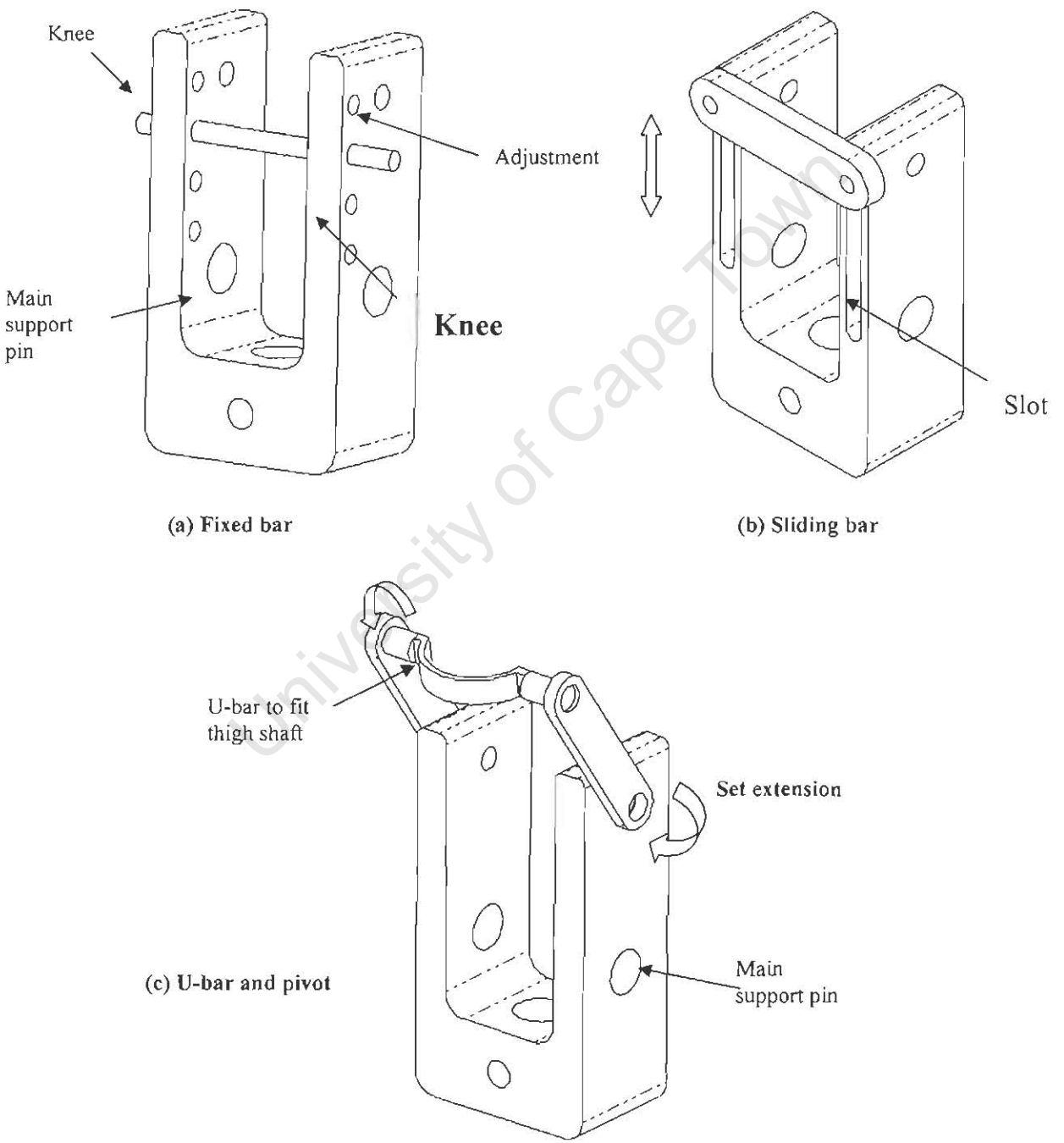

Figure 3.23 Possible Knee-stop mechanisms (a) (b) and (c)

In formulating the final design several precursor ideas were evaluated. Beginning with the primitive obstructive effect of a simple bar spanning the knee, (see Figure 23a), the height of which is varied by numerous locating holes. These holes clearly limit the increment of knee extension and influence the centre of mass in an unsymmetrical manner.

In Figure 23b the concept is converted to a sliding bar fitted to the front face, which facilitates adjustment and reduces the mass imbalance. Refined further, the third variation utilised a modified U-shape bar with a curved midsection which, free to rotate, accommodates the thigh's impact more readily. The ends are attached slightly above the main weight-bearing pin on either side of the knee at which point the angular position, and thus degree of knee extension is fixed by tightening the securing bolts (not shown). If required an adjustable torsional spring may be added at these ends to absorb some of the impact. However including a damper may prove problematic due to the limited lateral space available between neighbouring knees.

The final implemented design shown in Figures 3.24 and 3.25 varies significantly from the precursors. This arrangement employed a sliding bolt housed within an aluminium bracket that in turn was fastened to the outer sides of the knee. On contact the bolt slid backwards compressing a spring, which served to retard impact and limit bounce. On flexion the compressive force is reduced to zero and the spring returned the bolt to its initial position. Adjusting the locknut allowed the protrusion of the bolt, as well as the extent of spring compression to be varied.

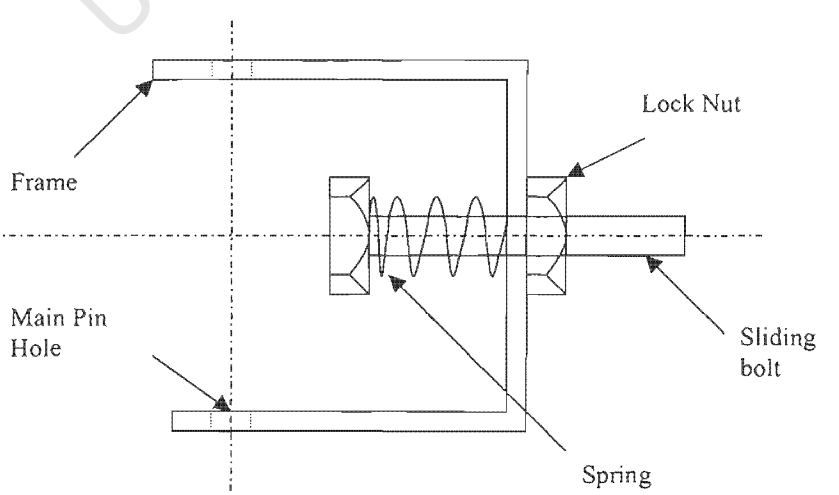

Figure 3.24 Schematic of implemented knee-stop mechanism

This paired system of components offered more elegantly the inclusion of an energy-absorbing spring, and if required an adjustable damper, all within a relatively compact volume. Further more the somewhat unavoidable asymmetrical addition of mass to the overall knee is minimised as all components are of aluminium save the bolt, which is the only component subject to direct stress and normal steel. Although the bracket transmitted the force of impact its high-strength profile allowed the use of lighter material. The overall mass of this arrangement is approximately 83g and shifts the centre of mass by less than 1.1mm.

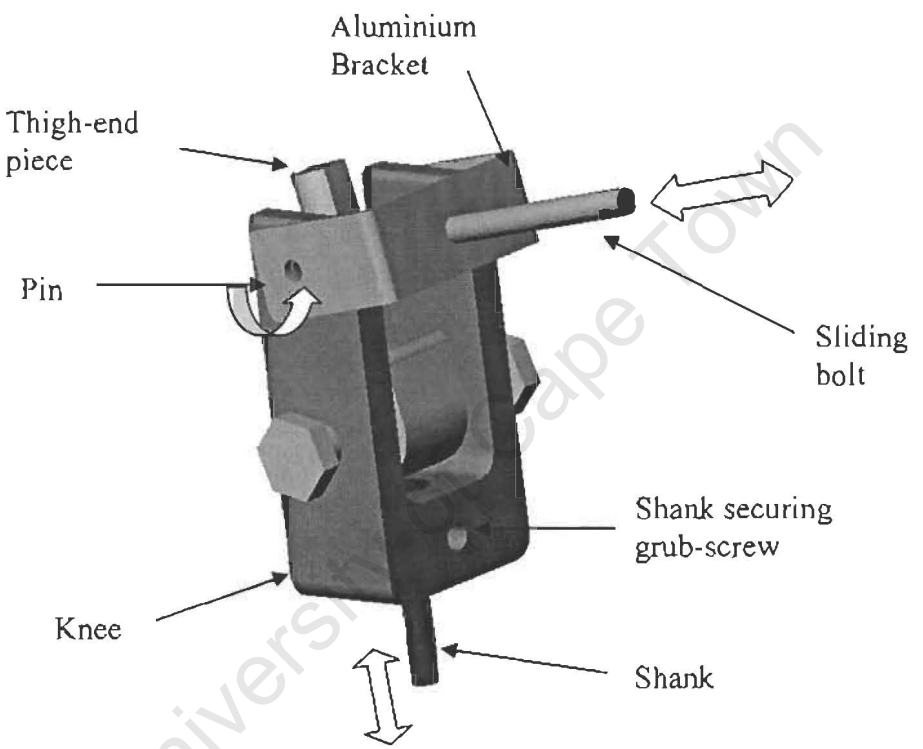

Figure 3.25 Knee joint assembly showing knee-stop and thigh-end piece

3.8 Ankle Joint

The ankle was required to be a rigid lightweight joint, allowing the simple adjustment of both angular and fore-aft position of the foot between trials. In accordance with the Garcia (1997) model of Figure 3.4, the foot edge where arc 'begins', and the shank centreline must be coincident. The evolution of possible ideas, which culminated in the implemented design, are illustrated in Figure 3.26.

Both the hinged-blocks and the triangular ankle are attached to a flat face machined onto the shank. The former utilises a slot along the foot face for fore-aft tuning and a hinge to adjust foot pitch. The latter has no such inbuilt adaptability and instead a new wedge for each angle must be machined. The next alternative retains the foot slot and replaces the hinge with a pin joint at the end of the shank. The stability and rigidity of this joint is favourable but rather expensive in terms of weight, approximately 124g.

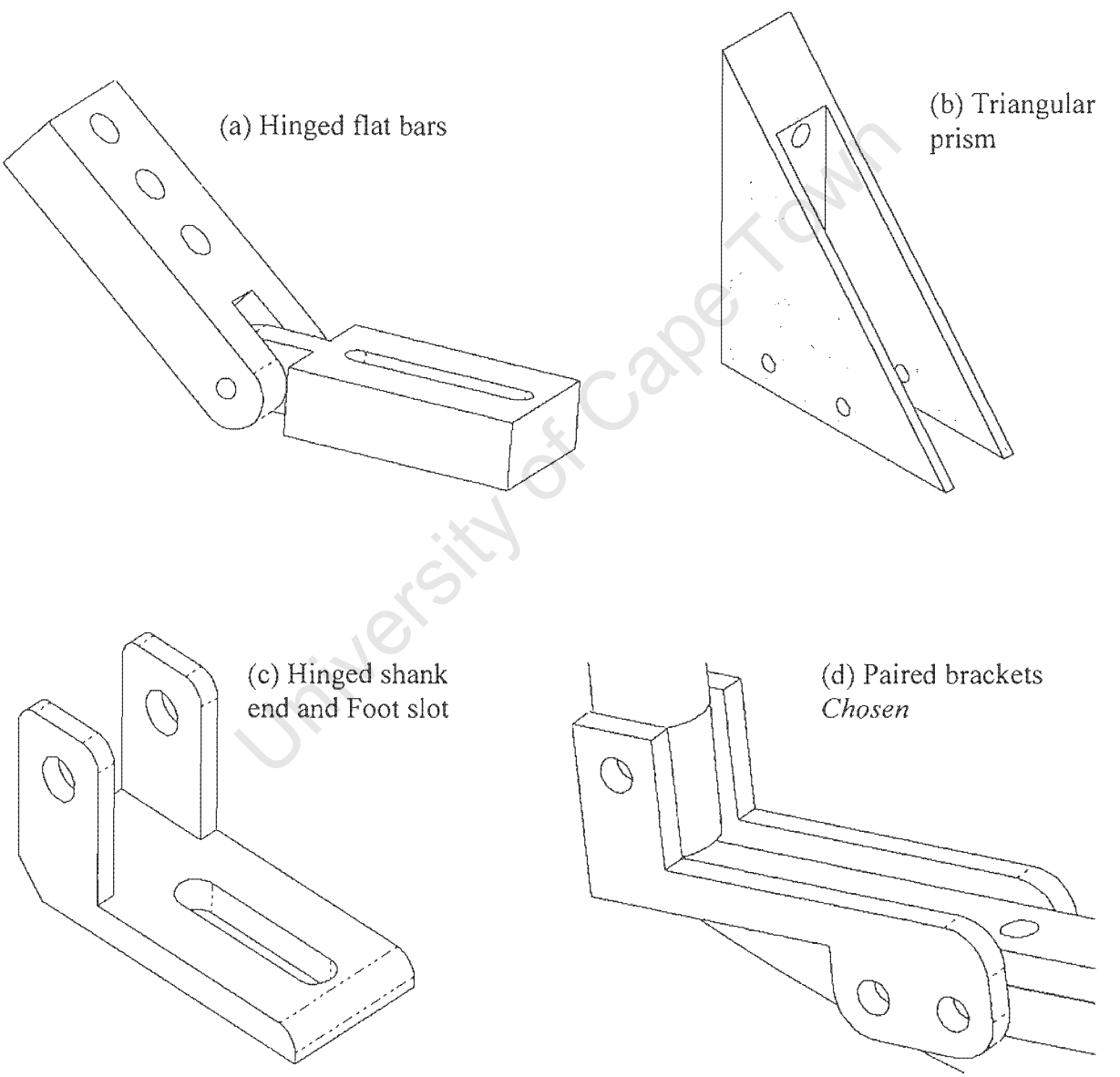

Figure 3.26 Evolution of the ankle joint concept (a), (b) and (c), with the final ankle design (d)

The final generation consisted of a pair of plates, sharing a common pin at the shank that, are fastened together by a pair of bolts passing through the already present foot slot, the total final weight of which was approximately 15g. To ensure rigidity is maintained during gait,

especially at heel strike, a flange is machined into the shank to fix the foot position and thus dispensing with the need to calculate the maximum joint torques and bolt strengths. The simple positional adjustment by release and tightening of the bolts, while remaining immobile during gait makes this lightweight design the preferred choice. The final dimensions are given in Figure 3.27 and Appendix D. Table 3.5 shows the final set of thigh and shank parameters of the thigh to be tested.

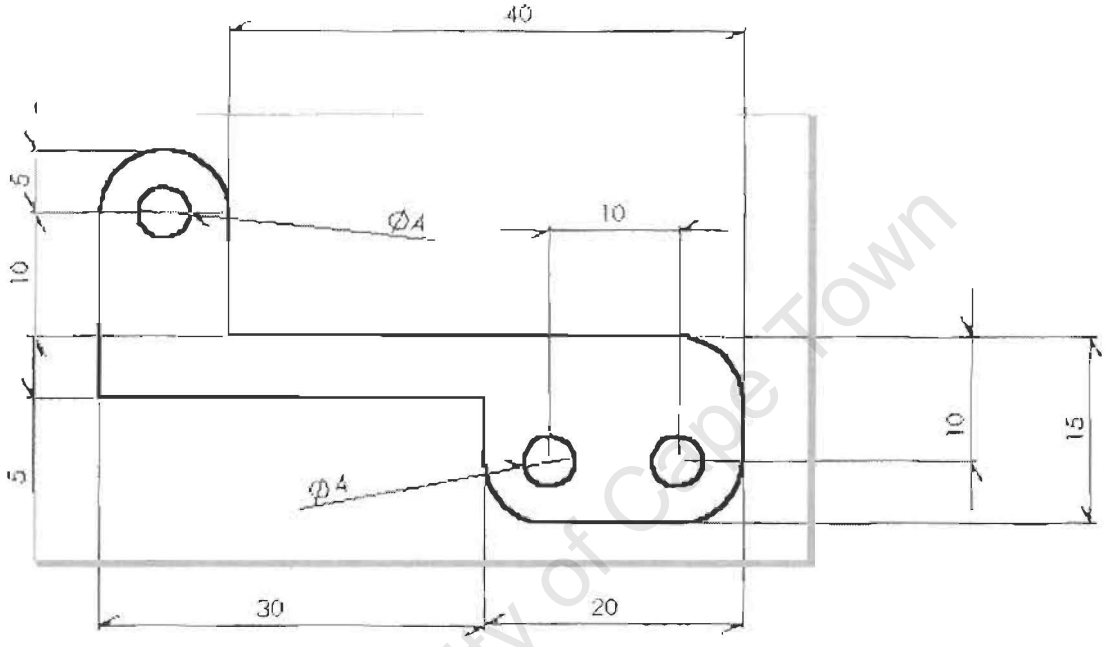

Figure 3.27 Dimensions of the ankle joint, Solid Works detail side view: two required per foot each of thickness of 3mm

Table 3.5 Final parameters for dynamically equivalent inner and outer thighs

Parameter	Thigh	Shank
Mass (kg)	5.1135	5.0946
COM position (mm)	103	101
Moment of Inertia (kgm^2)	77.351×10^{-3}	78.59×10^{-3}

Chapter 4

Performance of the Walker

On completion of the design, manufacture and assembly, the constructed walker's ability to exhibit an anthropometric, dynamically stable gait, independent of actuation, was investigated. The following trials assess the degree of stability and efficiency available within a purely passive system and evaluate the role of various defining parameters.

Practically this translates into ensuring zero foot scuffing while having no external assistance or power input other than gravity, and producing end-of-step conditions that are within range of the next step's initial conditions such that subsequent strides ensue in a repeatable and self sustaining fashion. In addition, the resulting gait reflects the effectiveness of the mechanical design at fulfilling the parameters of Garcia *et al.* (1997) and allowing limited variation of their quantities while ensuring the desired pendulum motion is preserved.

4.1 Method of Analysis

A 4 metre long stairway ramp and a large table provided the rigid walking surface. Fixing one end and elevating the other at different heights produced a working range of slopes, θ. Although of slightly different surface finishes, varnished and bare respectively, the rolling friction displayed by a uniform cylinder rolling unassisted down their lengths was virtually identical for testing purposes.

The primary testing phase aimed to establish a stable gait and involved evaluating the effect, both positive and negative, of key factors such as COM position on the stride. Based on mathematical reasoning and intuition borne from trial and error, as well as the previous research of most notably Garcia *et al.* (1997) and McGeer (1990, 2000), a number of relevant relationships between walker performance and parameter variation were achieved. Subsequent correction of the appropriate parameter (e.g. hip mass) was tailored according to the walker's shortcomings to better achieve the desired gait.

Before implementing any modifications, the design was tested virtually in Solid Works to confirm the geometry and COM positions, while the MATLAB simulation was employed as an indication of stability. Although rewarding, these procedures proved somewhat time consuming when quantifying the physical parameters (specifically I_{zz}) in Solid Works before making assumptions or design adjustments.

4.1.1 Descriptive Criteria

The criteria used to describe each stride are divided into the biped's temporo-spatial (i.e. step length) attributes and the external support imparted. The latter refers to the manual assistance provided as necessary, if at all, to the biped in order to bring about a complete stride. Support was applied at the hip joint either with a hand at each end of the main shaft or, for a finer touch, with a finger placed between the inner legs. Judged according to the demonstrator's touch, this force was inherently qualitative in nature. The level of manual support afforded was described according to whether its action was to retard or initiate motion as well as its direction and extent.

The point at which foot scuffing and knee strike occurred as well as the stride length were derived by sighting foot position (or other markers) along equally spaced lines drawn on the ramp surface perpendicular to the direction of travel. Yaw and heading were similarly judged by virtue of lines drawn parallel to the direction of motion. This method also enabled more accurate judgment of the extent of synchronisation between the outer shanks.

Foot clearance, however, proved difficult for a single person to judge due to the angle of viewing perspective. Though a second observer would improve matters his judgment, based relative to the stance leg or an incremented background (i.e. a ruler or lined board) would be subject to parallax error. However as we were primarily concerned with producing a sustainable swing-through, it was sufficient to aim for zero foot scuffing rather than to maximise clearance, which was of lesser importance at this stage.

An innovative method allowed the semi-quantitative measurement of a few additional spatial quantities. The point of foot contact at heel strike was evaluated by marking the under surface of each foot with equally spaced highlighter or heavy pencil lines depending on the surface. After heel-strike only the lines in contact with the ground are erased, while those on the untouched portion remain intact. Using the ratio between these areas an indication of the point of contact on the foot was evaluated.

This value, although not directly critical to performance, signalled whether heel-strike occurred at equal points for each pair of legs as well as judging the effect of parameter changes on the swing-through and knee-bounce portions of the stride. The above criteria thus allowed the evaluation of parameter influence on gait as well as identifying critical problems raised within each set-up, which were subsequently prioritised and dealt with accordingly.

4.2 Initial Results

Establishing testing protocol, the first step of every trial saw the outer legs act as the stance leg and the inner as the swing legs. Each trial began by discerning the corresponding inter-thigh angle, swing foot, hip velocity and slope for maximum knee flexion and foot clearance.

4.2.1 Foot Scuffing

Beginning with the original parameter set as given in Chapter 3, the biped was launched at the top of the ramp with differing initial conditions. However, the ensuing stride was found to be grossly unstable. Gait stopped abruptly at mid-swing where foot interference of the inner legs halted forward motion followed quickly by buckling of the knees. The outer pair displayed a similar run of events but showed a lesser, but still disruptive, degree of foot scuffing. By holding the ends of the main shaft after launch and applying a substantial force, hip movement could be delayed long enough to allow the outer legs to swing through. Despite similar manual assistance over several slopes ($1^\circ < \theta < 8^\circ$) the inner knees failed to flex sufficiently to clear the ground at mid-swing. Our problem thus involved two

spheres: insufficient foot clearance, and discrepancy between dynamic performance of the inner and outer pairs.

Mismatched dynamic performance of the limbs owes itself to the non-symmetrical arrangement of the connecting links giving differing thigh parameters, specifically C_t, M_t and I_t. The shank sections were assumed identical in this respect, as the linkages between them were minimal in comparison to their overall weight.

According to the findings of McGeer (1990), foot scuffing may be thought of as the stance leg's hip "falling" forwards too fast, not allowing the swing leg enough time to swing through to "break" its fall. This inconsistency was attributed to an excessively large hip mass, which decreases the swing period of the inverted pendulum motion of the stance leg. Similarly Garcia *et al.* (1997), while fine-tuning their physical model, found foot clearance improved by adding a mass of 0.8 kg at C_t (91 mm) and 0.178 kg at 30 mm from the hip.

4.2.2 Reducing Outer Link Mass

Thus informed, our next step was to reduce the hip mass of each leg. As the simulation did not detect any foot scuffing with the original setup, the method of adjusting the hip mass was one of trial and error. The inner and outer link masses were reduced from 0.5 kg and 1 kg to final values of 0.1 kg and 0.4 kg in increments of 100 g by firstly drilling holes and then slots along their lengths. As this step was somewhat irreversible each condition was tested thoroughly with a minimum of ten launches using various slopes and initial conditions.

A degree of flexibility was incorporated into the change in hip mass by using the free threaded hole on the hip surface to attach small blocks of +/-50 g that could be added two at a time, allowing a 200 g window of hip mass variation. By reducing the outer link to a greater degree than the inner it was hoped the dynamic behavior would be more similar. At this stage, however, this was secondary to finding the correct hip mass for both legs, thus allowing ample and repeatable foot clearance.

In the second group of tests, having reduced the mass of the links, the biped's gait faired much better. Slightly flexing the swing leg at launch, the inner legs swung through unaided to the mid-point, whereon ground contact occurred at the middle of the foot. Again scuffing could be eliminated by manually delaying the hip, signifying that the hip mass of the outer stance leg was still far too heavy. The outer pair managed to swing through with significantly less hip support.

We thus ascertained that the inner hip, when acting as the stance hip, is of appropriate mass, but is not currently replicated in the outer pair. The root cause of this was the exclusive contribution of the main support bar to the outer leg mass. During concept formation this problem was highlighted but only with respect to the end of step velocities and inter-thigh angles. As the simulation showed stable gait for both inner and outer parameter sets, foot clearance was assumed guaranteed, although as shown in the test, this was not the case.

4.2.3 Main Shaft

Rectifying the mismatched distribution of the main shaft mass between the inner and outer legs would necessitate significant machining and restructuring of both the hip assembly and that of the individual legs. Rather than redesign the structural layout, the author opted to first reduce the scale of the discrepancy. The solid mild steel shaft of 20 mm diameter was replaced with a hollow aluminium pipe of diameter 19 mm and wall thickness of 3 mm, effectively reducing the mass from 1 kg to 220 g and lowering the thigh's centre of mass (C_t) by 12 mm, making the biped less top-heavy. The dissimilarity in materials of the rotating elements necessitated adding a layer of machine grease to the outer hip's pipe surface to reduce friction. This simple step also allowed reduction of the hip weight exactly at its centre of rotation, preserving the moment of inertia.

Improving on these issues, the third test set saw overall foot clearance fare better, but by no means independent of external support, albeit to a lesser extent. Despite the implemented

changes a stable, autonomous gait was not easily achieved as several new problems arose, including excessive knee bounce, inner knee friction and intermittent yaw.

The most notable by far was the presence of unrestrained recoil of the shank at knee-strike . The current spring-loaded bolt arrangement only partially absorbed the swing shank energy, causing the knee to bounce open again before heel-strike, adding a stronger spring and a longer sliding bolt to increase kinetic energy absorption was somewhat beneficial. Unfortunately the extra spring energy present had the negative effect of destabilizing the stance leg, which lead to inappropriate flexion during the stride that if unattended set off buckling.

On the other hand, adjusting the limit of knee extension between 170° and 190° had catastrophic and ineffective results respectively. With a slightly flexed knee, rebound became more pronounced as did buckling of the stance leg at knee and heel strike. Conversely slight over-extension afforded the stance leg better stability throughout the stride but unless provided with substantial aid, produced inadequate foot clearance.

A further observation was that shank swing was delayed by not only the size and position of the COM but also increased friction and jostling of the thigh-end within the knee joint. During stages of the trial, inner-swing was smooth with adequate foot clearance if provided with manual aid, whereas at other times swing was restricted to less than midway. Such inconsistency was attributed to amplified wall friction at the knee joint as a result of over tightening of the inner foot link. The resulting tension also led to misalignment of the shank and thigh centres that further impeded swing. These highlighted the need to measure and match the foot link length with inter-knee distance, as during assembly one would easily over tighten the locknuts.

Foot clearance of both leg pairs improved with the addition of detachable 80 g weights to the shank at the centre of knee rotation. The resulting swing had a higher velocity at inception, leading to greater knee flexion and thus minimizing scuffing. When placed at the centre of rotation of the shank it was assumed the weight does not add to the shank's

rotational inertia about this point but rather seems to cause the stance thigh to swing forward more aggressively and so allowed more pronounced flexion.

Geometrically foot obstruction, simply put, was the result of the stance leg not raising the shared hip adequately above the ground. Increasing the angle, ξ, between foot and shank amplified this distance. Adjusting the ankle angle from 77° to 90° produced both better swing and foot clearance using less manual support. However beyond this limit the reorientation of the force at heel strike led to slipping which retarded the release of the new swing leg. Conversely, a reduction in the ankle angle brought the force at heel strike toward the vertical retarding the horizontal motion of the biped less. Moreover, the stance leg began to pivot earlier, diminishing the available time for the swing leg to advance.

An increase in limb length had no major changes on the biped's gait but did increase the stride period as confirmed by the research of McGeer (1990), who states that the legs pendulum motion are in a similar manner affected by an increase in the moments of inertia. Furthermore, increasing the separation of the leg pairs eliminated yaw. However this came at the price of a longer, and therefore heavier main shaft that would disrupt the gait cycle further. In this light leg separation was sacrificed for minimal shaft length, while affording a token amount of hip separation to guarantee sufficient lateral stability and eliminate yaw.

4.2.4 Compass Gait

In passing the biped was also reduced to a straight-legged walker by removal of the knee joint and slotting the shank directly into the thigh end. Alternatively, when the knee mass is required a locating pin was passed through the knee joint behind the thigh (via the bracket support hole), with the stop-bolt set directly in front, locking the leg in full extension.

So arranged, the compass biped was tested with curved feet and point feet. As is expected when restrained to 2D both arrangements failed to negotiate foot clearance with the curved feet displaying a lesser degree of interference, owing to the smaller are of contact. The McGeer (1997) solutions of a checkered-board surface of varying elevations or active

ankles were not attempted, as the time required would have detracted from the main theme of this project.

The quantities of tests carried out when ascertaining the bipeds gait were numerous involving several repetitions for each variation in parameter at several slopes and initial conditions. For this reason individual tests are not listed, rather Table 1 gives a summary of the key findings and the main aspects of the observed performance and subsequent evolution of parameters made when optimizing gait. Each step was evaluated according to the biped's ability to complete a single stride, of which the main criteria constituted: foot clearance, the degree of external support, knee buckling and knee bounce.

Table 4.1: Summary of evolution of tuning biped parameters and consequent results.

Biped Parameter	Observed motion & External Support
Original	Knee-strike too early with respect to heel-strike; Inner pair does not pass mid point but outer pair swings through fine; Knee bounce causes swing leg to flex at heel-strike leading to immediate buckling on outer legs; Inner knee-strike slightly later hence effect of bounce less marked, though knee flexed on impact, no buckling; Hip moves forward before swing leg can break its fall. Requires large assistance at hip and knee.
ΔM_{hip} and C_t	Lessened hip mass reduces Ct (Mc); Inner legs flex well at toe-off but drag slightly further than midline, outer fine; Knee bounce if unattended causes immediate buckling of outer legs, 2nd inner-pair heel-strike occurs very close to stance leg, +/-20mm; Smaller Ct delays heel-strike, causing greater knee bounce and less anthropomorphic gait.

Δ Ankle Angle	Reducing angle allows stance leg to roll forward earlier; Reasoning suggests increase may stop hip "overtaking" knee, allows shank enough time to "break fall" of hip [Mc].
Δ Knee Extension	If too acute, (<77°,) buckling at double support occurs; If >90° allows forward hip movement but impedes inner swing leg (does not pass mid-point); Simulation shows outer knee to hyper extend, but knee bounce in physical model eliminates this, thus causing buckling.
Δ Limb Length	Thigh +/- 50m and/or Shank +/- 30mm – Of little consequence other than increasing the swing period of the inverted pendulum, as does increasing the moments of inertia [Mc];
Δ Initial Conditions	Outer stance leg separation of 20mm gives good swing if yaw limited Inner pair, 5cm allows swing through, but 3cm with hip support gives excellent swing, but not consistent.
Δ Knee Mass	Adding 200g mass 10mm below knee joint improves shank swing Knee bounce worsened as KE of shank increased
Δ Inner Foot Separation	Foot scuffing very apparent even with support; Difficult to set exactly equal to knee distance;
Δ Hip Friction	Lubrication vital for swing leg motion leg; Foot clearance better but still irregular, less aid needed; Knee bounce does not allow true heel strike to occur.

Δ Compass Gait	Although stable till mid-swing, foot clearance was not achieved even with support at the hip; Trials done with and without the knee joint's extra mass and with round and point feet, neither showed promise of avoiding scuffing.

The final optimised set-up still did not allow adequate foot clearance when unassisted as the swing leg seemed to have insufficient kinetic energy to ensure early knee flexion and thus foot clearance. However, with a slight manual delay of the hip, clearance was achieved. Of major concern however were the presence of excessive knee bounce and the mismatched performance of the leg pairs. It is from this point that we investigated the pertinent modifications to be added to the design.

4.3 Design Modifications

Despite minor adjustments made to the biped during fine-tuning two major areas of concern were dealt with separately as their design and implementation were additions to the biped design rather than variation of its parameters. Other than foot scuffing, which may be temporarily avoided by some manual guidance, the major challenges impeding gait are dissimilar dynamic performance of the outer and inner legs, and the presence of excessive knee bounce.

4.3.1 Knee Joint Stiffness

On either side of the knee joint, additional individually machined brass collars replaced the standard set of steel washers currently used. This arrangement effectively reduced sidewall friction as well as afforded accurate and simpler alignment of the thigh and shank centrelines. Counter-sunk bolts allowed for a flush finish aiding assembly and reducing the chance of interference between legs.

4.3.2 Knee Bounce

Having the most catastrophic effect on gait, causing immediate buckling on heel-strike, reducing knee bounce was an obvious priority. Several design approaches were taken when finding an appropriate solution.

McGeer (1990) proposed the use of naturally occurring torques within the gait cycle to lock the swing knee. However, considering the increased mass of our biped, the torques required would need a much larger slope to generate sufficient angular velocities. As tested on the tuned biped at slopes greater than $\lambda = 5^{o}$ stability is lost altogether, while lesser slopes do not generate adequate locking torques. Thus although advantageous, this strategy was rendered ineffective for our set-up.

Alternatively decreasing the time between the knee and heel strike, served to lessen the extent of rebound. This was implemented by finding the correct ratio of the thigh and shank COM via simulation and implemented by the use of sliding weights. Although plausible and physically realizable, this is not a true solution but rather a means of skirting the opportunity for buckling. Such an approach may lead to further complications at differing slopes or leg lengths as the required weights would need to be be re-designed and re-machined.

The chosen option was to redesign the knee-stop mechanism entirely to unconditionally guarantee the knee remained closed between knee and heel strike regardless of slope, limb angular velocity or limb length. The new knee-stop was not to hinder knee flexion at any stage of the cycle, see Figure 4.3. As far as possible the original COM was maintained and when unavoidable the deviation for both sets of leg pairs was made equal. As per previous design steps the new shank parameters were first simulated to confirm stability before implementation.

The mechanism employed to achieve these attributes was chosen for simplicity of both construction and adjustment of the time delay while preserving the passive theme of the bipedal system. Some of the concepts considered are described below:

a. *Damper and spring*: Modified to produce a first-order damped response by addition of a one-way variable damper to the original set up, as in Figure 4.1. On extension

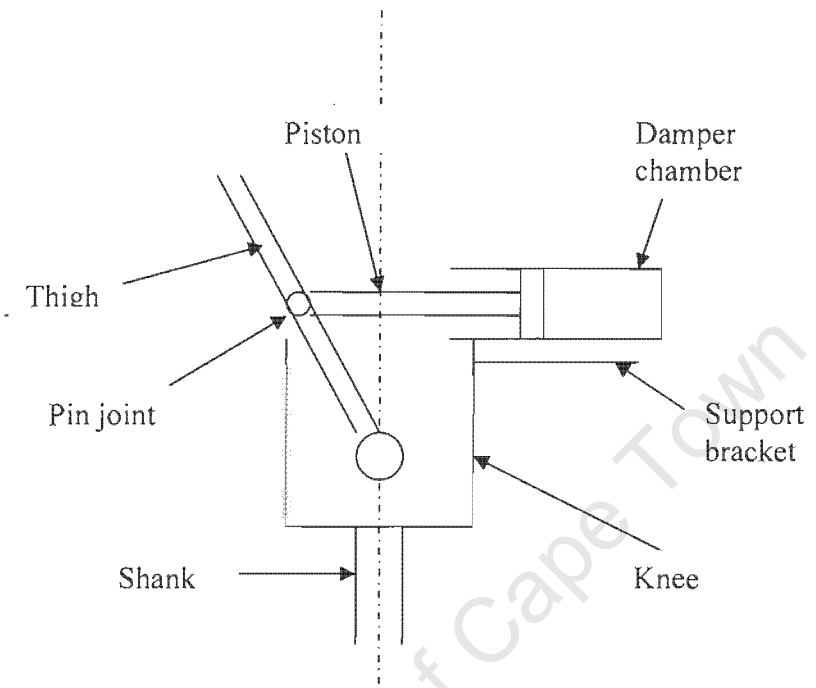

Figure 4.1 Schematic of knee-stop damper arrangement

the plunger, mounted on the thigh with a swivel, passes forwards freely, thus decreasing the volume of the chamber. During flexion the piston reverses direction, the returning fluid flow is impeded by a variable aperture. By adjusting these openings the return stroke, and thus knee flexion, may be retarded between knee and heel strike. However, during the stance-leg phase the damper is not reloaded and thus will resist flexion at toe-off with an equal amount of force. This as well as the added mass of the components negates the effectiveness of this concept.

b. *"Socket and Ratchet"*: Figure 4.2 shows a spring-loaded ball bearing housed within either the sidewall or lower face of the knee. The ball bearing protrudes from its housing and making rolling contact with the thigh-end. Knee motion is secured/halted when, at a specified angle, the bearing lines up with a dimple machined on the thigh-end surface. The spring's compressive force as well as dimple radius and depth is proportional to the locking and unlocking torque

provided and thus used to fine tune extension. Although the former may be adjusted between trials, it remains constant throughout the gait cycle, see Figure 4.3, thereby inhibiting the inherent unlocking torques responsible for flexion at toe-off. The advantages of its compact and simple nature are outweighed by this lack in functional requirements, as the distortion/interference of unlocking torques is too critical an aspect to overlook.

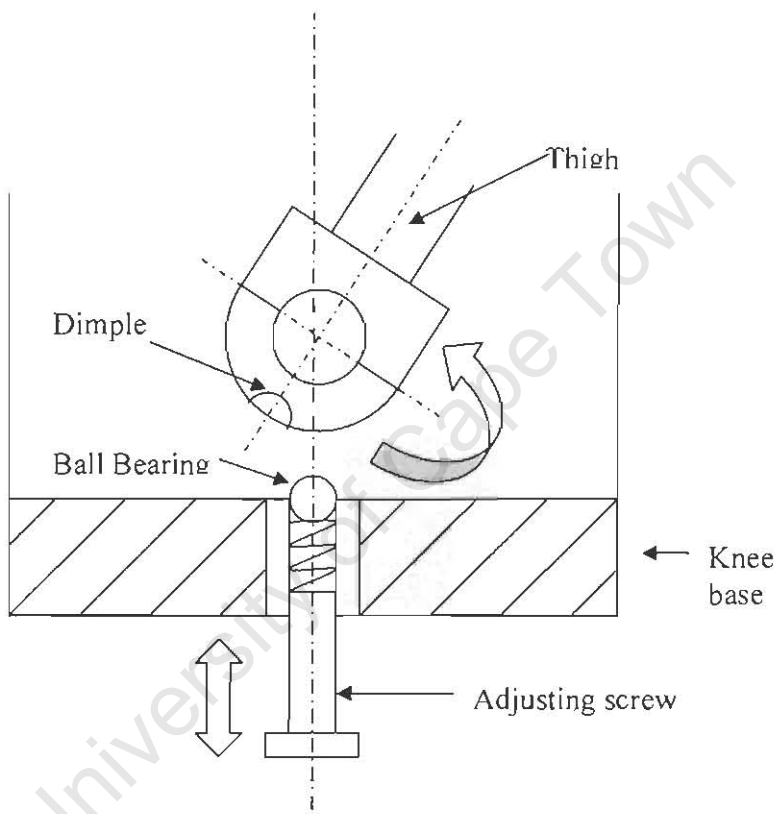

Figure 4.2 Socket and ratchet mechanism: Spring loaded ball bearing housed in base of knee, mates with dimple on thigh end.

c. *Timed Magnets*: A permanent magnet of sufficient strength would similarly require greater unlocking torques for flexion. However using an electromagnet whose activation is timed with an appropriate event in the gait cycle, for example the passing of the inner and outer knees, the magnetic attraction may be localized to the required period. The difficulty arises when implementing the electro-mechanical interface between event and magnetic activation. A possible form includes placing either an ultrasonic or infrared sensor on the side of each knee, which, on detecting

the passing of their neighbor will activate or disengage the magnetic field. A lower-end microcontroller may be incorporated to ensure the correct switching occurs, that is activation on swing forward and visa versa. Although a viable system the required volume to house the magnet, its power supply, sensors and control board as well as the additional complication of wiring and mounting is possibly avoidable with a simpler fully mechanical option. This choice is not altogether shunned but is by no means ideal.

d. *Eccentric Centres:* Although requiring extra machining, mechanically revising the knee joint to pivot about eccentric centers uses the thigh mass to maintain extension after knee-strike. Over extension is prevented by a slight overlap of the shank and thigh. This idea however was quickly rejected as the offset between thigh and shank centres is a deviation from the limb dynamics of those described by the McGeer (1997) mathematical model.

e. *Suction Cup Arrangement:* Thus far the vast majority of constructed bipeds such as McGeer (1997), Garcia *et al.* (1998) and Collins *et al.* (2001) utilize a suction cup mounted on the thigh facing the direction of travel while a flat plate extending from the knee makes contact with the cup at a specified knee angle. On impact of the two parts a vacuum is generated which maintains a straight leg until heel strike. An adjustable valve in the rear of the suction-cup allows the timed entry of air back into the cup. Using this adjustment the suction cup is set to release the plate before toe-off, hence limiting the suction-cup effect solely to the crucial period.

This mechanism is well liked, as it is self contained, independent of the bipedal mechanism ensuring an undisturbed natural motion as well as allowing simple adjustment of the time delay and the positioning of the suction-cup.

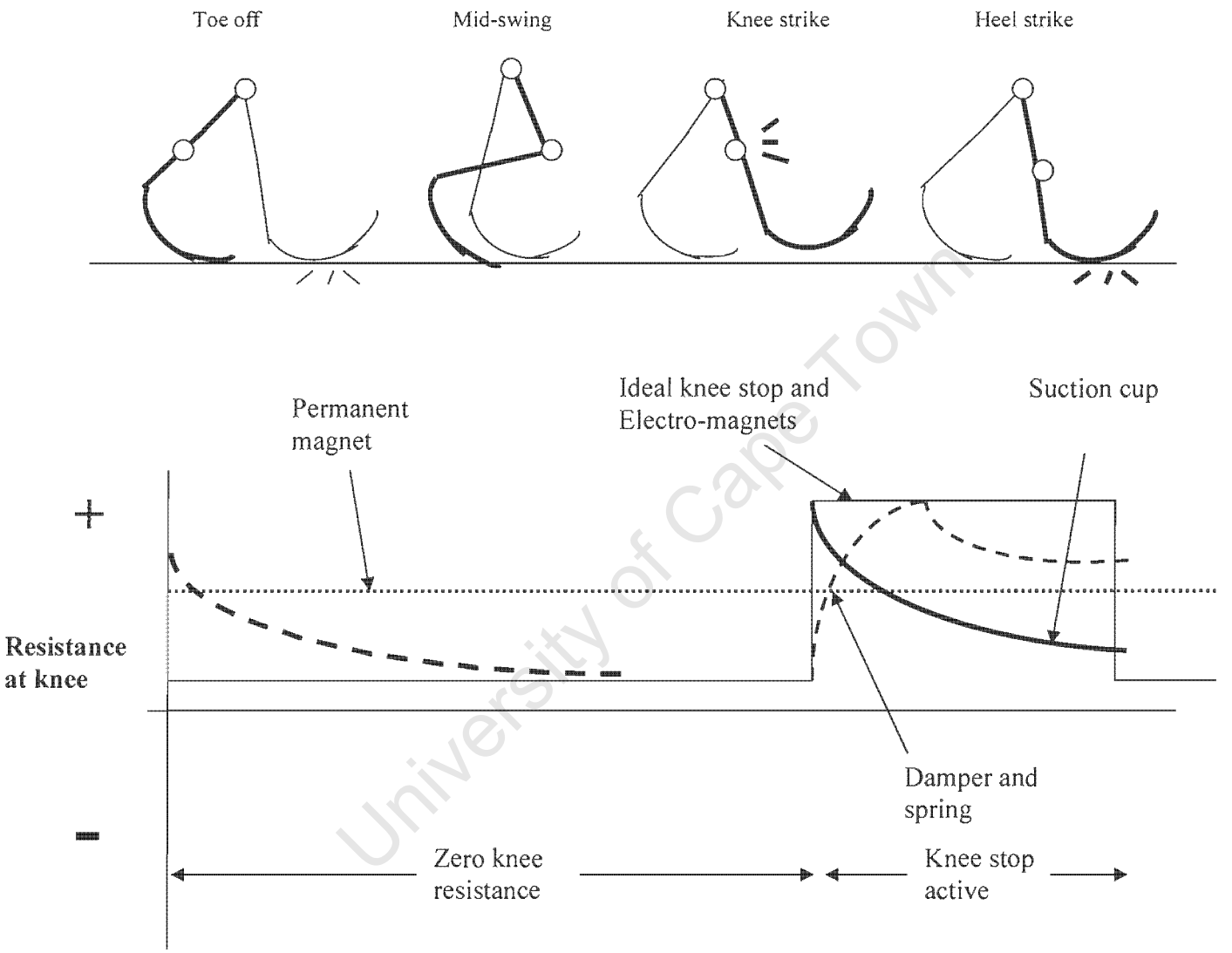

Figure 4.3 Required performance of knee arresting mechanism compared to performance of possible designs with respect to the critical events in a stride as per the animated gait given above.

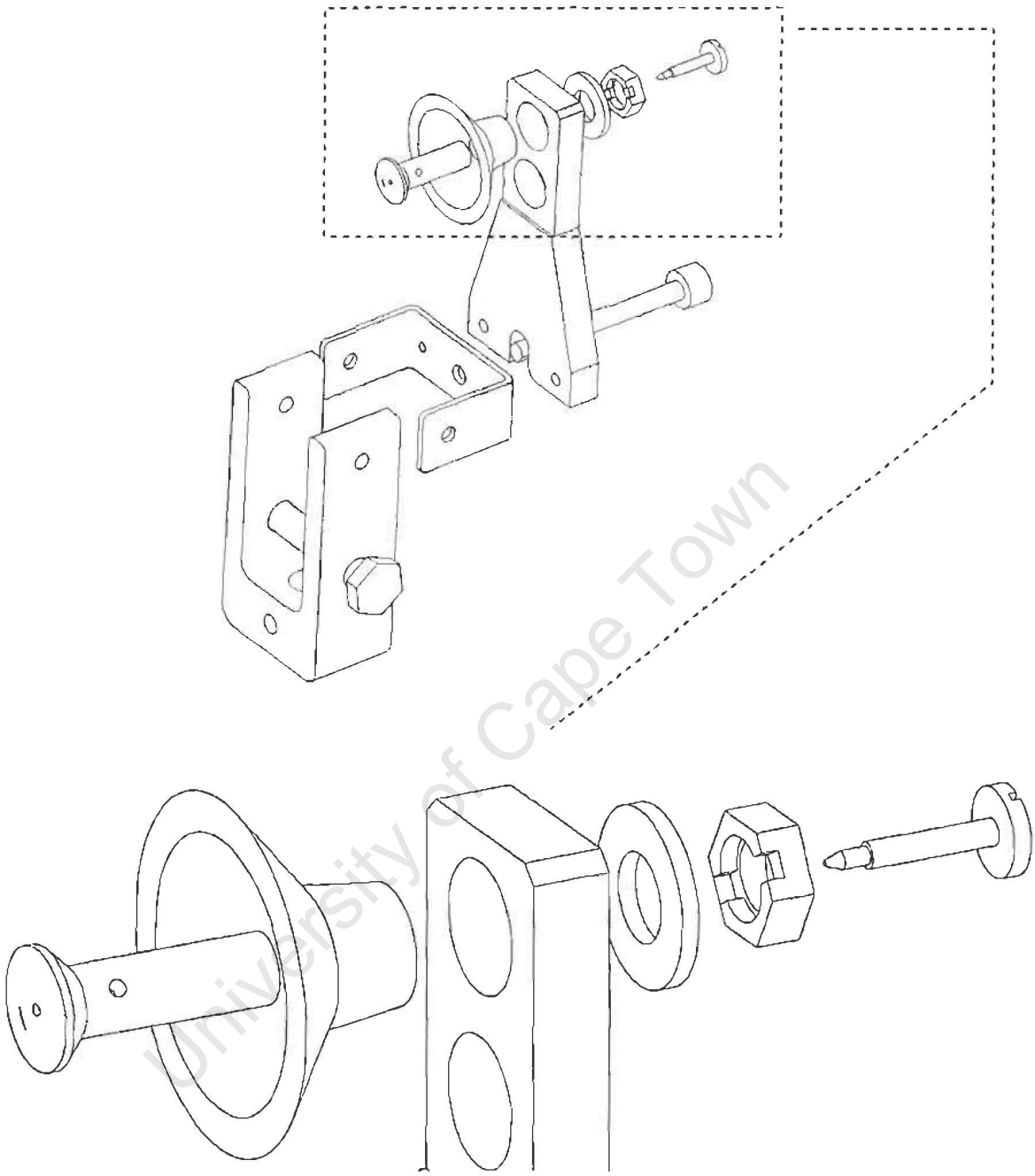

Figure 4.4 Implemented suction-cup and needle valve knee stop, (a) general layout; (b) exploded view showing detailed arrangement of parts

Our version of the McGeer suction cup method, shown in Figure 4.4 and Appendix D, shares the same timed-release principle but is modified in two main areas. Firstly, the mounting of the contact plate and the suction-cup assembly are on the thigh and shank respectively, with the latter attaching to the current knee-stop bracket via a pronged

aluminium plate. This permits both varying moment arms along with an offset for the contact plate. Secondly, air release is accomplished via a centre hole within the brass support bolt while a steel needle valve at the exit hole controls rate. The material selection utilizes the opposing ductility of brass and the hardness of the steel pin to permit accurate and fine adjustment of the aperture. Lastly, the securing locknut, an ordinary steel bolt, has a slot cut into the outer ring to allow communication with the outer air.

4.3.3 Dynamic Equivalence

The nature of the method of synchronisation of the 4-legged biped causes a discrepancy of parameters between the outer and inner pairs. As the outer link passes above the inner link and spans a greater distance, its effect on the outer thigh parameters is more pronounced. Fortunately this inconsistency is limited to the thigh section as firstly physical difference is restricted to the hip joint and secondly the shanks themselves are virtually identical and thus do not contribute to the problem. The key areas of concern are the overall mass, its position along the limb and the moments of inertia.

In order to produce identical pairs of legs an array of additional weights are added to the thigh-hip subassembly. The procedure outlined in Figure 4.5 is identical to that followed by Garcia (1997) barring certain practical considerations unique to this particular set-up.

Initially we take the inner and outer pairs as single rigid bodies of masses M_1, M_2 positioned at C_1, C_2 along their centrelines, with moments of inertia I_1, I_2 about their respective COM's. The aim is to equalise these parameters by addition of practically realisable weights. Notation is similar to Garcia (1997) where subscript denote the pair of legs and a "*" superscript denotes any dimension that is different in value from the original.

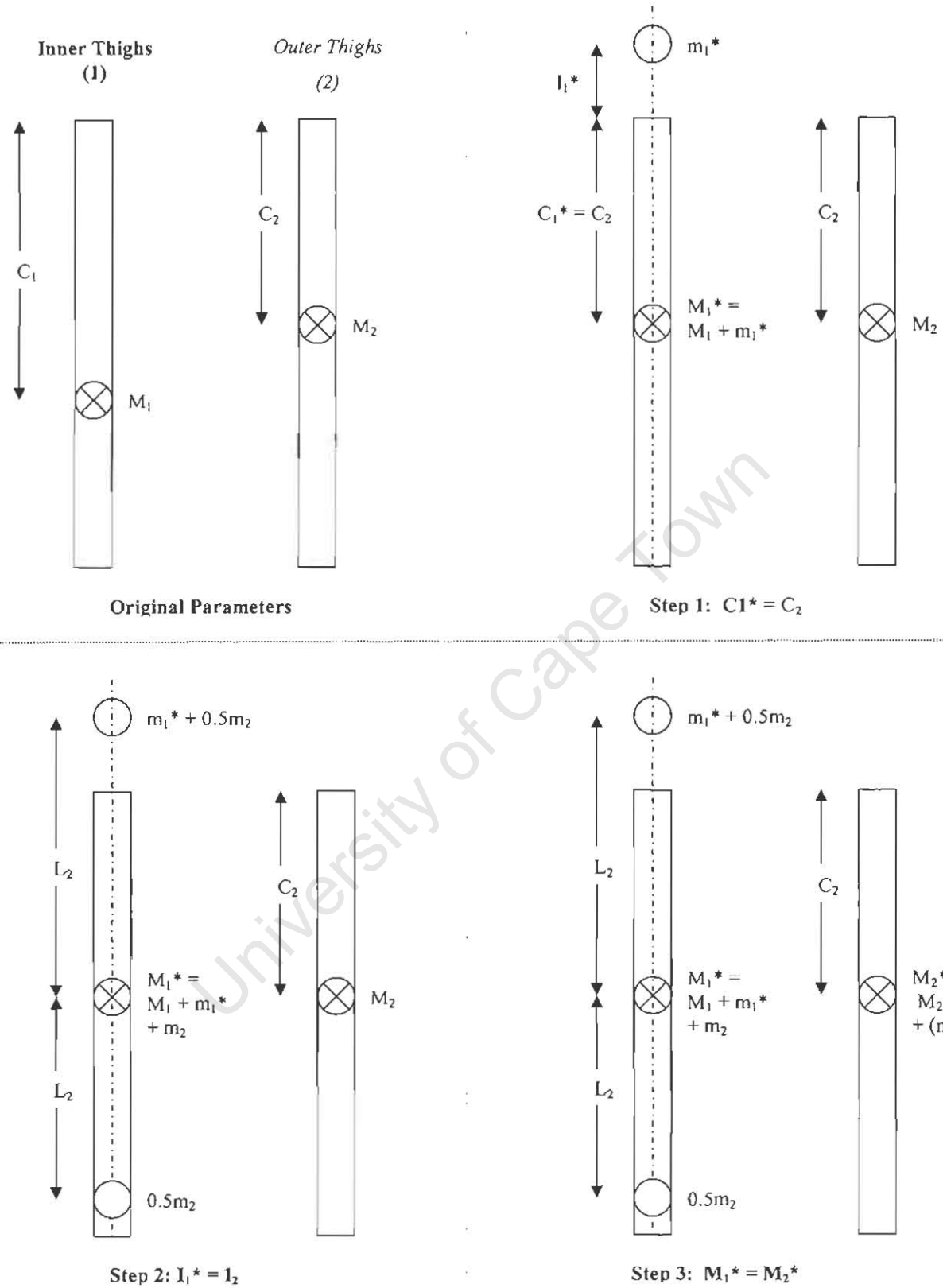

Figure 4.5 Steps to achieve dynamic equivalence. Subscript 1 and 2 refers to the inner and outer pairs of thighs respectively

Using a three step procedure, the overall masses M_1 and M_2 are equalised by addition of a smaller mass $m_1 = M_2 - M_1$ to the lighter limb which in our case is the inner pair, at a distance l_1 from its COM. Subsequently the new COM position of the inner pair C^*_1 will be:

$$C_1^* = \frac{M_1 C_1 + m_1 l_1}{M_1 + m_1} \qquad \textbf{4.1}$$

Knowing that $C^*_1 = C_2$ we may solve for l_1

$$l_1 = \frac{C_2(M_1 + m_1) - M_1 C_1}{m_1} \qquad \textbf{4.2}$$

Substituting for $m_1 = M_2 - M_1$ gives

$$l_1 = \frac{M_2 C_2 - M_1 C_1}{M_2 - M_1} \qquad \textbf{4.3}$$

On application to the original thigh parameters in Table 4.2 gives $m_1 = 400$ g and $l_1 = -45.5$ mm, the negative distance indicating the required position of m_1 is above the common axis of rotation. Practically this is extremely tricky to implement as it implies passing a connector through the outer link's locus of movement.

Table 4.2 Original non-dynamically equivalent thigh parameters

Parameter	Inner Thigh (1)	Outer Thigh (2)
Mass (M)	4.546 kg	4.946kg
COM position (C)	113.9 mm	101 mm
Moment of Inertia (I)	68.19 x 10^{-3} kgm^2	78.57 x 10^{-3} kgm^2

Alternatively a new mass m_1* may be used at a maximum permissible distance, which considering the clearance required, would be at the COM of the inner link, giving l_1= -25 mm. Recalculating m_1* by balancing of moments as per Figure 4.6, gives m_1*= 465.2 g.

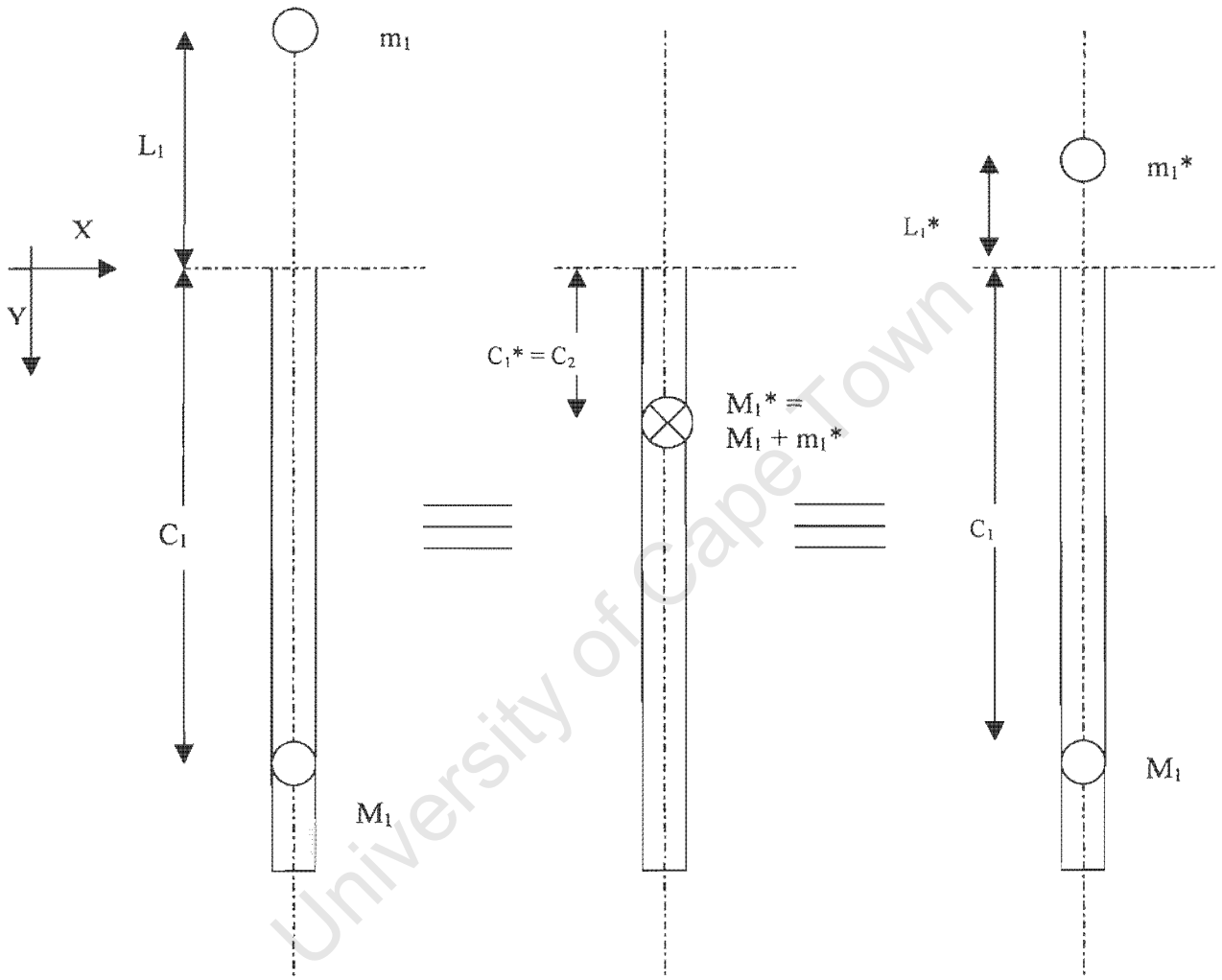

Figure 4.6 Design steps for the equivalent mass m1 if incorporated as the inner overhead link

The moment of inertia of the inner thighs now becomes I_1*, which may be derived directly from Solid Works or using the equation below:

$$I_1^* = I_1 + M_1\left(C_1 - C_1^*\right)^2 + M_1^*\left(C_1^* + L_1^*\right)^2 \qquad 4.4$$

The third step is to balance the moments of inertia by adding a mass m_2, at a distance L_2 from the COM. However in order to maintain the COM the mass is split symmetrically above and below the COM. The exact value of the mass is dependent on the maximum distance L_2:

$$m_2 = \frac{I_2 - I_1^*}{L_2^2} \qquad 4.5$$

In our case as $I_1^* < I_2$, the mass is added to the inner pair. At the maximum distance of $L_2 = L_1^* + C_1^* = 126$mm, which places the upper $0.5m_2$ weight with the inner link COM, gives $m_2 = 142$g.

The final step is to balance the overall weight by adding a collar at the COM of the outer thighs. The final masses of each pair are:

$$M_1^* = M_1 + m_1^* + m_2 \qquad 4.6$$

$$M_2^* = M_2 + m_2 + \left(m_1^* - m_1\right) \qquad 4.7$$

Table 4.3 shows the final set of thigh parameters of the set-up illustrated in Figure 4.7, with required additional weights to be added take the form:

1. A new inner link of mass and dimensions
    - Mass = $m_1^* + 0.5m_2 = 537$ g
    - Height = 9.5 mm
    - Length = 172 mm
    - Width = 42 mm

2. Two collars on each inner thigh at a distance of 224 mm from the axis of rotation
    - Mass = $0.25m_2 = 35.6$ g
    - Height = 6 mm

- Outer radius = 20 mm and inner radius = 12.5 mm

3. A set of collars on the outer thighs coincident with its original COM, 72.5 mm from the axis of rotation
    - Mass = $0.5(m_2 + m_1^* - m_1) = 104.2$g
    - Height = 17.5 mm
    - Outer radius = 20 mm
    - Inner radius = 12.5 mm

Table 4.3 Final parameters for dynamically equivalent inner and outer thighs.

Parameter	Inner Thigh (1*)	Outer Thigh (2*)	Difference
Mass (M*)	5.1135 kg	5.0946kg	18.9g
COM position (C*)	103 mm	101 mm	2mm
Moment of Inertia (I*)	77.351 x 10^{-3} kgm^2	78.59 x 10^{-3} kgm^2	1.24 x 10^{-3} kgm^2

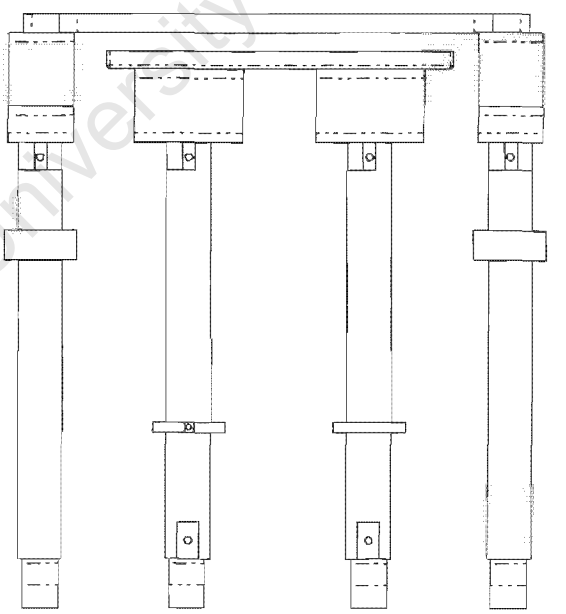

Figure 4.7 Final thigh arrangement showing additional collars and new inner link added to achieve dynamic equivalence between the inner and outer thighs

4.4 Subsequent Results and Improvements

Overall the outer legs displayed a significantly improved swing with the knees flexing earlier in the stride and adequate foot clearance was achieved with less support. A slope of $3^{\circ} < \theta < 5^{\circ}$ and an initial stride length of approximately 9 cm produced the best stride, but in a number of trials heading and yaw were compromised when heel-strike of the left outer foot preceded that of the right. Subsequent leaning encumbered inner-leg motion, as the main shaft is no longer perpendicular to the direction of travel.

This condition demanded either a U-shaped bar or a similar link between the outer feet. However, practically isolating such a link from other components and the ground, makes possible designs cumbersome and destroys the elegance of the system.

The swing of the inner pair was much enhanced overall, although still required slightly more external delay at the hip for the majority of trials. The end stride-length, 8-10cm, of the inner set lay within range of the outer pair at 9- 12cm, which were almost identical to the start condition of the opposing pair. These observations illustrated the virtually identical dynamic behavior of the new biped setup.

Knee bounce was also greatly improved with 70% of the trials having no trace of its effects. Some problems did occur, specifically a sudden loss of suction in mid stride or just before heel-strike. This was attributed to the reduced pliability of the plastic cup after several trials and in some cases drying of the oil/Vaseline layer on the contact surface. In addition, incomplete or misaligned initial contact between the perimeter of the cup and its plate jeopardized the suction.

Knee Lock - Unlike the "Constrained Compliant" model of Dankowicz *et al.* (2001), where knee lock was allowed to exist slightly after lift-off of the new swing leg, the suction cups in our physical model were timed to allow release well before toe-off. When not the case "toe-dragging" consistently occurred, as expected with rounded, protruding feet.

The moment arm of the suction cup was sufficient to exhaust enough air to produce a vacuum of the appropriate strength at large slopes but performed not as consistently at smaller slopes. In some cases to safeguard the needle valve mechanism, impact energy was limited as required by adjusting the length of the protruding steel bolt. The air release mechanism proved well suited to quick and accurate adjustment, individually tailored to each leg.

On the other hand the inner feet would lose alignment after approximately every 10 trials, arising for the most at the knee-shank connection. Although easily rectified between trials the possibility of occurring during gait demanded a more robust method of torsional security. In a similar manner the ankles also proved to be not entirely rigid. Although their angular and fore-aft position would hold for three to four trials, to ensure accuracy the locating screws were tightened after each trial.

In conclusion, the modified biped displayed a significant improvement in the areas of assisted foot clearance, elimination of knee bounce, dynamic equivalence and stability. However several shortcomings are still apparent:

- External support at the hip was still needed, although the degree was reduced to the extent of a single finger placed at mid-hip to delay motion just before swing through.
- Knee bounce was not always eliminated due to the incomplete exhausting of air from the suction cup which was possibly a result of the plate being perpendicular to the cup at impact. A slightly oblique angle of attack would allow the bottom of the suction cup to make contact earlier, leaving the upper portion free for the escape of air.
- Yaw and heading were still apparent in some trials but were regarded as symptoms of other problems.
- Lack of synchronization of the outer shanks was an unexpected occurrence that could not be attributed to unequal knee friction, limb lengths or ankle position.

Chapter 5
Simulation Results

As the physical model did not produce a stable and repeatable gait with sufficient autonomy, the variation of the Froude Number and dimensionless velocity over differing sizes was investigated by means of the Garcia *et al.* (1997) simulation of 2D kneed passive gait. Although this model does not describe the physical situation perfectly, this alternative has the advantage of allowing the constructed biped to be scaled over a greater range of otherwise difficult and cumbersome sizes using smaller increments and slopes.

5.1 Scaling the Biped and Determining Relative Parameters

According to the dynamic similarity hypothesis of Alexander (1976), the comparison of the gaits of different sized bipeds is only valid if they are geometrically similar. In our case we take the maximum hip height above the ground as the reference dimension that is multiplied accordingly.

Hip height is defined as the vertical component of the simulated biped's shank, L_s and thigh, L_t Limb lengths and foot radius R, as given in Figure 5.1 and calculated as follows.

$$\text{Hip height} = a + b = \left(L_t Cos\varepsilon_t\right) + \left(L_s Cos\varepsilon_f\right) + R\left(1 - Cos\varepsilon_f\right) \qquad 5.1$$

As all original angles are preserved, multiplying hip height by the scaling factor is equivalent to individually multiplying L_t, L_s and R by the same scale factor.

Determining the dimensional parameters associated with each size began by multiplying the original foot radius, shank and thigh lengths by the scale factor. The only further calculation was to find the equivalent limb length of the shank section, L_{limb}, for the stipulated shank length L_s, this follows similar geometric procedure as of section 3.2, specifically:

$$L_s - R = \left(L_{limb} Cos\varepsilon_k\right) - RCos(0.5\beta) \qquad 5.2$$

$$L_{limb} = \frac{L_s + R\left[Cos(0.5\beta) - 1\right]}{Cos\varepsilon_k} \qquad 5.3$$

Hip, knee and ankle joints preserved their original structure and size, as did the radius of the limbs. The feet and accompanying slot are scaled up and down accordingly, maintaining the foot's angular offset, ε_K, in all cases at 14°. Having geometrically scaled and assembled the biped, the new mass and inertia properties of the thigh and shank are derived using Solid Works.

If drawn on paper each profile of the walker at different sizes will display a linear progression of stature. Five separate sizes ranging from twice (*i.e.* scale factor of two) to half the current model are investigated. The descriptors available for simulation constitute the dimensional variables illustrated in Figure 5.1. Specifically these are; the shank and thigh moments of inertia, I_s, and I_t,, their COM position and mass, (i.e. Ct, Cs, Ws, Wt and M_s, M_t), and their lengths Ls and Lt.

As explained in Chapter 4, the structural layout of the hip joint and the accompanying links produce an inherent discrepancy between the inner and outer thigh mass parameters making them dynamically non-equivalent, (referred to as non-DE). The necessary additional masses needed to achieve dynamic equivalence are calculated for each new size in Excel using the equations from Chapter 4, and implemented in Solid Works. As a result, for a single scale factor three separate parameter sets are possible, namely those of the inner and outer legs as they appear without additional collars (i.e. non-DE) and that the biped with dynamically equivalent legs. The biped was thus scaled entirely and is as it would appear if constructed with longer or shorter limbs and accompanying feet.

5.2 Locating Stable Gaits

Having scaled the biped, the MATLAB simulation was used to firstly investigate the presence of stable gait and secondly determine the associated dimensionless velocity.

Each set of parameters, (i.e. dynamically equivalent, non-dynamically equivalent outer and inner thighs) were tested individually by running the simulation at a host of slopes. Beginning at an arbitrary maximum and minimum, the slope was incrementally converged toward each other eventually locating the limits of the stable range. If however no stable gait occurred within this

range of slopes, the most promising slope for each set-up was selected and thereafter the physical parameters of the biped are adjusted in a sequential fashion.

So as to avoid confusion during this process, each parameter was varied in isolation, its effect noted and returned to its original value before commencing with the next parameter. With experience and an appreciation of pendulum dynamics, as well as consulting the research of Garcia *et al.* (1997) and McGeer (1990, 2000) an understanding of the interplay between parameter choice and the gait produced was formed making the search for stable gait more efficient.

The most influential parameter as found by McGeer (1990) and Garcia *et al.* (1997) during their fine-tuning stages, and thus the first to be altered, was thigh COM distance from the hip, denoted as C_t.

5.3 Calculating the Dimensionless Velocity (β)

Beginning with the parameters of the constructed dynamically equivalent biped the simulation was run to confirm stability and determine the maximum and minimum slopes at which period one gait occurred. Along with two additional slopes, the change in the McGeer angles θ_{st}, θ_t and θ_s were plotted against dimensionless time. In this form stride length, stride period and hence dimensionless velocity were calculated in the following manner:

In Figure 5.1, stride length is the sum of the separation between the centre points of the leading and trailing feet at double support $2x$ and the foot curvature ψ through which the stance foot rolls. At double support, inter-foot distance x is calculated by multiplying the hip-to-foot-centre distance, (i.e. sum *a* and *b)*, by sine of angle θ_{st}.

- Stance leg separation = a + b = $2x = \left[\left(L_t Cos\varepsilon_t\right) + \left(\{L_s - R\} Cos\varepsilon_f\right)\right] Sin\theta_{st}$ 5.4

- Foot curvature = $\psi = 2\pi R\left(\frac{\theta_{st}}{180^o}\right)$ 5.5

- Stride period = $\Delta T = Time = t\sqrt{\frac{L_s + L_t}{g}}$ 5.6

- Stride Length = $L = 2x + \psi$ 5.7

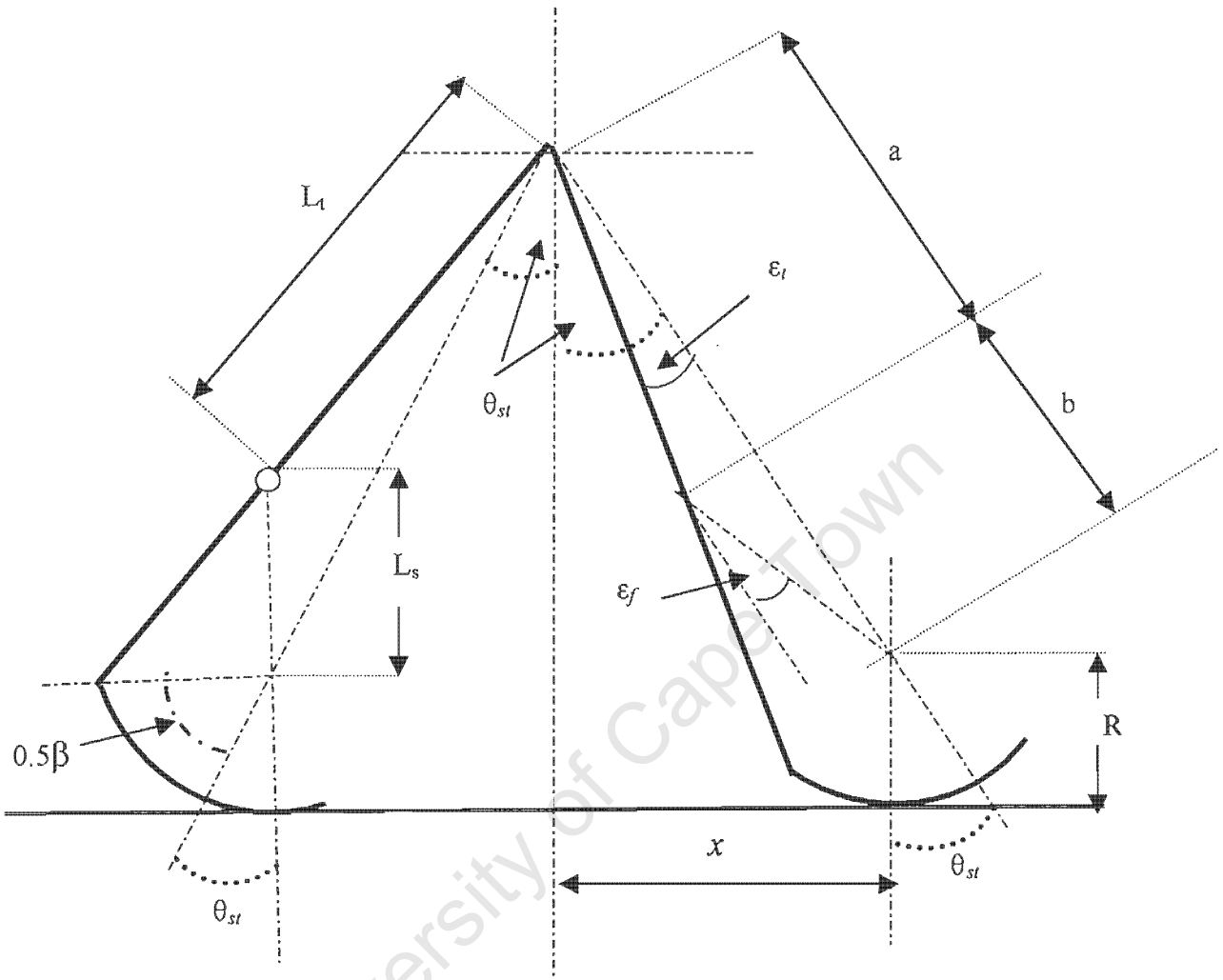

Figure 5.1: Schematic of leading leg at double support phase showing dimensions and angles used to calculate stride length; x- half stance leg distance; a + b = hip to foot centre distance separation.

Step velocity is given by overall stride length divided by stride period. The latter is measured physically from the printed graphs and using equation 5.6 the step period is converted from dimensionless time to seconds.

The Froude Number as explained in Chapter 2, is the ratio of stride velocity squared divided by the product of overall limb length and gravity.

- Step Velocity = $v = \frac{2x + \psi}{\Delta T}$ 5.8

- Froude Number = $Fr = \dfrac{V^2}{g(L_s + L_t)}$ 5.9

- Dimensionless velocity = $\beta = \sqrt{Fr} = \dfrac{V}{\sqrt{g(L_s + L_t)}}$ 5.10

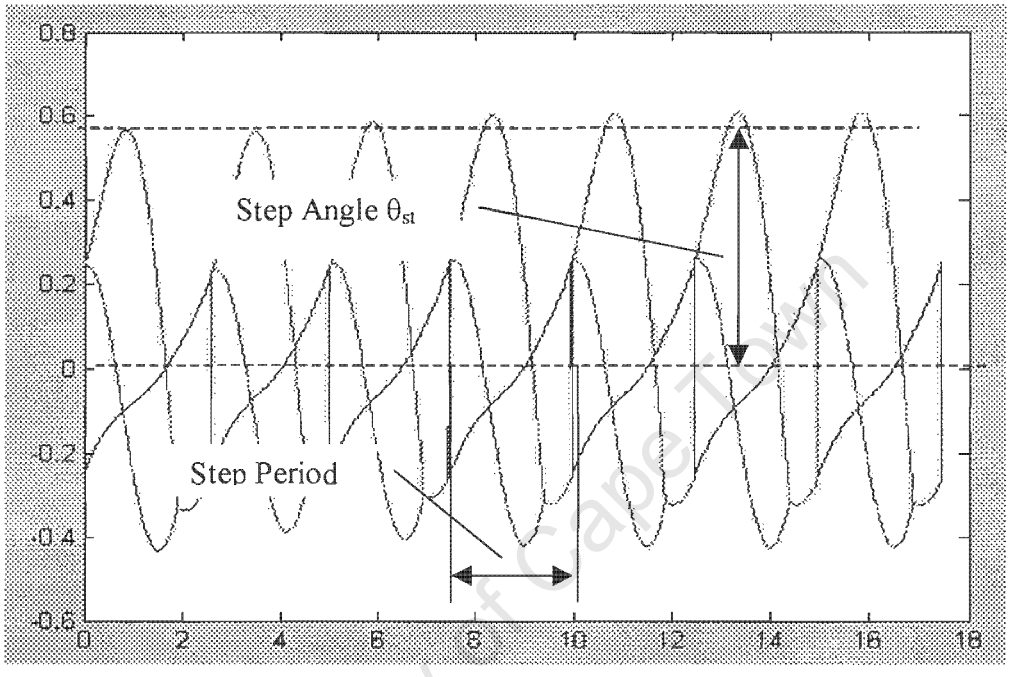

Figure 5.2: The Garcia simulated gait cycle showing McGeer angular displacement against dimensionless time, using the parameter set of the physical model (i.e. scale factor of one with the dynamically equivalent set of leg parameters).

Each set-up was tested for a minimum of fifteen complete steps to ensure a stable gait had been established and to determine the number of cyclic repetitions of the stride lengths (*i.e.* period 1, 2 or 3 gaits). As this project was concerned with understanding bipedal motion and more so anthropometrical gait, the definition of stability is restricted to period one gait where the end conditions are repeated after every step. In this light the step length and period was required to be identical between each step. Although several alternative stable gaits were discovered for each set-up, those displaying period two gait (*i.e.* limping) and above are noted but excluded from the results.

5.4 Results

The findings of the simulation are displayed graphically in Figure 5.3 and in tabular form in Table 5.1. Each point in Figure 5.3 represents the dimensionless velocity achieved during stable period one gait at scale factors ranging from 0.67 to 1.67. The slope at which each gait occurs is given alongside the respective data point, while the shape indicates whether the parameter set used was formed from either the inner or outer dynamically non-equivalent (*i.e.* non-DE) legs or the dynamically equivalent set (DE). In some cases deviation from these original values was necessary in order to produce a stable gait, the value of the specific adjustments are listed in the second column of Table 5.1.

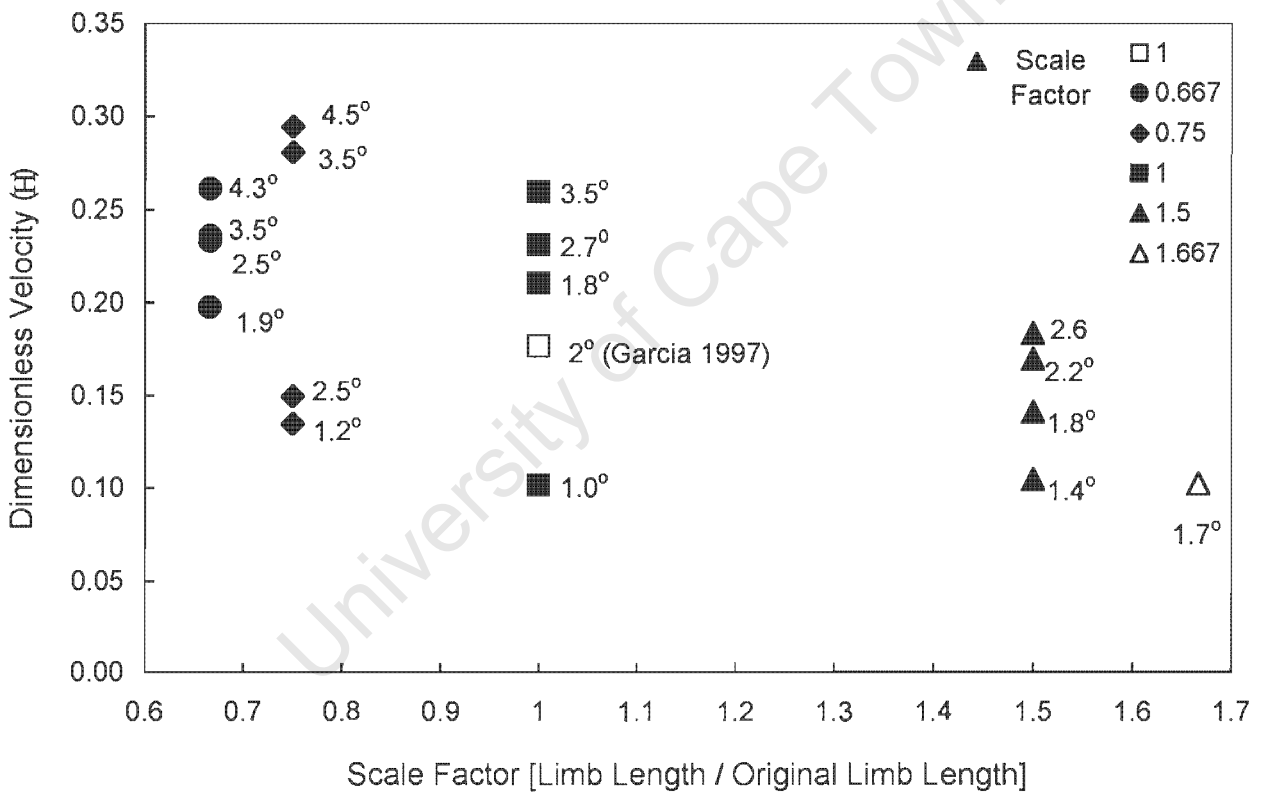

Figure 5.3: Dimensionless velocity β, of simulated scaled biped against scale factor. Each size has a maximum of 4 slopes at which gait was tested, point shape refers to parameter set used as follows;

▲ = Inner non-D. E; ◆= Outer non-D. E; ■= D.E set as with calculated additional weights

Table 5.1: Results from simulation showing; specific parameter set-up, either D.E or inner/outer non-D. E pairs; specific parameter changed; stride Length; stride velocity; slope; Froude number; Dimensionless velocity

Trial #	Description	Scale Factor	Slope	Froude Number	Dimensionless Velocity
		x	Degrees	Fr	β
	Garcia et al. (1997)	1	2	0.03	0.18
	Unstable	**0.5**	N/a	N/a	N/a
1	Outer Thighs Non-DE Ct = 26.7; Period 2	**0.667**	4.3	0.068	0.260
2			3.5	0.055	0.235
3			2.5	0.054	0.232
4			1.9	0.039	0.197
5	Outer Thighs Non-DE Ct = 55 Ct = 40 Period 2	**0.75**	4.5	0.086	0.293
6			3.5	0.078	0.280
7			2.5	0.022	0.149
8			1.2	0.018	0.134
9	Dynamically Equivalent Physical Model	**1**	3.5	0.067	0.259
10			2.7	0.053	0.230
11			1.8	0.044	0.210
12			1	0.010	0.101
13	Inner Thighs Non-DE Ct = 195.74	**1.5**	2.6	0.034	0.183
14			2.2	0.029	0.169
15			1.8	0.020	0.141
16			1.4	0.011	0.104
17	Inner Thighs Non-DE Ct = 220.2 Period 2 Period 2 Period 3	**1.667**	1.7	0.010	0.102
18			1.6	N/a	N/a
19			1.5	N/a	N/a
20			1.4	N/a	N/a
	Unstable	**2**	N/a	N/a	N/a

The first tentative steps at finding a stable gait at different, geometrically similar sizes began by defining the maximum and minimum limits. For our particular parameter combination these were found to occur at double and half the original size respectively. As Figure 5.4 shows at a scale factor of 0.5 the biped is stable for a single step with the satisfactory completion of knee and heel-strike followed by unstable support transfer. The gait pattern of the larger size limit, with a scale factor of 2, Figure 5.5, shows a greater degree of instability with knee-strike barely accomplished and heel-strike failing to occur altogether.

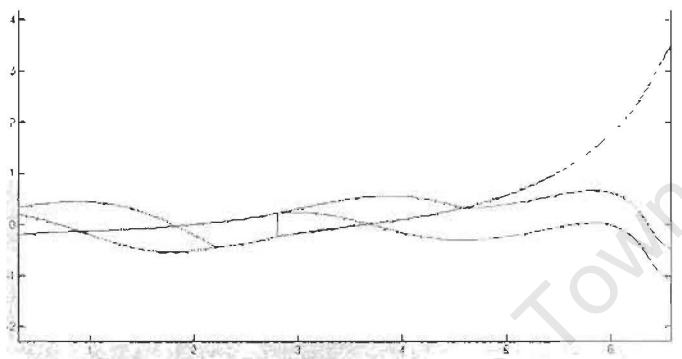

Figure 5.4 An example of the unstable gait produced when using the unmodified parameter set relating to half the original limb length.

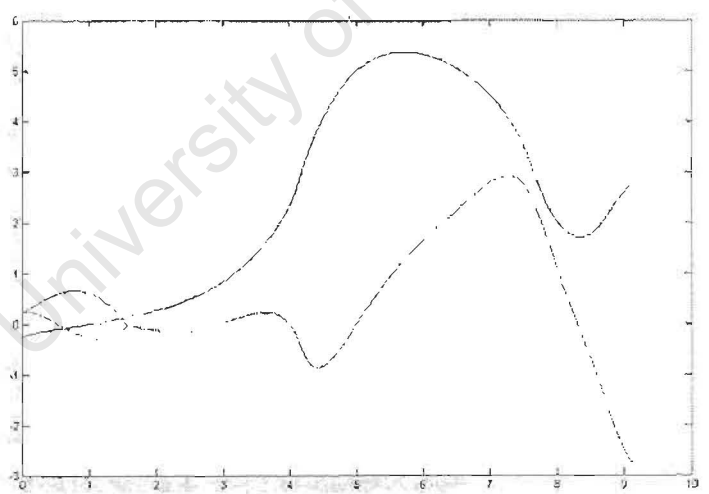

Figure 5.5 An example of the unstable gait produced when using the unmodified parameter set relating to twice the original limb length.

Having determined a set of upper and lower limits to biped size, (more may occur which we may not be aware of due to the limited domain of our trial-and-error search approach), the first set of

stable parameter sizes we simulated represented the constructed model. With a scale factor of one and using the DE set of parameters; the maximum and minimum slopes at which stable period one gait was possible are 3.5° and 1°, each with an assigned dimensionless velocity of 0.259 and 0.101 respectively. At two further slopes of 1.8° and 2.7° the accompanying velocities at which the biped travels are 0.21 and 0.23.

Increasing limb length to 1.5 times the original stable, gait appeared only with the inner non-DE set, without any need for modification. The slope limits decreased to 2.6° and 1.4° with velocities of 0.183 and 0.104, while the intermediate slopes of 2.2° and 1.8° the velocity follows a predictable linear increase to 0.169 and 0.141 respectively. In Figure 5.6 the DE parameter set when tested at a slope of 0.9° gave a typical exponential decay of the stride length, which despite several parameter changes could not be salvaged.

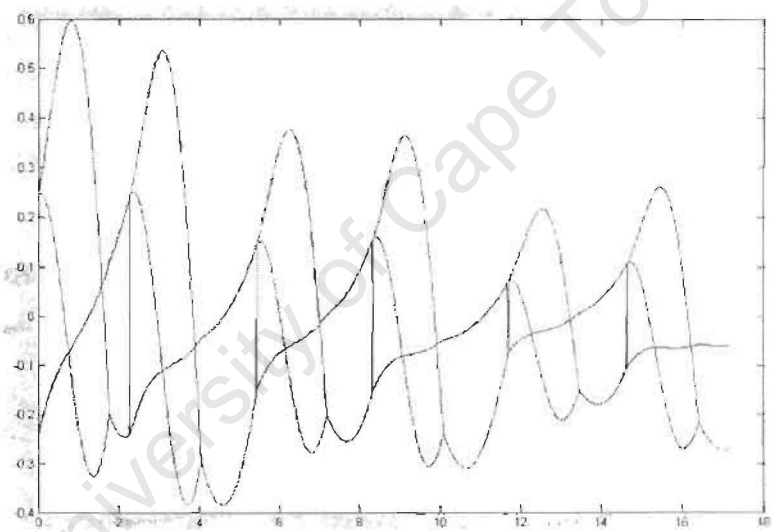

Figure 5.6: Typical exponential decay of stable gait marked by the decreasing inter-thigh angle θ_{it} .Here a scale factor of 1.5 is used with the inner legs non-D.E. parameter set at a slope of 2.5°

Distinctively at a maximum scale factor of 1.67, only a single stable slope was found at slope of 1.7° giving a minimal velocity of 0.102, using the inner non-DE set. The evolution to this stable gait is illustrated in Figure 5.7 where, after beginning with a promising first few steps the DE set ended in "over-stepping". Opting for the inner DE set stability was greatly improved, although the stride was distinctly period two which despite an increased slope did not improve. After several parameter variations, increasing Ct from 20 mm to 270.2 mm attained a period one gait.

A further two stable gaits at slopes of 3.5° and 4.1° were evident with the outer non-DE, although these and their preceding forms were markedly period two and three respectively, despite several combinations of parameter variations could not be reduced to period one and were thus excluded from the results.

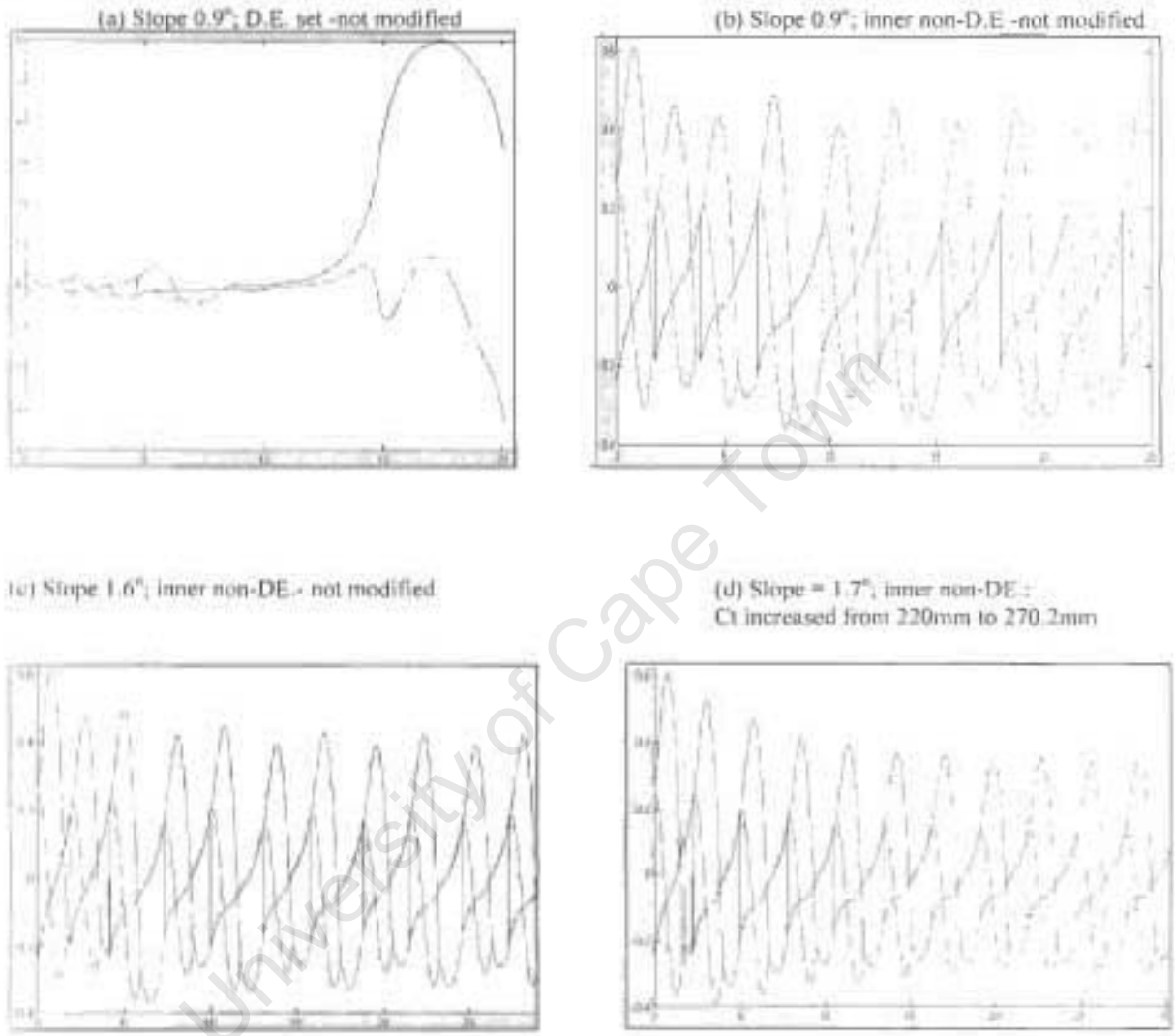

Figure 5.7: Evolution of a stable gait at a scale factor of 1.67; (a) The most promising slope produces three stable steps followed by "over-stepping" and instability, (b) a change in parameter gives a stable period two gait; (c) increasing slope improves this discrepancy somewhat d) Finally a stable period one gait is achieved by increasing Ct from 220mm to 270.2mm. [D.E refers to leg parameters of dynamically equivalent inner and outer legs]

At the other end of the scale, multiplying limb length by 0.75 did not produce a stable gait across the tested range of slope from 0.01° to 10° , with any of the three variations of parameter sets. Despite changing COM position of the thigh and shank, the inner non-DE set allowed only a single stride followed by multiple swinging of the shank. Similarly the DE set buckled immediately after

knee-strike. The outer thigh non-DE set, although initially also plagued by multiple swinging of the shank, proved more promising after decreasing I_s from 34.78 kgm^2 to 2534.78 kgm^2.

Further stability was achieved by reducing C_t from 76.7 mm to 40 mm, Figure 5.8(a) Care was taken with these variations as the second step was on the verge of buckling. Fortunately by increasing Ct to a final value of 55mm, Figure 5.8 b), although the first step is barely completed the flowing settle into a steady pattern of equal stride lengths after five to seven strides. Decreasing Ct too far to 26.7mm, Figure 5.8c), despite allowing more robust initial steps increased the period to two.

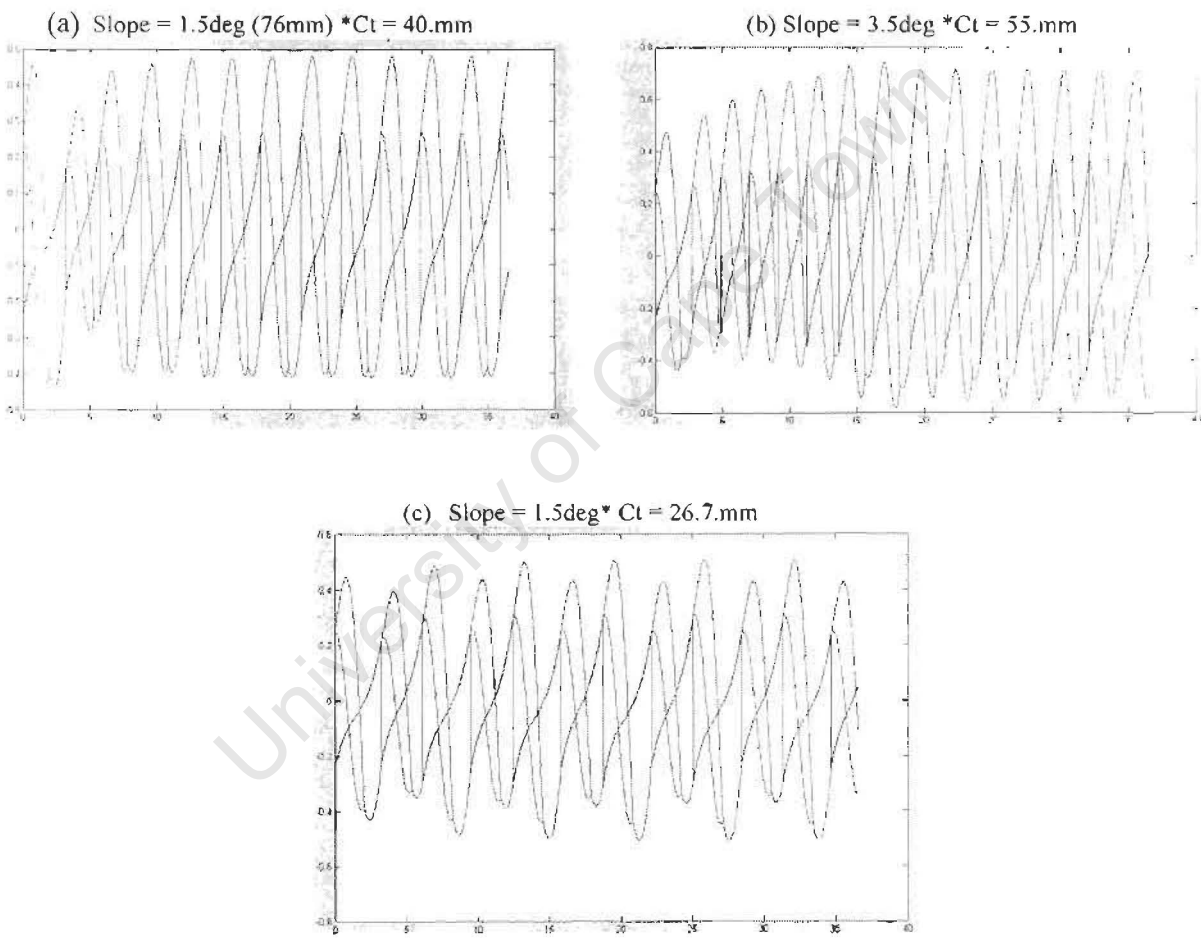

Figure 5.8: The effect of altering Ct on gait at a scale factor of 0.75 with the non-dynamically equivalent (referred to in the text as non-DE) parameter set of the inner legs.

When combined, as in Figure 5.3, a wide spectrum of velocities was eventually determined ranging from a maximum of 0.293 at a slope of 4.5° to a minimum of 0.134 at 1.2°. The intermediate slopes, although equally spaced at 2.5° and 3.5°, produced vastly different velocities of 0.149 and

0.280. Interestingly at a slope of 1.5° and with Ct = 26.7 mm the outer non-DE set produced an exceptionally stable period two gait, without the momentary unbalance in the first step as was the case in the period one cycle.

Further shrinking limb length by a factor of 0.667, instability was once again evident in all three groups with slopes from 0.1° to 10°, with the inner non-D.E set displaying two increasingly smaller steps ending in a final double support stance with both feet next to each other. Employing a change in C_t from 66.9 mm to a final value of 26.9 mm, stability for the outer non-DE set was achieved, although the first three steps displayed inconsistency beyond this the gait settled into a truly stable period two gait. However, for our purposes, the difference between stride periods of 0.1 is considered negligible and thus included in the results.

This final 0.67 combination produced a similar range of angles as the previous scale factor, 0.75, of between 1.9° and 4.3° with a modest accompanying increase in dimensionless velocity of 0.197 and 0.260. When tested at similar slopes as the previous set, 2.5° and 3.5°, β was almost identical at 0.235 and 0.232, opposite to the vast difference of the former. Once again an alternative gait, this time of period three was also present but again displaying a more robust initial phase occurring within the slope range at a slope of 4.1°.

(a) Slope= 3.5°; (66.9mm)*Ct = 26.9 mm

(b) *Slope = 4.1°; (66.9mm)*Ct = 26.9mm Period 1 Period 3

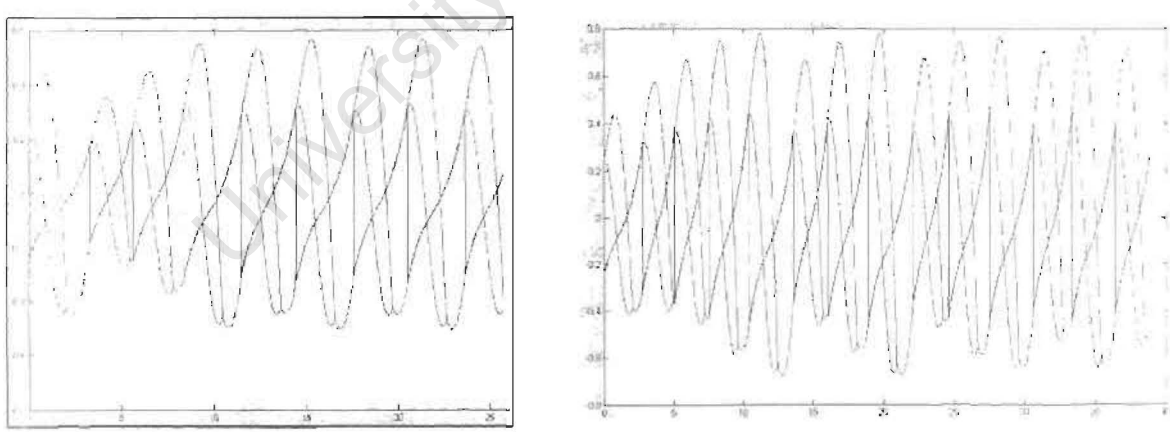

Figure 5.9: At a scale factor of 0.66, using the outer legs non-DE parameter set shows sensitivity to adjustment of Ct at slopes of 3.5° and 4.1°; (a) Period 2 gait with an unfavourable 2nd and 3rd steps; (b) Period 3 gait beginning with smaller stable steps and settling to larger steps.

It must be noted that the parameter changes undertaken were aimed solely at generating stability and not concerned with the ease or potential for construction. With some variations, particularly for

scale factors 0.667 and 0.75, although they originated from easily designable combinations, their final states were not necessarily physically realisable with the current model. For example, stability of the 0.667-parameter group required C_t to be reduced from 66.9 mm to 26.9 mm. This is equivalent to placing a mass of 3.5 kg at 2mm from the hip centre, which is physically challenging to incorporate without corrupting the other parameters such as the moment of inertia etc.

5.5 Parameter Change and Performance

As with the physical model, the corrective steps undertaken to establish a stable gait were based both on the author's intuition as well as the research of Garcia *et al.* (1997) and McGeer (1990, 2000). The most significant relationships exploited are outlined below.

For a given parameter set, if the first few steps of the simulation were stable but followed by exponential decay of stride length, decreasing C_t was the most beneficial parameter to change. In the majority of cases a 50% reduction of the original value was a viable starting point for iteration. On the other hand, decay of stride length could be rectified by use of steeper slopes. Conversely, gait stability was extremely sensitive to changes in C_s where either an increase or decrease led to "overstepping".

Another common aspect of instability occurred when the leading shank swing back and forth several times per stride. Reducing the shank moment of inertia, I_s by a small percentage limits the swing direction to forward only. It must be noted that although the animation displays a degree of multiple swings during defined stable gait, this is regarded as overextension of the knee rather than outright instability as at heel-strike the limb straightens.

During simulation more than one type of stable gait was observed. Several set-ups produced both period one and period two or three gaits. The transition from a stable period two gait to an equally stable period one gait is accomplished by increasing $C_{t,}$. The variation of this parameter must be treated with caution as the walkers 1st step tends to be extremely sensitive, leading to instability. Hence a balance must be struck between producing period one gait from period two with that of solving the stride length decay. However if the 1st step is even barely completed the ensuing strides converges to a stable repetitive gait at a greater velocity. If at the onset of a stride, before the first step has been completed, the walker tends to fall backwards or forwards the slope had to be increased or decreased respectively. If however no stable gait was found using this convergence of slope procedure, it was assumed no stable gait existed for the particular parameter set tested.

Chapter 6

Discussion

The following discussion comprises two elements of research on which this study is based. The first consists of the physical trials conducted with the constructed walker. Although unable to produce a sustainable, stable gait the evolutionary approach to the optimisation of parameters allowed for several insights into the behaviour of passive dynamic gait in two-dimensions. Also highlighted are possible reasons for the constructed walker's inability to produce a stable and repeatable gait as derived from observation in conjunction with the simulated model and the prior literature.

The second component discusses the investigation into varying size and the effect on gait. The effect of scaling the biped up and down on the dimensionless velocity has been investigated using the model of Garcia *et al.* (1998) and will be discussed in light of the parameter sets used and the slopes at which each gait occurs.

6.1 Physical Passive Walker

Although a truly independent stable passive gait was not achieved by our version of the McGeer 2D biped, the evolution of the biped's parameters and performance as described in Chapter 4, coupled with the relationships established beforehand by, amongst others, McGeer (1990), Dankowicz *et al.* (2001) and Garcia (1999) afforded the author some insights into the role of key parameters in producing a stable gait. The most notable challenges of foot scuffing, outer limb non-synchronisation, knee hyperextension and dynamic equivalence were overcome to varying degrees of success, with the status of the first two still currently unsatisfactory.

Foot Clearance

Throughout the initial results of section 4.2 as well as following the improvements to knee bounce and dynamic equivalence in section 4.3, foot scuffing remained the most pronounced obstacle to stable gait. In the current biped parameter set up inadequate foot clearance was seen as originating from two main areas.

First and foremost was the limited, retarded swing of the trailing leg. Despite implementing the rewarding parameter adjustments listed in Table 4.1 - namely a change in hip mass, initial launch conditions, inner foot separation and lessening hip friction - it remained a major setback characterised by delayed and deficient knee flexion of the biped's trailing leg. While the former measures had a direct bearing on the biped's centre of mass profile and ultimately the stride function, the latter adjustments role was to better mimic simulation conditions by minimising the real-life problems of joint friction and alignment.

The inadequacy in swing-through was improved by manually delaying hip motion at mid-swing. The equivalent parameter change that would accomplish this delay is attributed by McGeer (1990) and Garcia *et al.* (1998) to adjusting the distance of the thigh centre of mass from the hip, C_t .Although investigated, the exact extent of the required change was difficult to determine. The proportion in which these parameters acted in conjunction to decrease foot scuffing was not apparent.

The second sphere lay in the performance of the stance leg. The meagre time available for swing-through before the hip "falls" forward was a major impediment to the formation of a stable and independent gait as outlined in section 4.2. These discrepancies lead to the inadequate straightening of the swing leg. Despite the knee-lock mechanism, the gait could not be salvaged as it relied on natural torques to extend the leg. As pointed out in Chapters 4 and 5, McGeer (1990) attributes this to an inadequate lengthwise offset of the thigh centre of mass, C_t. This was been confirmed physically by addition of sliding weights along the thigh, thereby amplifying C_t and effectively extending the inverted pendulum length, and thus the period of the stance leg motion.

As the initial results of section 4.2 show, adding mass to the knee centre of rotation also reduced the degree of foot scuffing by improving knee flexion. This perceived earlier flexion is not ascribed to an increased affinity for the shank to delay forward progression. Rather it was seen as the tendency for the bottom-heavy thigh to swing forward more aggressively in accordance with compound pendular mechanics, ultimately producing a greater degree of flexion.

In addition, the extra mass at the knee improved swing by attributing a greater portion of the gravitational energy available to the lower limb. Poor swing-through was ascribed to

insufficient kinetic energy of the swing leg shank sub-assembly. Such additional shank weight was treated with care as the proportion of energy lost at knee strike increased tending to buckle the trailing legs and requiring an increased slope to prevent excessive energy expenditure. This observation complimented the findings of Garcia *et al.* (1998) where knee-strike energy loss dominated at small slopes (*i.e.* $\gamma \rightarrow 0$) in relation to hip associated dissipation of energy.

Ankle Angle

Geometrically, foot obstruction was also viewed as the result of either the knee not flexing sufficiently or the stance leg not raising the shared hip adequately above the ground. Increasing the angle ξ between foot and shank was found to amplify the latter distance as well as aid earlier and more pronounced knee flexion.

As mentioned previously in sections 4.2 and 4.4, it is thought that reducing the ankle angle brings the impact force at heel strike more vertical, reducing the tangential component and therefore allowing the hip COM to conserve a greater portion of its momentum and progress forward in a smoother fashion.

Conversely, the degree of jolting, (also referred to as impact or jerking), was beneficial when initiating flexion of the trailing leg. The induced knee flexion occurred earlier and was more pronounced, thus making adequate foot clearance more likely. This generally occurred at long step lengths and although it produced a rigid-looking, less anthropomorphic, gait this set-up depended the least on manual guidance and support. As always care was taken when exercising this option as, if the support transfer was not sufficiently robust (*i.e.* when the hip had insufficient momentum), this form of aggressive heel-strike lead to buckling of the trailing leg in some trials. This was attributed to the hip not having the required kinetic energy to pass over the front leg but just enough to take weight off the trailing leg, allowing it to unlock. At acute ankle angles this was not the case. The new swing leg failed to bend suitably as the tangential component of the produced heel-strike force was minimal, which brought about smoother foot contact leading to smaller step lengths, or as Garcia *et al.* (1998) termed it, a short-step gait.

From the stance leg's point of view, a "flexed" ankle meant the foot began to roll forward earlier. Consequently the period during which the trailing leg was to swing through was reduced significantly, leading to termination of the stride.

Knee Extension

The results of section 4.2 demonstrate the role of knee flexion on gait stability. As expected from observation of human walking with a fully extended stance-knee, a small degree of hyperextension affords the biped increased stability in the double support phase and the stance leg throughout the stride. However, in our passive biped, the initial lift-off of the swing foot was impeded by the additional extension through which the shank must pass (*i.e.* from $>180^{o}$ to $<180^{o}$), forcing protracted ground contact of the trailing leg. Moreover, the shank COM lay either in line with, or in front of, the thigh COM. This effect promoted knee extension until such time as the stance leg moved the hip up and forward sufficiently to reverse this condition. This further impinged on the time and energy available for swing-through as the hip had traversed a significant portion of its arc.

Conversely, slight flexion of the knee, similar to normal human gait where full extension does not occur as per Winter (1987), allowed earlier bending of the new swing leg and thus promoted foot clearance. However, as the stance leg was responsible for the forward and upward progression of the hip, it was countered by the tendency of the stance leg to buckle almost immediately after double support.

Limb Synchronisation

Once adjustments for dynamic similarity and excessive knee bounce were made (as described in 4.2 and 4.3 respectively), the subsequent tests showed the outer and inner pairs of the biped to have near identical kinematics, baring one aspect. A significant problem remained which was faced exclusively by the outer pair of legs; the unequal occurrence of heel strike, where the left-foot contact preceded that of the right. Hence, despite adequate foot clearance when supported at the hip, subsequent jostling and leaning of the hip led to reduced inner foot lift-off, and thus jeopardised stability.

As the thighs were coupled sufficiently rigidly by the outer link, which in turn coupled the entire leg via the suction-cup mechanism after knee strike, the discrepancy thus occurred during the three-link portion of the cycle, from toe-off to knee-strike. The difficulty was thus

attributed to the asymmetrical dynamic behaviour of the outer pair's shank section when free to swing forward independently. Possible reasons for this lay in the discrepancy between the shank subassembly geometry (*i.e.* overall length, ankle angular position) or centre of mass distribution (*e.g.* dissimilar component masses) or the link to the upper limb (*e.g.* unequal knee stiffness, shank misalignment, release of suction at knee).

Maintaining consistency of the biped within these areas depended on the manufacture and assembly of the biped subassemblies. Although minor differences no doubt occurred, they were considered negligible and preventable if adequate time and care were given to each process, in particular the setting of the ankle angular position and the release valve of the suction-cup mechanism was set before each trial. A guaranteed way to enforce synchronisation between the outer shanks is to incorporate a physical link at some point along their lengths. This however would be cumbersome and difficult to implement without interfering with the ground or the inner pair of legs.

Although these points are seemingly minor in their role of guiding the biped towards stable gait in comparison to prudent defects such as excessive knee-bounce and foot scuffing, the assembly procedure is vital in ensuring overall consistency within the array of parameters. Further relationships between parameter and performance, as observed from the initial operation of the biped, (section 4.2) and after the modifications of section 4.3, are listed below:

- Shank Mass Moment of Inertia I_s related directly to the shank's ability to swing through and had a useful and influential role in rectifying simulated gait when shank swing occurs more than once in a single stride.

- Limb Length - Confirming the findings of McGeer (1990), an increase in limb length increased the pendulum period and kinetic energy of the swing motion, thus requiring more potential energy in the form of a steeper slope.

- Yaw and Hip Separation - Increased separation of the hips decreased yaw and improved heading as the turning angle was decreased. This did not solve the root of the problem but reduces its effect.

6.2 Scale and Dimensionless Velocity β

It must be noted that the scaling undertaken in this study does not focus on the isolated variation of either limb length or mass independent of each other. Rather we deal with a unique set of parameters originating by scaling only the linear dimensions of the physical model, with the aim of conserving geometric similarity, which as explained by Alexander (1977) is mandatory when comparing for dynamic similarity.

Mass and mass moments of inertia of the newly sized biped were as they would appear in a manufactured model and were determined individually by modelling in Solid Works. For this reason our results were not expected to follow exactly the explicit trends put forward by, amongst others, Garcia *et al.* (1998), McGeer (1990), Dankowicz *et al.* (2001) and Witte *et al.* (2004). Rather they displayed a combination of each trend.

The array of dimensionless velocities produced for different sized bipeds at their maximum and minimum slopes is shown in Figure 5.3. For all but the largest, at 1.67 times larger than the original, four separate slopes were found at which a stable period one gait occurred for a minimum of 15 steps, after which it was assumed that a stable gait has been established.

The Sacrifice of Speed for Stability

Shown clearly in Figures 5.3 is the steady decrease of the maximum dimensionless velocity of with size. Starting from a maximum of 0.29, at a scale factor of 0.75, the dimensionless velocity decreases to a minimum of 0.08 at the largest size of 1.66 time the original. In Figure 6.1 the dimensionless velocity within each size subset increases linearly with slope. The larger sizes occupy the lower end of the scale, while smaller sizes are stable at steeper slopes and experience greater dimensionless velocities.

This trend was thought of as a sacrifice of maximal speed in return for stability. However, the sacrifice was too great at double and half the original sizes, and no stable gait is evident. Furthermore the largest sized biped, 1.66 times larger than the original, occurs at a slope of 1.7°, at the lowest dimensionless velocity 0.103 and a relative stride length of 0.3. This seemed counter intuitive as one expected longer, heavier pendular legs to swing faster with longer strides.

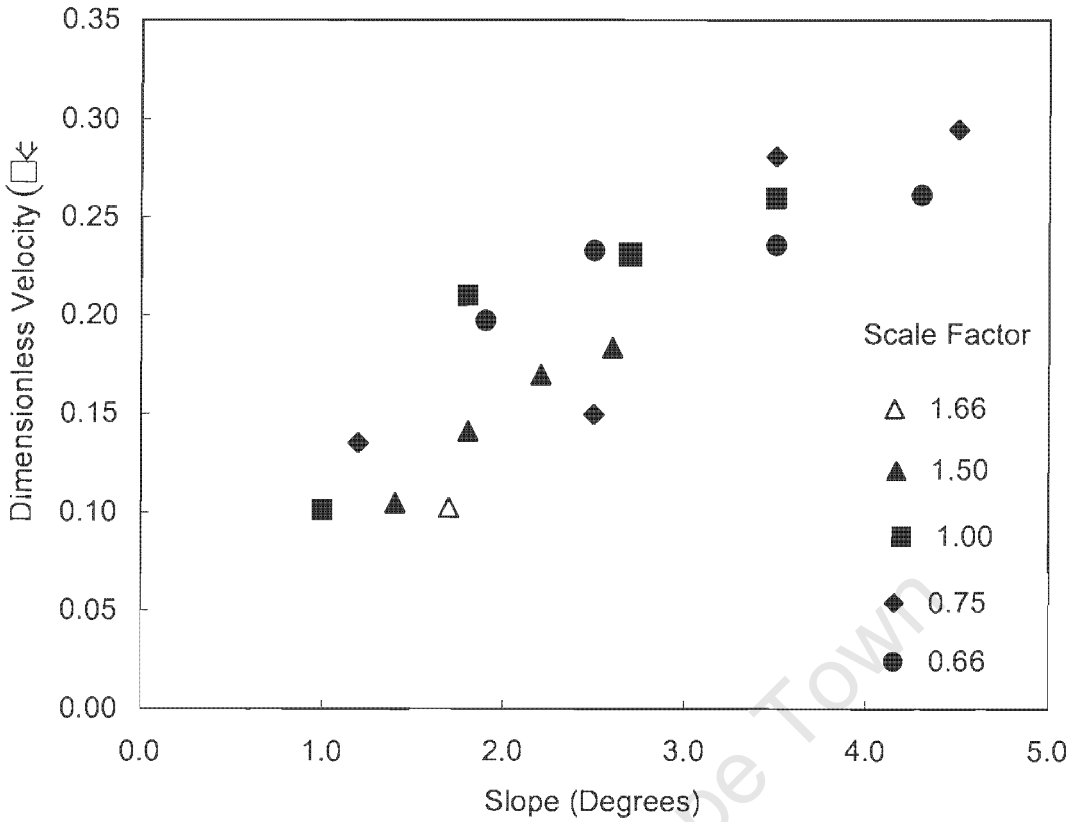

Figure 6.1 Reinterpretation of simulated results showing the variation of dimensionless velocity β with ground slope. Each point is labelled according to limb length relative to the physical model and referred to as the scale factor

This sacrifice of speed for stability was attributed to either to the trial and error technique relied on to find fixed points on the Poincarè map. Alternatively, stability was limited by an unfavourably excessive amount of knee and heel-strike energy losses. It is this latter point that we will be the focus of our attention.

Energy Loss at Knee Strike

As McGeer (1990) states, the scaling of limb mass was not to disrupt the inherent characteristics of a given gait, but rather served to modify the quantity of the collision forces involved. As mentioned in Chapter 2, baring joint friction and ground friction, the collisions at knee and heel-strike are primarily responsible for energy losses in the biped system and are thus pivotal in producing any stable gait. If these exceed the available energy, (*i.e.* potential energy gained with each stride and the kinetic energy from initial conditions), motion will cease.

For kneed walkers, McGeer (1990) and Garcia *et al.* (1998) mention that a prerequisite for stability was for the shank mass of a biped to be sufficiently small compared to the pelvic mass. In doing so knee strike expends a relatively small amount of energy compared to that at heel-strike. When sustainable, this energy may be recovered by the biped before the inception of the next step as it moves down the slope.

As knee-strike occurred first chronologically it expends a growing percentage of the available energy, till eventually the remainder was insufficient to maintain the overall momentum after heel-strike. In an effort to minimise this effect the maximum velocity of the heavier bipeds was forced to decrease as collision losses during each step were proportional to the colliding foot speed squared (Garcia *et al.* 1998).

In our case, although the proportion of energy losses at knee and heel-strike are maintained, a growing shank and thigh mass meant the quantity of the collision losses were amplified while the available reservoir of potential energy, determined by ground slope and stride length, decreases significantly with increasing size.

Size, Slope and Stride Length

The question thus arises: why not subsidize the larger knee-strike losses by simply increasing the available potential energy with an increased slope?

Intuitively, amplifying the mass and limb length of a stable bipedal system would demand greater energy in the form of steeper slopes and in turn lead to higher speeds. From Figure 5.3 we see that this was not so in our case. Stable gait occurred within a narrow band of slopes, the range of which decreased for both greater and smaller sizes in comparison to the original. For the smaller bipeds the range decreases from 2.5° to 1.4°, while the larger sizes of 1.50 and 1.67 showed a rapid decrease in slope range of 1.2° and 0°respectively.

A possible reason for this limiting envelope was deduced from the plot of stride length against slope in Figure 6.2. As biped size increases the rate at which stride length increases with slope is amplified. From the simulation's animation we observed that at the maximum slopes the biped displays an "over-stepping" gait where the stride length is too large and the robot cannot recover its balance. That is the momentum needed to raise the centre of mass above the

new stance foot far outstripped the energy available. Conversely, as slope decreased so did the stride length, until eventually the steps were so small that the biped fell forwards.

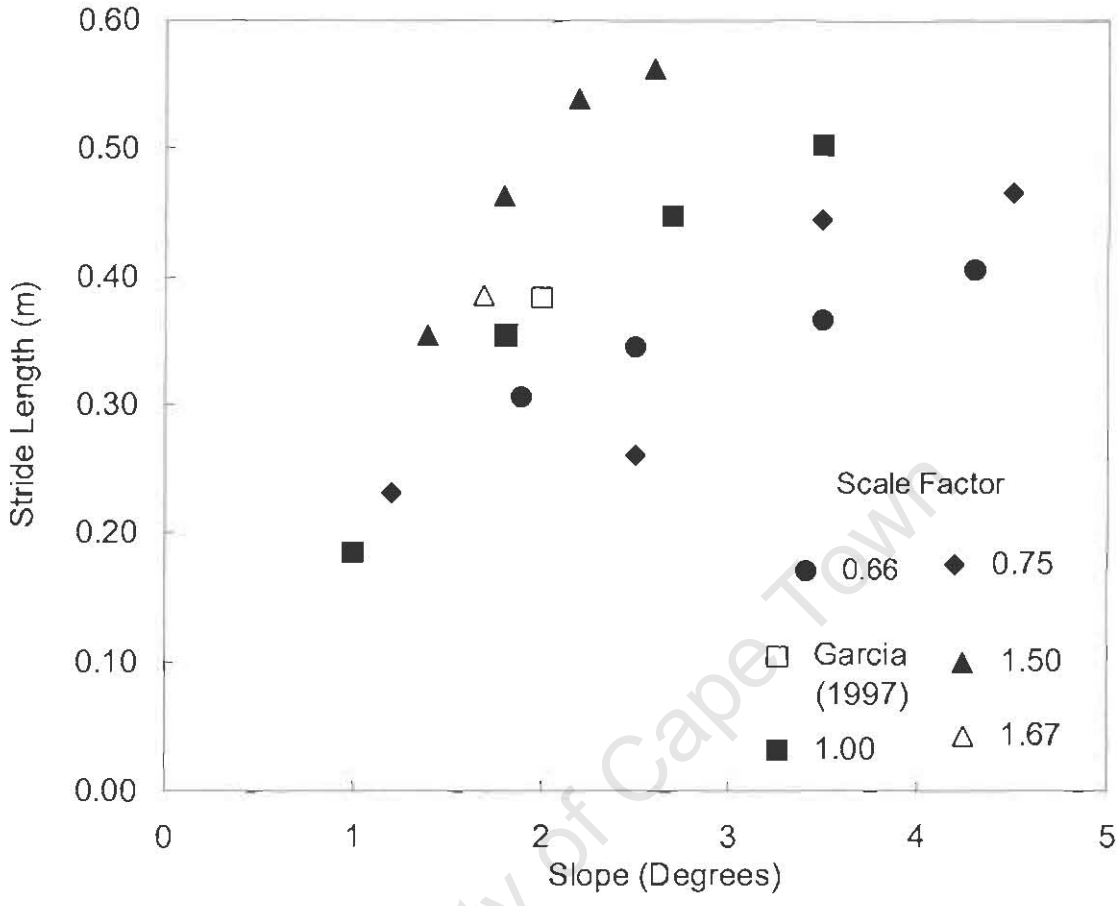

Figure 6.2 Stride length in metres against ground slope for the simulated data The size at which each gait occurs is labelled according to tbe legend in the top left corner.

It must be remembered that in Figure 6.2 stride length is not dimensionless, and hence the larger sized walkers, having larger feet, show longer strides for a given slope and thus reach their maximum stride length limit at lower slopes than that of their smaller counterparts.

These restrictions to stride length were extended by the relationships derived and listed in Chapter 5. Firstly, to extend the upper slope limit, the vertical offset of the shank centre of mass from the knee (C_s) must be adjusted. The reduction in C_s served to limit the moment arm of the shank, which consequently reduced both the kinetic energy requirements of the shank and the energy expenditure at knee-strike. The lower limit was extended by decreasing the thigh centre of mass offset (C_t) from the hip by approximately 50%.

Size and Dynamic Similarity

The dynamic similarity of gait between different biped sizes is apparent in Figure 6.3, where dimensionless velocity β is plotted against the biped's relative stride length which, as per Alexander (1984, 2004), Kubat (2000) and Pratt (1999) took as the stride length λ divided by the height *h* of the stance leg hip above the ground at mid-stride. As Kubat (2000) reported, both Donelan *et al.* (1997) and Pratt (1999) believed that dynamic similarity was only truly present if both the Froude number and the relative stride length were equal.

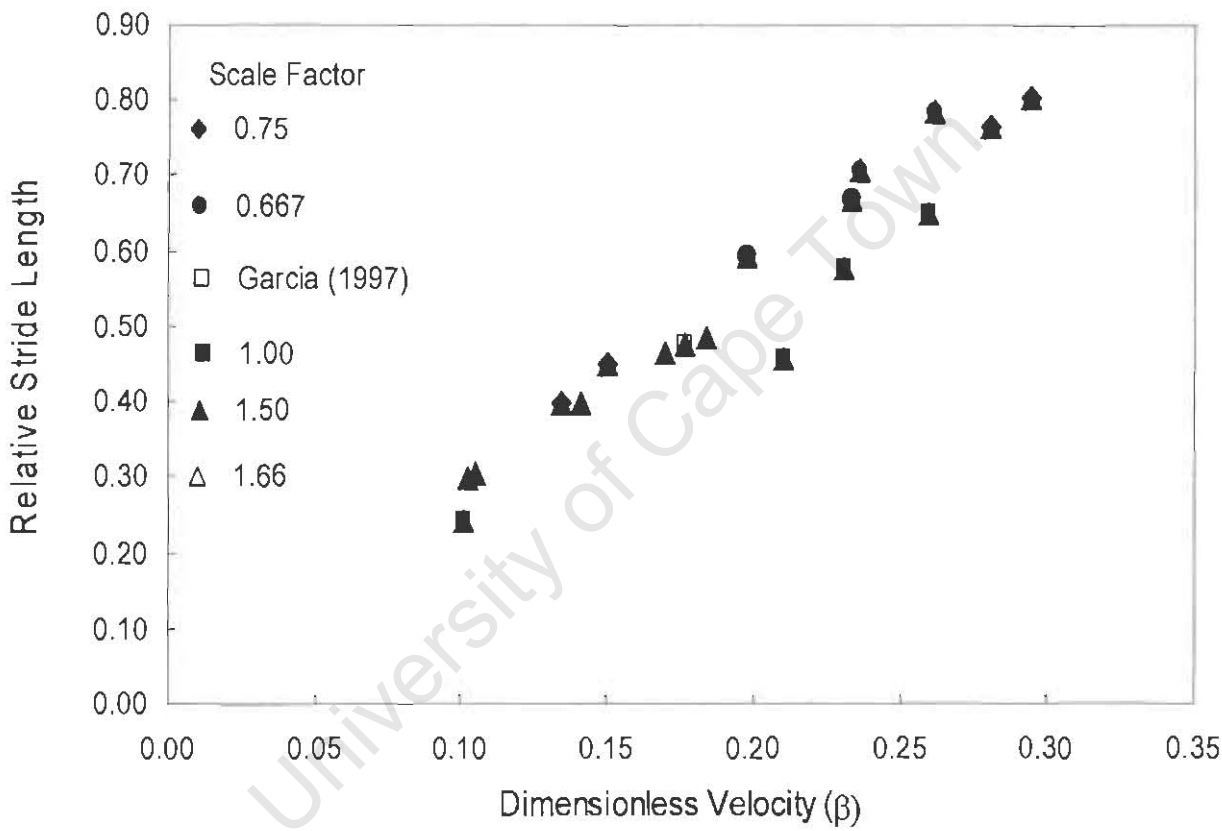

Figure 6.3 A reinterpretation of simulated results showing the variation of dimensionless velocity β with relative stride length (L_{stride}/L_{limb}). Each point is labelled according to limb length relative to the original physical model limb length, referred to as the scale factor.

Pendulum and Elastic Mechanics in Gait

The strong linear relationship bears testimony to the ability of the Froude number and its square root, the dimensionless velocity β, to predict the dynamic similarity of our passive dynamic walker at different sizes and slopes. The Froude number, also defined as the ratio of gravitational forces to centripetal forces, lends itself well to predicting simulated passive bipedal gait as pendulum mechanics are the sole mechanism employed.

The trend of Figure 6.3 follows the findings of Alexander (1976, 2004), given in Figure 2.10, very well despite occurring at much smaller dimensionless speeds.

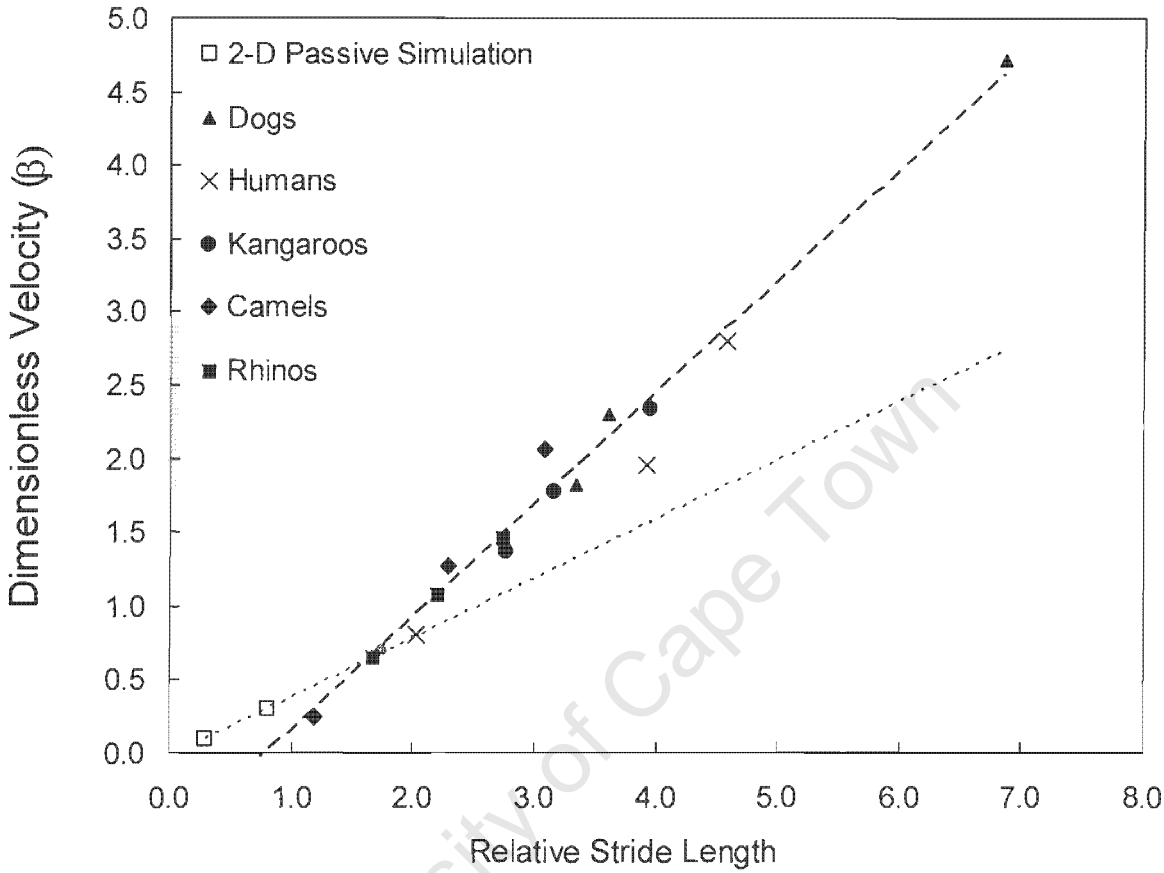

Figure 6.4 Extrapolated linear progression of dimensionless speed against relatives stride length for the results of Alexander (1976) and our simulated bipedal walker.

When plotted on the same set of axes, Figure 6.4, and extrapolated so as to overlap each other, we find the slope of the simulation to be slightly shallower than that from Alexander (1976). This difference in slope implies the purely passive pendulum-based simulated gait has a slightly lower efficiency. Furthermore at dimensionless speeds below 0.7, a faster speed is achieved by the passive simulation at the same relative stride length. Above a dimensionless speed of 0.7, the passive mechanics of the simulated gait loses its advantage, with an ever widening gap between dimensionless velocity of at a given stride length. This change occurred at a Froude number of 0.5, well before Alexander's (1977) value of Fr = 0.7 for the transition from walking to running,

It is proposed that although the exclusive use of pendulum mechanics is more efficient at very low speeds, in reality there must exist an additional mechanism that bolsters efficiency sufficiently well beyond these low speeds to make the sacrifice of its inclusion worth while at higher walking speeds and running.

It has been well documented by Farley *et al.* (1998), Witte *et al.* (2004) and others in section 2.3 that, unlike passive dynamic bipeds, bipedal walking is not the exclusive product of pendulum motion because of the anatomical nature of animals, including humans, elastic tendon forces have an inescapable contribution to gait mechanics. As reported by Bullimore *et al.* (2004), this contribution occurs in a non-linear, size-independent fashion. Their reasoning extends to dynamic similarity, which is not conserved amongst Nature's bipeds at equal Froude numbers. Even if perfectly geometrically similar, the Froude number does not scale all the contributing mechanics with size, specifically the ever-present elastic-tendon moduli.

This hypothesis fits well with the comparative results of Figure 6.5, where assuming pendulum-based motion of the limbs are the foundation of gait mechanics, at low speeds it is restricted somewhat by the inherent elastic tendon forces present in the muscular-skeletal system. At higher walking speeds, between $\beta = 0.7$ and 1.0 for our parameter set, the same elastic mechanics help to augment the pendular recycling of energy, increasing overall efficiency. This approach as neatly suggested by Garcia *et al.* (1998) to describe the role of neuro-control of gait as one of "gentle guidance rather than imposing control".

Neuro-Maturation of Children's Gait

The results of Vaughan's (2002) study of 204 children between the ages of 14 to 169 months, reproduced in Figure 6.6 with the inclusion of our results, we see that as children grow, dimensionless velocity increases with limb length. As the essential mechanics of the lower limbs remain the same the increased speeds attained are more a product of increasing neural control than anatomical and physiological growth.

If compared to our simulated results in Figure 6.5 we find the opposite occurs with a purely passive mechanism. Here larger sizes, being less stable and expending more energy at knee-strike, appear stable at comparatively much slower speeds. These comparisons again suggest that purely passive pendulum mechanics has its limits when applied to the same set of parameters as it is scaled upwards. As size increases, the growing instability and diminishing

speed of pendulum-based legged motion must be countered by an increasing involvement of neural control.

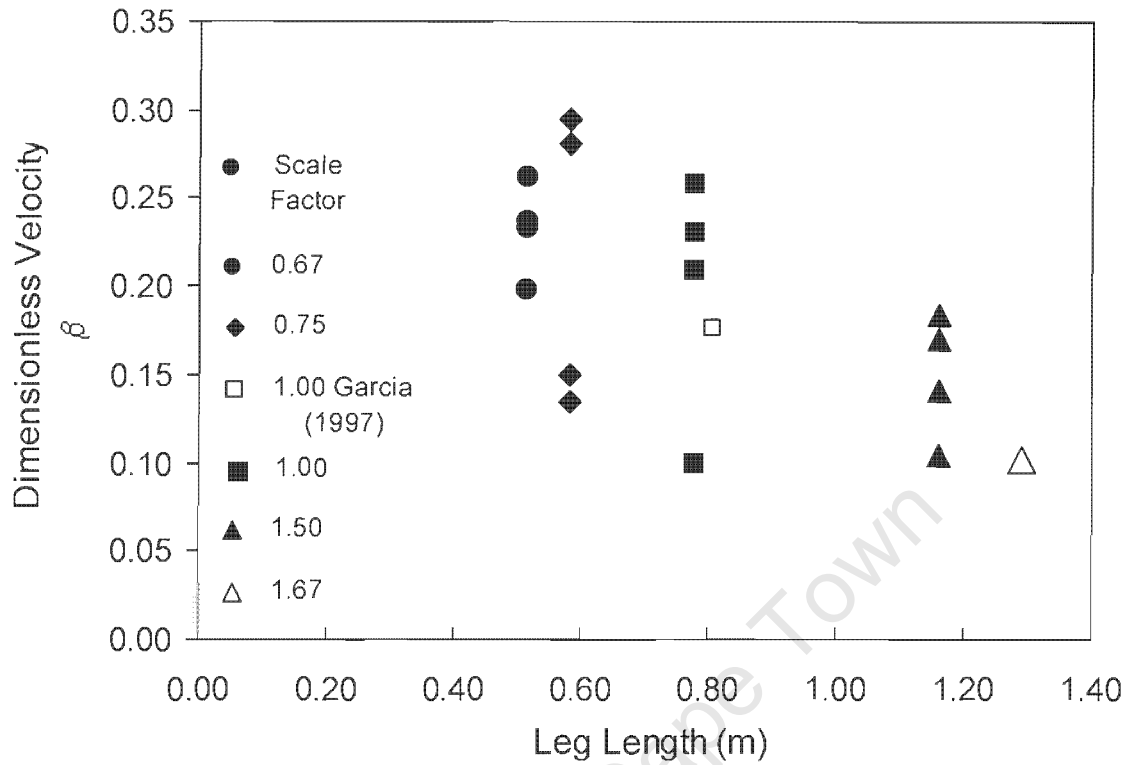

Figure 6.5 Simulated data of scaled 2D biped motion, dimensionless velocity versus Limb Length [taken as Hip height in accordance with Alexander (2004)]

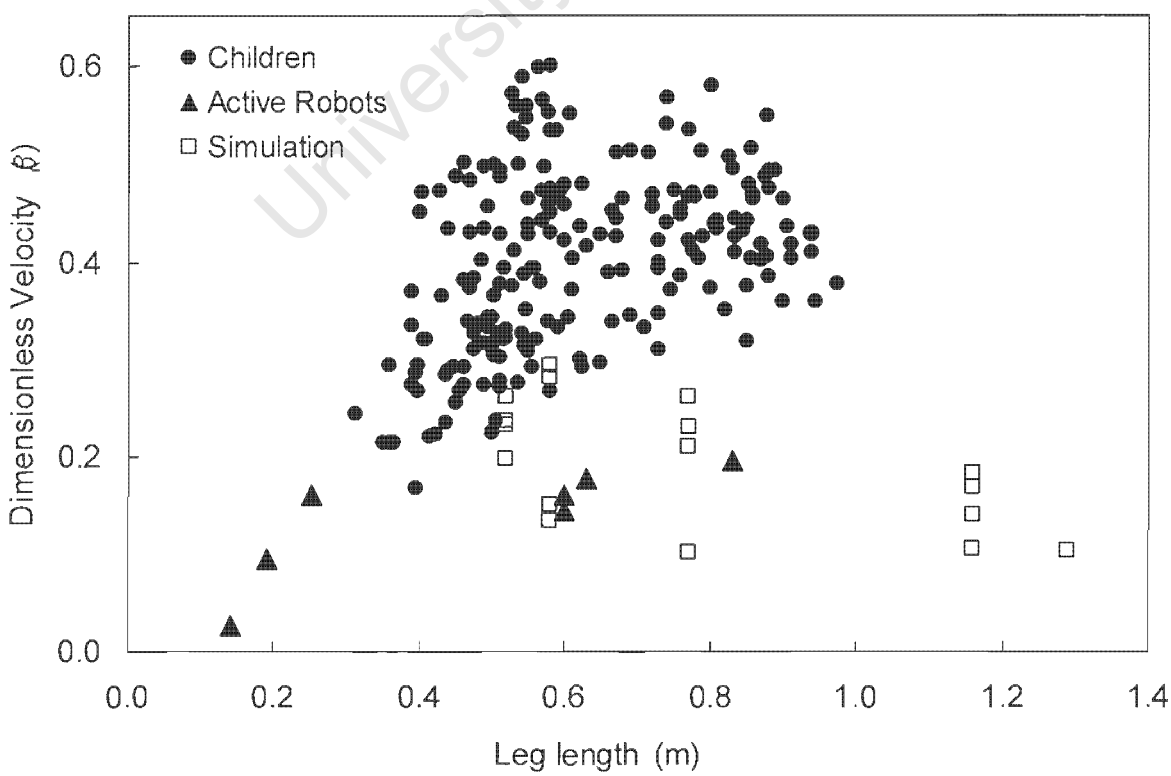

Figure 6.6 The results of Vaughan (2002) showing the dimensionless speed against leg length of 204 normal children between the ages of 14 and 169 months, as well as a collection of modern active robots. Incorporated are the current simulation results of Figure 6.5

In reality passive-dynamics is augmented by both neural control and elastic tendon forces. This is supported by Ivanenko *et al.* (2004) who show that toddlers, although possessing the mechanical "equipment" for pendulum based gait, are not inherently adept at using it efficiently and must employ an increasing degree of neural-control when learning to utilise the system. This neuro-maturation maybe roughly translated as learning to walk.

McGeer (1990, 1993) and Witte *et al.* (2004) have shown that as with pendulum motion, biped speed increases in proportion to the square root of the limb length, contrary to our findings in Figure 6.2. This discrepancy arises due to the inclusion of mass increases in our model that are proportional to limb length, whose effect on stability via energy dissipation outweighs the length increase effects.

On a cautionary note, one must exercise care when viewing these results with respect to actual data as by definition the current simulation deals only with the two-dimensional environment. By expanding to three dimensions, as the physical model of Collins *et al.* (2001), (L=082m, $v=0.51ms^{-1}$, $\beta=0.18$) one may find the decrease in dimensionless velocity to be less dramatic, as well as afford a greater range of sizes and slopes at which stable, passive gait may occur.

Furthermore, when comparing the increase in dimensionless velocity of growing children to that of the simulated biped, our method of scaling parameters should not be taken as an interpretation of normal musculo-skeletal growth. Such growth not only varies greatly among individuals but is no doubt poorly represented by the linear geometry-based scaling method used in this study. Our aim is to show the viability of using passive pendular dynamics at increasing biped sizes of a particular parameter set, which are geometrically similar, and compare the dynamic similarity of their gaits.

Chapter 7
Conclusions and Recommendations

As illustrated by the results of Chapter 4, the biped owes its current unstable status to underperformance in certain key areas. These shortcomings may be overcome by implementing the following alternative strategies at both the design and assembly levels. Their aim is to facilitate both the physical interpretation of the required passive dynamic system including the implementation of various physically non-existent assumptions such as frictionless joints and inelastic knee-strike, as well as improving the ease and more importantly the consistency of assembly.

7.1 A New Revised Biped Design

These alternatives must begin with the key aim of reducing the weight of each limb by half to reach that specified by Garcia *et al.* (1998). The current misinterpretation arose very early in the design specification process and was only detected in the test phase when the problems of knee-bounce and foot-clearance, as well as the biped's sensitivity to changes in hip mass, lead to a re-evaluation of the assumptions within the entire system.

Nonetheless, although designed quantitatively beyond specification our physical model and subsequent simulation retain the ratio of masses per leg and has given rise to valuable insights. We note however the increased shank and thigh masses are possibly responsible for inducing the excessive energy losses at knee-strike. Moreover the extra weight demands steeper slopes for stable gait to occur. The higher limit is governed by the knee-strike energy losses, which combined with heel-strike, leave an inadequate amount of energy for support transfer to occur.

Implementing the correct masses for the existing limb lengths necessitates the manufacture of a new biped using a modified selection of materials. Aluminium is preferred to form the majority of the frame as the current mild steel cross-section would

be reduced to unrealistic diameters. However weight-bearing pin-joints at which rotation occurs may remain of mild steel.

In turn a new limb cross-section is required to compensate for the loss in material strength as well as accommodating the hip, knee and ankle joints. The most likely alternative to the steel shafts used currently would thus be limbs of C-cross section, similar to the models of McGeer (1999) and Garcia *et al.* (1998), with the use of independent attachments for each joint. Fine-tuning of the produced gait would still rest on the biped's ability to allow subtle changes in mass distribution. These changes may be achieved by use of detachable, interchangeable "ballasts" attached to either side of the limb by straight pins passing through holes spaced equally along the length of the leg. As opposed to the sliding collars currently employed, placement is incremental and can only provide limited accuracy that, as the overall leg mass is much less, may not provide the required sensitivity.

7.2 Modifications to Current Biped Design

The gait of the current biped is not entirely autonomous and may be improved upon by the inclusion of the following adaptations.

The ankle joint proved reliable during the course of each test but required constant checking and adjustment between trials. Moreover the current line-of-sight method of setting each foot did not guarantee identical angular position and may contribute to the mismatched dynamic behaviour evident in the outer pair of legs.

Two possible redesigns require the addition of an adjustable stop-rod/limiter, which may be housed either within the "heel" of the foot, or externally above the foot parallel to the limb, as illustrated in Figures 7.1 and 7.2 respectively. In both versions ensuring contact between stop-rod and the lower face of the shank or the top of the foot respectively sets the minimum angle between the limb and the top of the foot.

In Figure 7.1 a small adjustable counter-sunk bolt within the heel acts as the limiter. The restricted available volume and the need to maintain a smooth ground contact surface limits the size of the bolt and demands the bore be placed at an acute angle with respect to the upper foot surface. Unfortunately, as this demands intricate manufacture and more importantly compromises the strength of the ankle, it is retained as a secondary option.

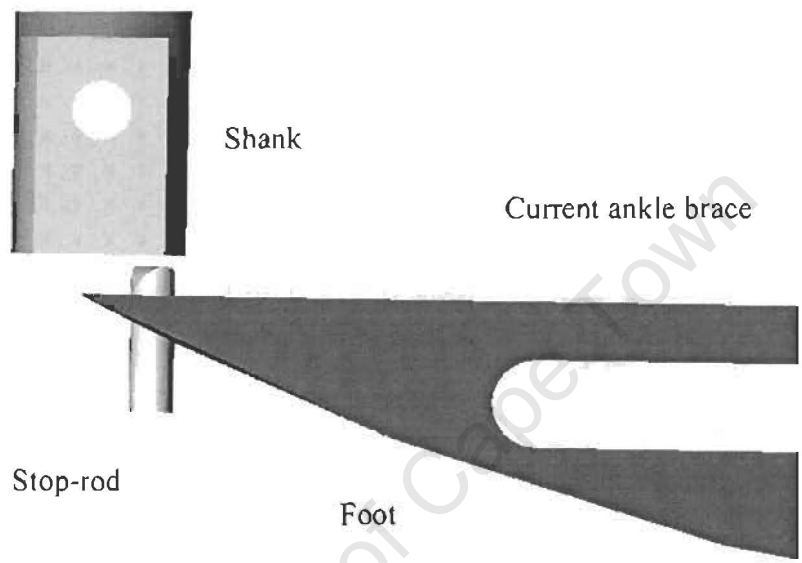

Figure 7.1 The redesigned ankle joint showing the position of the additional stop-rod in relation to the current ankle joint. Housed within the heel, stop-rod angle of inclination is more acute and length has been exaggerated for clarity.

The second arrangement in Figure 7.2 has a fixed governing stop-rod housed in a separate elongated collar that slides along the shank limb. Once more the stop-rod contacts with the upper foot, and is adjusted by grub screws. Despite the impact of heel-strike and the following foot-roll in stance phase where the moment arm at which the contact force acts gradually increases, "dorsi-flexion" of the foot is impeded.

Adjustment in minimally demanding, allowing for the accurate, reproducible, rigid angular positioning of the feet. The sacrifice of fore-aft freedom is felt, at present, to be minor in comparison to these advantages. The disadvantage that may deem this approach ineffective is the corruption of the shank centre of mass by the extra parts. However, if sufficiently minor these may be easily countered for elsewhere in the shank subassembly.

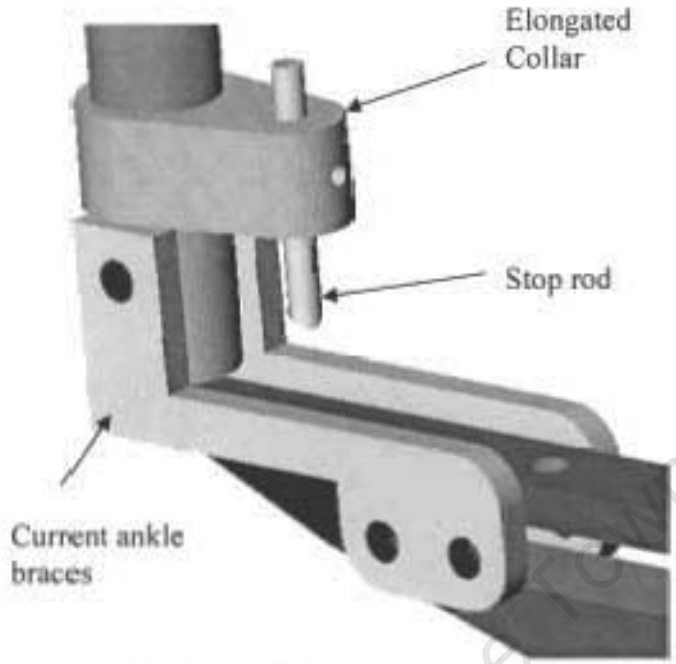

Figure 7.2 Alternative ankle joint design with additional elongated, overhead collar attached to shank limb with a similar stop-rod.

Another vital area to be addressed is the unequal distribution of the main supporting shafts mass between the leg pairs. This proved a major discrepancy that, although extensively minimised by replacing the mild steel shaft with an aluminium tube, influenced the unequal dynamic behaviour of the leg pairs.

With this in mind the hip joint would be better suited to linking the outer and inner pairs of legs if redesigned according to second structural design, Figure 3.7, described in Section 3.4. This common-inner-bearing configuration, where the main shaft acts as the outer link and the inner bearing housing as the inner link, dispels with the need for overhead links that offset the centres of mass unequally. The proportions of the new "linkages", (*i.e.* diameter, cross-section, material) may be adjusted to avoid mass based discrepancies. Furthermore the bearing set up minimises hip friction more effectively and

The knee joint performed satisfactorily during the majority of trials. The silver steel pin and associated brass washers provided adequate frictionless rotation, minimal sidewall

friction and maintained alignment of the shank and thigh. Our accompanying version of McGeer's (1990) suction based knee-stop, although the passive and self-contained nature is well suited practically to the biped's requirements, its inability to function consistently over several trials proved disruptive. This is particularly problematic when such inconsistencies occur between individual legs during a single stride. The critical period requiring improvement is the initial contact between cup and plate when the suction hold is established. Although addressed by the provision of an increased moment arm for the suction-cup to act and a gel-like coating, at low speeds the effectiveness of this method is currently temperamental as either an insufficient amount of air is exhausted from the cup.

Alternatively a different mechanism altogether may be utilized to achieve the delayed knee-lock required for the last two-link portion of the swing phase. A likely candidate is a simpler version of the electro-magnet arrangement proposed in Chapter 4, where a compact sensory and power unit is provided that does not jeopardize the motion of the legs nor their mass properties. These stipulations however, are a marked difficulty and are unlikely to be solved adequately enough so as not to distort and pollute the passive theme of the biped.

7.3. Simulation: Efficiency and Stability with Size

The distinct trends established between the dimensionless velocity, stride length, ground slope and size of the scaled parameters of our bipeds parameter set are listed below:

- Increasing size and/or leg length decreases dimensionless velocity;
- Increasing relative stride length increases dimensionless velocity and;
- Stride length increases with ground slope, where the rate of change decreases with biped size.
- The smallest passive bipeds reach speeds comparable to children, but;
- Larger sizes loose speed by loss of stability.
- At higher speeds passive dynamic walking is progressively unstable, even though supremely energetically efficient,

- The inherent energetic advantage of passive gait, although slightly reduced is not lost with size.

We conclude that generally, for a given parameter set, the effectiveness of purely passive pendulum motion at larger sizes is limited by increasing energy demands at knee-strike, which leads to increased instability. Compensation occurs in the form of a sacrifice of speed for stability as size increases. Conversely at smaller sizes knee-strike energy losses are less problematic as they utilise a smaller and more sustainable portion of the available energy. Higher maximum speeds are thus attained.

In both larger and smaller sizes, the maximum ground slope is limited by overly large foot separation at double support, for which the remaining momentum of the system is insufficient to instigate support transfer. Similarly the minimum ground slope, and thus the available potential energy was limited by exceedingly small foot separation at double support which restrict knee flexion and likewise foot clearance.

The raised rate at which stride length increases with slope for larger sizes is indicative of the greater potential energy available per stride.

In addition the useful comparison the results of Alexander (1986) and Vaughan *et al.* (2002) allowed for valuable insights into the role of pendulum based mechanics in the walking gait with biped size and growing children. In summary we may conclude the following:

- Purely passive pendulum gait is more efficient at very low speeds, equating to Fr < 0.49, compared to the elastically augmented locomotion of real animals;
- The inherent energetic advantage of passive gait, although reduced is not lost with size;
- Speed is sacrificed for stability with increasing size as the smallest passive bipeds reach speeds comparable to children, but larger sizes steadily reduce speed in order to compensate for increasing instability;

- Increasing instability is attributed to unsustainable knee-strike energy losses;
- In developing children the growing instability of passive mechanics is negated by similar increases in neural control allowing the increase in speed with size while retaining the energetic advantage of pendulum motion;

Improvements to the Simulation

The main improvement recommended is an expansion of the sample size of the stable period one gaits found. This should include a larger maximum and a smaller minimum scale factors with smaller increments to guarantee that there are in fact no other stable sizes beyond the current limits considered. In addition, in an effort to better track the relationships between slope and dimensionless velocity, the number of stable slopes investigated should be expanded to at least six per size.

To improve the overall efficiency of the data capture and simulation procedure in addition to providing greater accuracy the MATLAB code should be modified to include a section that allows for the automatic detection, measurement and calculation of stride length, stride period and dimensionless velocities of the various stable gaits. As for the majority of gaits investigated, a stable and consistent period one gait was established only after several steps. For this reason it is thought best to ignore the first two or three strides of every trial as well as use the average value of several steps rather than a single stride.

Appendix A

Geometry and Centre of Mass Calculations

A.1 Thigh Sub-Assembly

(Please refer to Excel spreadsheet Design_Equations.exl Thigh COM on attached CD)

Using the parameter set as outlined in Table 3.2, the biped thigh must display the following properties.

Table A.1 Table (3.2) Thigh subassembly parameters

Parameter	Symbol	Value
Thigh Length	L_t	0.35 m
Thigh Mass	M_t	2.345 Kg
Thigh Centre of Mass Distance	C_t	0.091 m
Thigh Centre of Mass Offset	W_t	0 m
Thigh Radius of Gyration	r_t	0.099 m

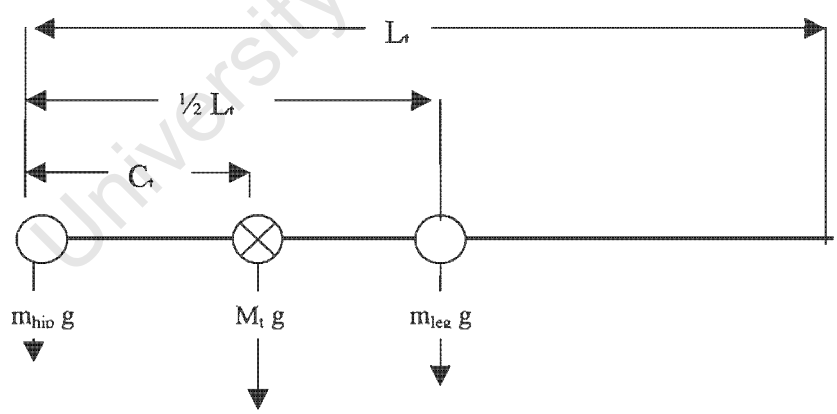

Figure A.1 (Figure 3.8) Free body diagram of thigh subassembly

Taking moments about the centre of mass (COM) as in Figure A.1 gives us the following:

$$M_{hip} \times g \times C_t = \left(M_{leg} g\right) \times \left(\frac{L_t}{2} - C_t\right) \quad \text{A. 1}$$

$$M_{hip} = \left(M_{leg}\right)\left(\frac{L_t}{2C_t} - 1\right) \quad \text{A. 2}$$

Substituting $M_{leg} = (M_{thigh} - M_{hip})$

let $$x = \frac{L_t}{2C_t} - 1 \quad \text{A. 3}$$

$$M_{hip} = M_t\left(\frac{x}{x+1}\right) \quad \text{A. 4}$$

Substituting the values in Table 3.2 the required mass of each limb comprises of a hip and thigh of masses M_{Hip} = 1.1256 kg and M_{thigh} = 1.2194 kg respectively.

Having calculated the mass of each limb of the thigh, and having specified the hip to knee length, 350 mm, the maximum cross sectional area, A, available is determined from the volume available.

$$A = \frac{M_t}{L\rho} \quad \text{A. 5}$$

ρ = Density of mild steel = 7850 kgm^{-3}

Solid circular shaft = $A = \pi r^2$ r = 12 mm

Hollow circular shaft = $A = \pi\left(r_{outer}^2 - r_{inner}^2\right)$ r_{outer} = 13mm r_{inner} = 5 mm

A.2 Shank Sub-Assembly

(Please refer to Excel spreadsheet Design_Equations.exl:Shank COM on attached CD)

The necessary limb length L_{leg}, and foot dimension and position as given in Figure 3.3 are determined geometrically and by balance of moments respectively.

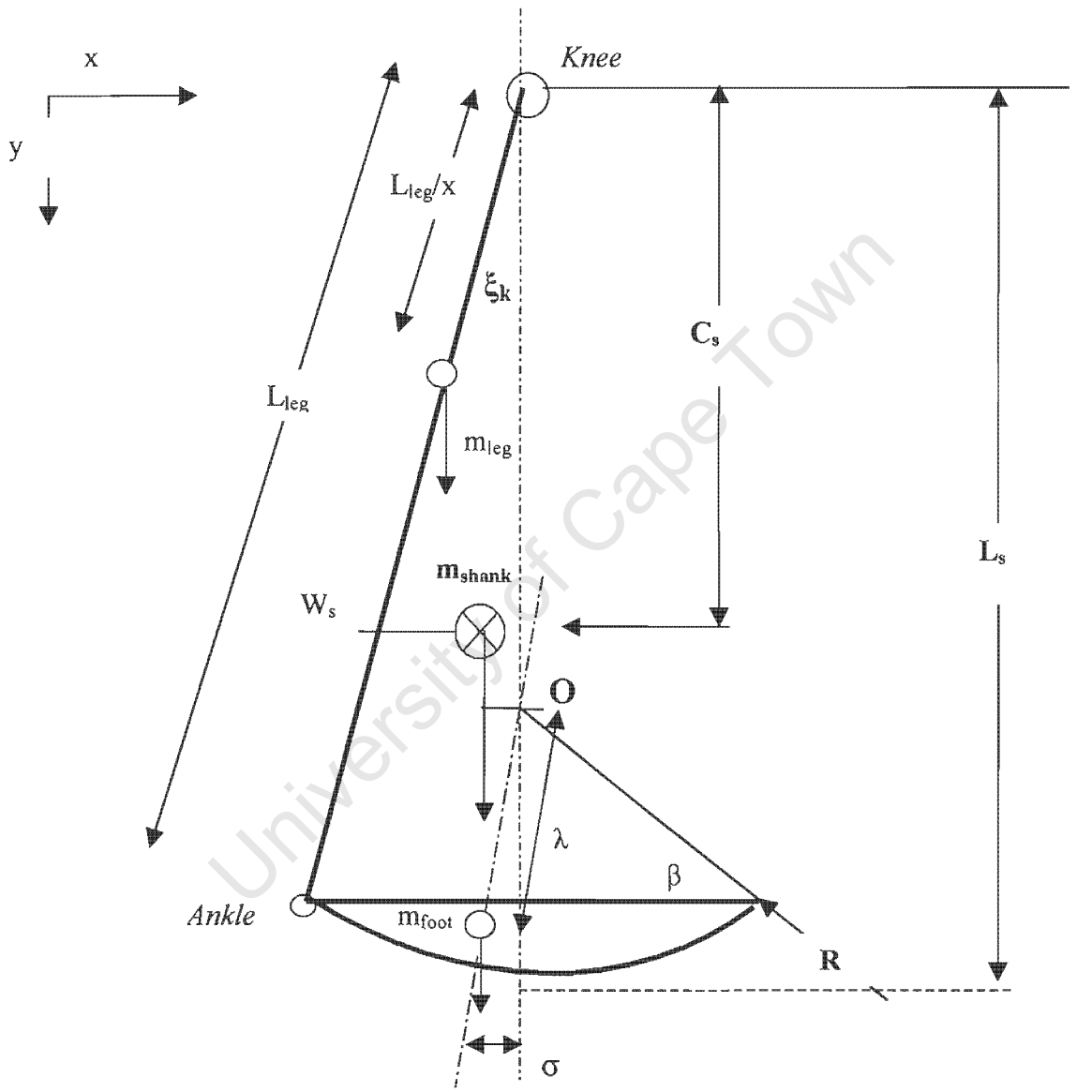

Figure A2:/3.9 Free body diagram of shank subassembly, set parameters from Garcia et al. (1998) are bold, design specific parameters are in

Initially the application of the Cosine rule in conjunction with the list of known parameters as given by Garcia *et al.* (1997), allows us to determine L_{leg} in the following manner.

$$R^2 = L_{leg}^2 + 0.26^2 - 2\left(L_{leg}\right)(0.26)\cos\omega \qquad \textbf{A. 6}$$

$$R^2 = L_{leg}^2 - \left(L_{leg}\right)(0.52)\cos\omega + 0.0276 \qquad \textbf{A. 7}$$

$$L_{leg} = (0.5)(0.52)\cos\omega \pm (0.5)\sqrt{(0.52\cos\omega)^2 - 4(0.0276)} \qquad \textbf{A. 8}$$

Substituting $\omega = 14^\circ$ gives a required leg length of $L_{leg} = 0.441$ m.

The next step is to specify the quantity and position of the centre of masses (COM) of the limb and foot such that the overall shank COM produced is $C_s = 0.17$ m and $W_s = 0.025$ m. We begin by taking moments about the x and y-axes using the hip as our reference point, as shown in the simplified free body diagram of Figure A3.

Taking moments about the y-axis:

$$M_{shank}\, C_s = M_{leg} L_y + M_{foot}\, F_y \qquad \textbf{A. 9}$$

As $M_{shank} = M_{leg} + M_{foot}$, we may write;

$$M_{shank}\, C_s = (M_{shank} - M_{foot}) L_y + M_{foot}\, F_y \qquad \textbf{A. 10}$$

Rearranging gives:

$$\frac{M_{shank}}{M_{foot}} = \frac{F_y - L_y}{C_s - L_y} \qquad \textbf{A. 11}$$

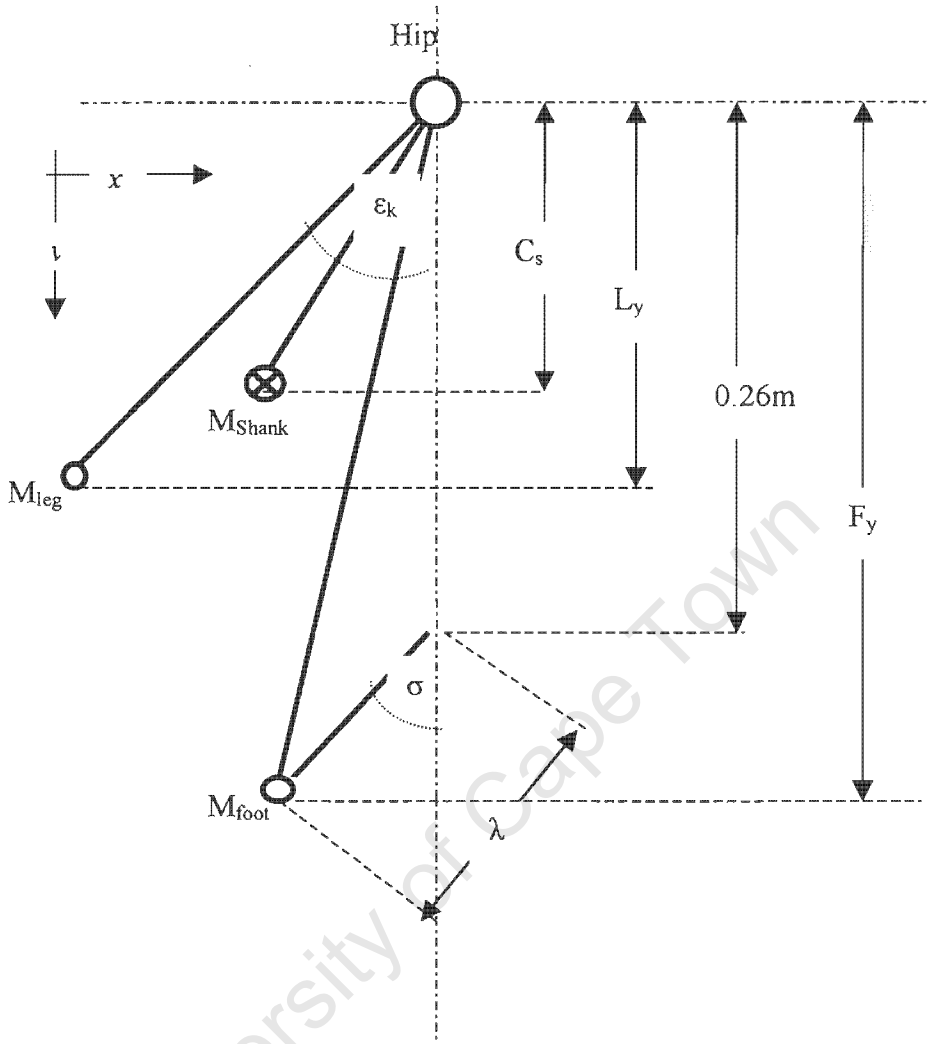

Figure A.3: Simplified free body diagram of the key masses and their positions within the shank sub-assembly. The origin lies at the hip joint, the distance from which is given by the first letter of the component followed by the axes of the measurement, except with the overall COM where the labelling of Garcia *et al.* (1997) is maintained.

Similarly by taking moments about the x-axis the initial equation is rearranged:

$$M_{shank}\, W_s = M_{leg} L_x + M_{foot}\, F_x \qquad \textbf{A. 12}$$

$$\frac{M_{shank}}{M_{foot}} = \frac{F_x - L_x}{W_s - L_x} \qquad \textbf{A. 13}$$

Equating equations **A.11** and **A.13** gives us:

$$W_s(F_y - L_y) - L_xF_y = C_s\,(F_x - L_x) - L_yF_x \qquad \text{A. 14}$$

Substituting the following dimensional parameters from Garcia *et al.* (1997) namely, Cs = 0.17 m and Ws = 0.025 m, and from Figure A.2 we determine the following:

$$Fx = \lambda \sin\sigma \qquad \text{A. 15}$$

$$Fy = 0.26 + \lambda \cos\sigma \qquad \text{A. 16}$$

$$L_x = \frac{L_{leg}}{x}\sin\omega \qquad \text{A. 17}$$

$$L_y = \frac{L_{leg}}{x}\cos\omega \qquad \text{A. 18}$$

Where "x" refers to the distance along the shank limb at which it's COM is placed. This is necessary as the overall shank COM lies above the midway point of the limb. This implies that the current COM of M_{leg} is the combination of the limb COM, which lies midway along its length and an additional weight placed at the knee. The exact ratio between the two portions is determined numerically as explained further on.

The distance of the foot COM from its geometric centre is given by λ which is given by equation A.19.

$$\lambda = R^2(\sin^3\alpha)\left(\frac{\alpha}{\sin\alpha - \alpha\cos\alpha}\right) \qquad \text{A. 19}$$

Before substituting into equation A.14 we first define σ in terms of α. Again using the geometric relationships of Figure A.3 we may write the following:

$$R \sin(\sigma + \alpha) = L_{leg} \sin(\omega) \qquad \text{A. 20}$$

By expanding using trigonometry relationships and rearranging to make σ the subject of the formulae gives:

$$R(\sin\sigma\cos\alpha - \sin\alpha\cos\sigma) = L_{leg}\sin\omega \qquad \text{A. 21}$$

$$\sigma = \sin^{-1}\left(\frac{L_{leg}\sin\omega}{R}\right) - \alpha \qquad \text{A. 22}$$

Having determined l_{leg} = 0.441 m and taking R = 0.2 m and $\xi_k = 14°$ from Garcia *et al.* (1997), gives.

$$\sigma = 32.15° - \alpha \qquad \text{A. 23}$$

Finally substituting into equation A.14 gives us:

$$\begin{aligned} &0.0065 + (0.025\lambda)\cos(32° - \alpha) - \\ &0.025\left(\frac{L_{leg}}{x}\right)\cos\xi_k - (0.17\lambda)\sin(32° - \alpha) + 0.17\left(\frac{L_{leg}}{x}\right)\sin\xi_k = \\ &\lambda\left(\frac{L_{leg}}{x}\right)\cos(32° + \alpha)\sin\xi_k + 0.26\left(\frac{L_{leg}}{x}\right)\sin\xi_k - \lambda\left(\frac{L_{leg}}{x}\right)\sin(32° - \alpha)\cos\xi_k \end{aligned} \qquad \text{A. 24}$$

Solving the above equation numerically in Excel, gives final values of M_{foot} = 0.1785 kg and M_{leg} = 0.834 kg at x = 4.

As derived by the momentum balance in Figure A.4, we may determine the knee mass as M_{knee} = 0.201 kg giving the actual shank limb of M_{limb} = 0.201 kg

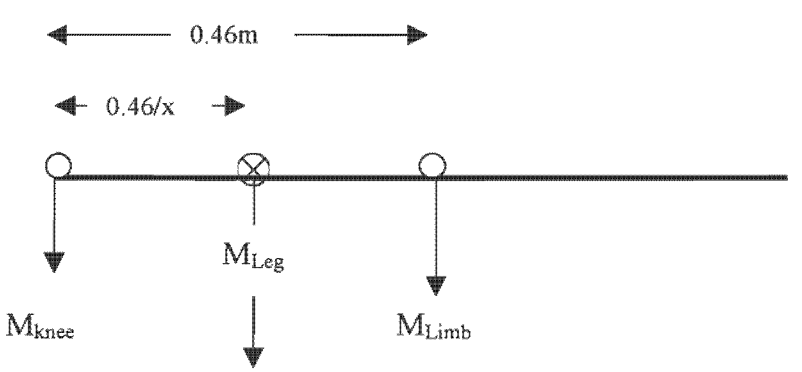

Figure A.4 Free body diagram of the knee-limb distribution of mass of the shank leg section

A.3 Cross-section: Foot and Limb

(Please refer to Excel spreadsheet Design_Equations.exl :Shank dimensions on attached CD)

Having found the necessary masses of the shank components it is a simple step to calculate the dimensions of the limb and foot. The knee, being a more involved component will be dealt with separately in the following Appendix.

Beginning with the shank limb, the required radius is calculated by means of the available cross sectional area, A as follows:

$$A = \pi r^2 = \frac{M_{Limb}}{L_{Limb}\rho_{steel}} \qquad \text{A. 25}$$

Thus the limb radius required is approximately 6 mm. Similarly the foot thickness is determined from the required mass, $M_{foot} = 0.1785$ kg and the angle of arc, $\alpha = 27.4^{\circ}$, giving:

$$A = \frac{\alpha}{180^{o}}\pi r^2 - r^2 \sin\alpha\cos\alpha \qquad \text{A. 26}$$

$$Thickness = T = \frac{M_{Foot}}{A \times \rho} \qquad \text{A. 27}$$

The final foot dimensions included an additional slot of length 80 mm and height 6 mm. This was placed at the level of the foot COM. Thus reducing the cross sectional area not only increased the foot thickness to a more hand able ≈ 10mm, but is to also provide a useful attachment for the ankle joint. Although the slot is offset by 15 mm from the centre line, in the x-direction, the resulting 0.8 mm deviation of the foot COM made the inclusion of the slot worthwhile.

The final parameters of the shank sub-assembly are given in Table A.2.

Table A.2 (3.4) Known dimensional parameters of shank subassembly

Parameter	Symbol	Value
Shank Mass	M_s	1.013 kg
Shank Length	L_s	0.46 m
Shank Centre of Mass Distance	C_s	0.17 m
Shank Centre of Mass Offset	W_s	0.025 m
Foot Radius	R	0.2 m
Foot Centre Offset	ξ_k/σ	0.197 rad

Appendix B

Joint Dimensions

(Excel spread sheet name Joint_equation.exl)

The design of the hip, knee and ankle joints are to primarily fore fill the role of attachment between the neighbouring components in a manner, which permits constrained movement. At the same time these transition pieces must be of specific mass and position, as determined in Appendices A1 and A2, to ensure the desired overall COM is produced.

This section of calculations will determine the dimensions of the chosen joint shape and form as discussed in Chapter 3. With the aim of ensuring the required mass is achieved and is focused about the joints centre of rotation while accommodating the attachment and movement of the parts concerned.

B.1 Hip Centre of Mass

The chosen structural layout of the hip requires the individual inner and outer hips to differ in profile. To ensure clearance of the inner link as it passes underneath the link spanning/connecting the outer hips, an inverted T-shaped profile is used to gain extra elevation of the outer link. Conversely the inner pair is required to be as low as possible; hence a simple rectangular cross section is used.

Outer Hip

Beginning with the mass of each hip, which is $M_{hip} = 1.126$ kg gives an available volume of $V = 143 \times 10^{-6}$ m^3 when using mild steel of density $\rho = 7850$ kgm^3. Mild steel is preferred over aluminium for both greater tensile strength; ease of machining and, for the increased density, which as will be evident later, allows for more compact components. Using the labelling of Figure B.1 we may write;

$$\text{Volume} = V = T \times (A_1 \times B_1)(A_2 \times B_2) \qquad \textbf{B. 1}$$

For both hips the volume of the main shaft hole is neglected as it is assumed the main shaft itself will act to replace the "missing" volume. Further more the difference in densities

between the mild steel hip and the silver steel shaft is relatively minimal, (i.e. 7.85 g/cm^3 and ≈8.02 g/cm^3 respectively) for the volumes involved.

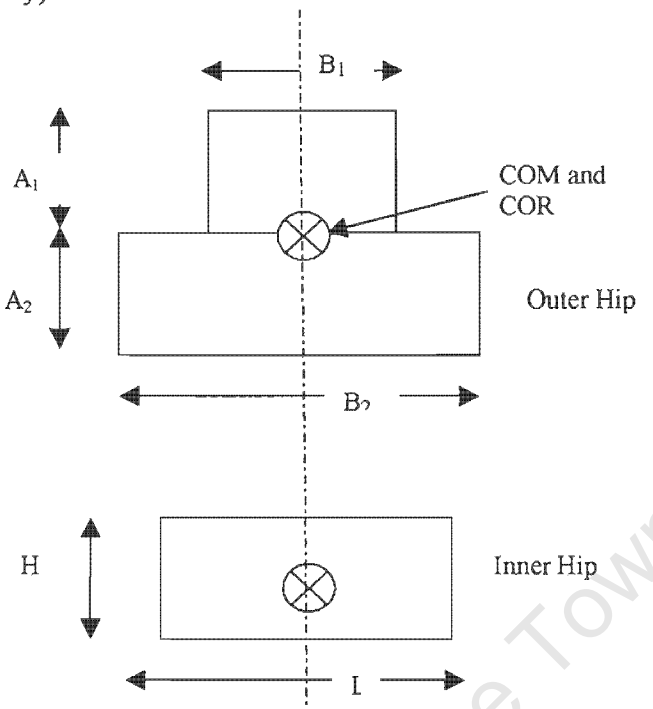

Figure B.1 Schematic of outer and inner hip profiles showing the equal distribution of mass about the centre of rotation

Figure B1 shows the position of the COM and centre of rotation to be coincident. As a result the mass above this point must be equal to the mass below. As each section shares the same density and depth, this is reduced to an equivalence of areas as shown below.

$$A_1 \times B_1 = A_2 \times B_2 \qquad \textbf{B. 2}$$

Using these two forms we arrive at an equation for the required thickness of the outer hip;

$$T = V/(2 \times A_1 \times B_1) \qquad \textbf{B. 3}$$

The values of the upper segments height (A_1) and that of the lower segments (A_2) depend on the clearance available for the outer link and the minimum threaded length necessary for the thigh attachment respectively. Generally a M6 threaded section of a minimum length of 15 mm is more than sufficient to support the 3.4 kg leg, while an additional 5 mm allows

adequate separation from the movement of the main shaft. In light of this strength requirement the minimum heights of the lower half of both the inner (i.e. ½H) and outer hips (i.e. A_2) must be a minimum of 20 mm.

Clearance is dependant on the dimensions of the inner hip. The maximum distance, from the COR to the corner must not exceed the height of the upper half of the outer hip and is given as:

$$A_1 < \tfrac{1}{2}\sqrt{(H^2+L^2)} \qquad \textbf{B. 4}$$

A minimum value of 36 mm for A1 is required. For added safety an additional 4 mm is bringing the final value to $A_1 = 40$ mm

The Excel spread sheet attached (**Joint_Equ_modified_2.exl**) is used to fine tune/optimise the hip dimensions according to the above relationships are entered while the value of A_1, A_2, B_1 and B_2 are varied. A stipulated maximum or minimum value for each quantity is determined by

B.2 Knee Centre of Mass

As shown in the schematic of Figure B.2 the knee joint constitutes a U-shaped yoke attached by a grub screw to the upper end of the shank limb.

Determining the dimensions necessary to produce a mass of $M_{knee} = 0.417$ kg at the centre of rotation is done in a similar manner to the hip design, namely equating the volumes on either side of the COM. Beginning with the overall volume available we produce the first governing equation below. The volume of the hole housing the support pin is considered filled by the pin which is of the same density, thus it maybe excluded from the volume calculations.

$$\text{Volume} = \text{Vol} = m/\rho = UVW - OBU - A\pi r^2_{shank} \qquad \textbf{B. 5}$$

$$B = UVW - \text{Vol} - (A\pi r^2_{shank})/OU \qquad \textbf{B. 6}$$

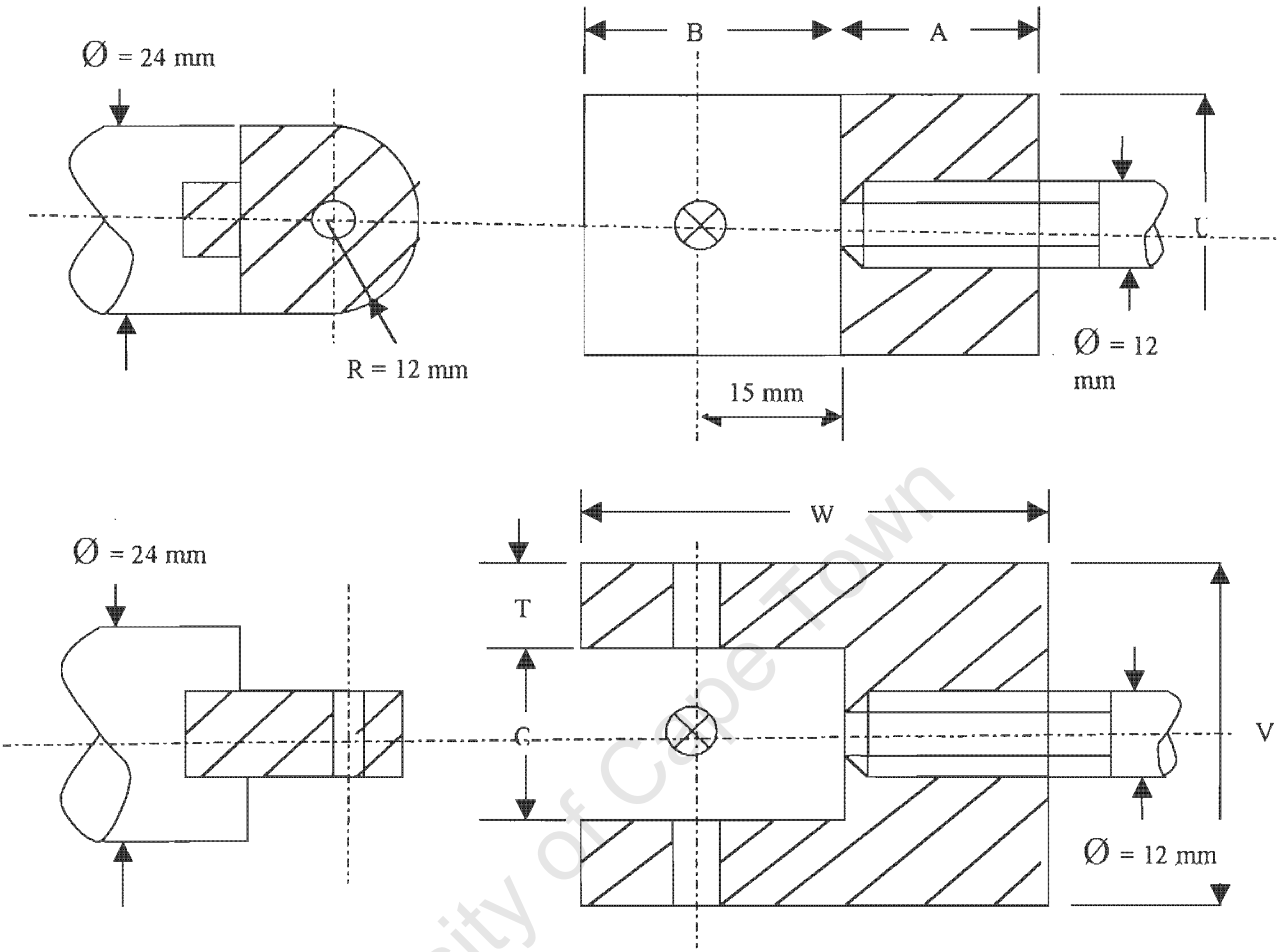

Figure B. 2 Schematic representation of the thigh-end and shank end of the knee joint. Note that the pin joint is placed 15 mm above the inner base of the knee to prevent interference of the thigh-end piece, which has radius of 12 mm.

Equating the areas and/or volumes about the COR produces the second governing equation:

Taking the relationship Area right-side = Area left-side

$$2T(B-15) = 2T(15) + AV - 2r^2_{shank}\,A \qquad \textbf{B. 7}$$

$$B = 30 + (\tfrac{1}{2}AT)(V-2r^2_{shank}) \qquad \textbf{B. 8}$$

The dimensions U, V, W and the gap O are specified by the author in relation to its ability to accommodate the thigh-end piece attachment and its opposing twin on the shank end. Once more Excel was employed to grant easy variation of these variables allowing the optimal ratio of sizes to be chosen. The final dimensions produced using the Excel spreadsheet "**Knee_joint_Equation.exl**" are given in Table 3.2 and the working drawing in Figure D.12

B.3 Thigh End- Piece

As explained in Chapter 3 and illustrated in Figure C.2, the shape and functional approach of the knee joint necessitates modification of the thigh-end at which the rotation is to occur. This modification took the form of a sliding element with a circular profile and minimal thickness, which allows sufficient clearance from the bottom and sides of the knee-joint yoke respectively. As the yoke of the shank-end of the knee had a gap of 29 mm, there was no need for an excessively long end-piece. Rather a short curved end of a minimal length of 15 mm was sufficient to house the pins of the knee, M8 and the sliding runner's threaded end as shown in Figure B. 3 and the working drawing in Appendix D.

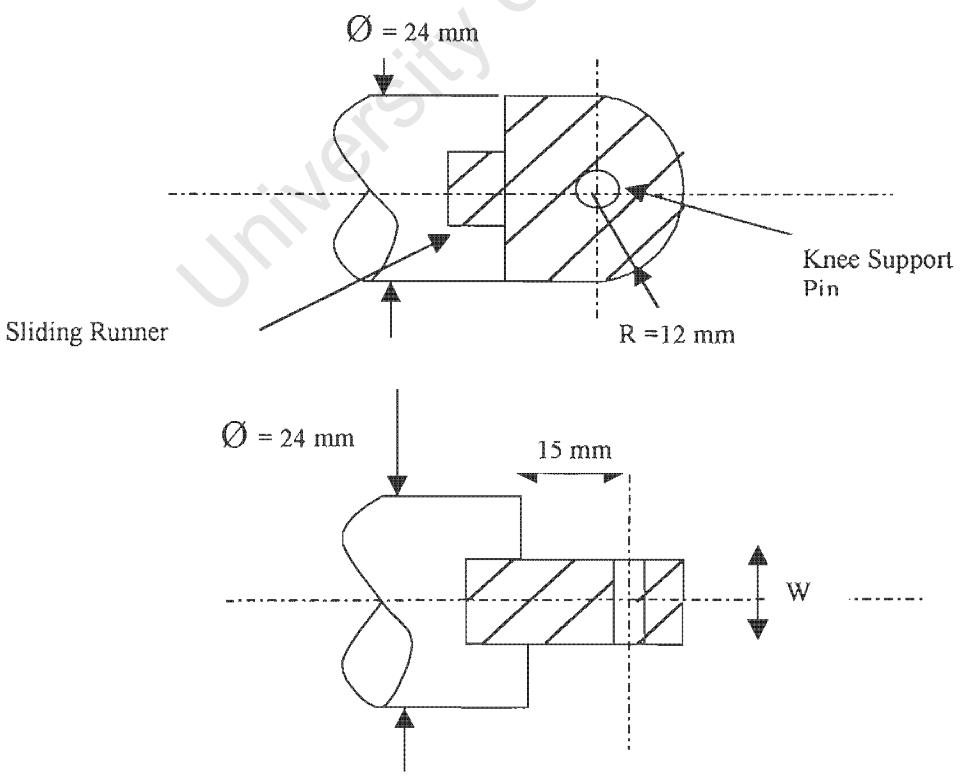

Figure B. 3 Dimensions of the thigh-end piece responsible for allowing rotation of the thigh. A 50mm long runner is added to the connecting end to allow for variation in thigh length, a small M3 grub screw achieves fastening.

In order to maintain the thigh's COM as previously calculated the weight of the end piece must be equal in mass to the length of thigh, which it replaces. In addition the point of rotation (i.e. pin hole) must be the same distance from the thigh end, thus conserving the overall Hip-knee length of the limb.

Volume of replaced portion of thigh = V_{thigh}

$$V_{thigh} = \pi r^2 \times 15 \text{ mm} \qquad \textbf{B. 9}$$

Volume of thigh-end piece = V_{TE}

$$\begin{aligned} V_{TE} &= 15\ r\ W + \tfrac{1}{2}\ \pi\ r^2\ W \\ &= W\ (15r + \tfrac{1}{2}\pi\ r^2) \end{aligned} \qquad \textbf{B. 10}$$

Equating the two governing equations above gives W = 20 mm.

Appendix C

Simulation: MATLAB Code

The MATLAB simulation by Garcia (1997) of a two-dimensional Passive Dynamic Walker was obtained partly from his personal web site (http://tam.cornell.edu/students/garcia/msghomepage.html) and via personal email correspondence. For the most part the code is unchanged and is as appears available for public, however some minor modifications were made to simplify several steps concerning the addition of extra masses along the thigh and at the hip and the accompanying effect on the second moments of inertia (i.e. I_{zz}) as these were derived directly from the Solid Works modelling package.

Further adjustments and additional plots were used initially to determine the Froude number but proved more cumbersome than the graphical and Excel based method outlined in section 5.2. The accompanying source code is not included in this appendix, as it remains unchanged to that of the original. The entire simulation however is stored on the CD accompanying this text under the folder name, 2D_Passive_Biped_for_Public.zip.

Modified UCT Version of MATLAB CODE

```
% 2D Passive Dynamic Bipedal Code
% Original version by Garcia (1997) adapted and slightly modified by
% Nazir Karbanee UCT,2004)
% Original comments and method retained for clarity.

% run_walker.m file initializes parameters for 2D kneed walker and
% integrates forward to simulate walking down shallow slope (gamma
% radians)

% Parameters should be entered for thigh(m2) and shank(m3) and
% extrapolated for straight leg combination- modifying this 11/4/94
% to eliminate inconsistent and/or incorrect parameter values

% At knee strike, the int_walker function calls the function "knee
% strike",
```

```
% which locks the swing knee and computes new angular velocities
% based on conservation of angular momentum.  Similarly, at heel
% strike,
% the function calls "heel strike" and computes new angular
% velocities,
% and also re-defines variables so the walker can take a new step.

% walking continues until t=tfinal
% modified 11/6/95 to turbo version to run faster

clf reset
axis equal
clear
format long

%        WORKING SECTION

% Thigh Subassembly
% without extra stuff

lt = 0.355*0.75;    % limb length multiplied by "scale factor"
ctold = 0.040;  % COM distance from Hip
wt=0;   % COM distance from centre line
m(2) = 4.289;       %   Total mass
Izz2noem = 0.03896;          % 2nd moments of thigh from Solid Works

% Following section was not required as Solid Works allows direct
% derivation of radius of gyration and COM position. However it is
included
% here for completness.

% Addition of extra mass
% emthigh = 0.1718; Garcia (1997)
emthigh = 0.0;
cem = 0.002;

% square masses add emthigh at cem down thigh (calculated 1 thigh)
```

```
% adjust thigh to include extra (non-cm) mass added

ct = (ctold*m(2) + cem*emthigh)/(emthigh+m(2));

Izz2wem = Izz2noem + emthigh*(cem-ct)^2+m(2)*(ctold-ct)^2;
rt = sqrt(Izz2wem/(m(2)+emthigh));
m(2) = m(2)+emthigh;

% extra mass at hip
% mh=0.773/2;
mh=0;
cth=(ct*m(2))/(m(2)+mh);
Izz2whm=Izz2wem + mh*cth^2 + m(2)*(ct-cth)^2;
m(2)=m(2)+mh;
rt = sqrt(Izz2whm/m(2));    % final radius of gyration; derived from
Solid Works
ct=cth;

%Shank Sub-assembly
m(3) = 1.88;     % Mass
rs = sqrt(0.03478/m(3));     % radius of gyration
ls = 0.315;          % Length
cs = 0.081;       % COM "y-axis" distance
ws = 0.0028;      % COM "x-axis" distance
R = 0.150;           % radius of foot

% Total Mass
m(1) = m(2)+m(3);

% Slope, & Gravity
gam = 4.0*pi/180;      % slope (degrees)
g = 9.81;              % gravity

% Short Hand
sgam = sin(gam)*g;
cgam = cos(gam)*g;
```

```
%eta (epsilon)values as defined in notes

etak = 12*(pi/180);
etat = atan((ls-R)*sin(etak)/((ls-R)*cos(etak)+lt));
etaf = etak-etat;

cs=csold*cos(etak)+wsold*sin(etak);
ws=csold*sin(etak)-wsold*cos(etak);

% Initial Conditions as used by Garcia et al (1998)
% fp for labwnks gam=0.036 em=0.8 and 0.1718 mh=0.773
theta1= 0.24395343514010;
theta2 = pi-etat-2*theta1;
theta3 = etak;
theta1dot= -1.04912725993148;
theta2dot= 0.74760219037376;
theta3dot= -1.18165555602257;

y0 = [theta1 theta2 theta3 theta1dot theta2dot theta3dot];

% vectors from origin of frame to next frame
% refer to Figure 3.2
p01x = R;
p12x = lt*cos(etat)+(ls-R)*cos(etaf);
p23x = lt;

%vectors from origin of frame to cm of leg bit
pc2x = ct;
pc2y = -wt;

pc3x = cs;
pc3y = -ws;

%compute cms of thigh and shank in coordinates of stance leg
%without hip mass
p1c2x = -ct*cos(etat)+wt*sin(etat)+p12x;
p1c2y = ct*sin(etat)+wt*cos(etat);
```

```
pcsx = -cs*cos(etaf)-ws*sin(etaf)+(ls-R)*cos(etaf);
pcsy = -cs*sin(etaf)+ws*cos(etaf)+(ls-R)*sin(etaf);
pcs=[pcsx pcsy]';

% compute cm of composite stance leg (thigh+shank)
pc1x = (m(2)*p1c2x+m(3)*pcsx)/m(1);
pc1y = (m(2)*p1c2y+m(3)*pcsy)/m(1);

% coordinates of stance knee from frame 1- used for heelstrike
p1kx = (ls-R)*cos(etaf);
p1ky = (ls-R)*sin(etaf);
p1k = [p1kx p1ky]';

% coordinates of hip from stance knee, used in stance knee torque
check
pkct1x = lt*cos(etat);
pkct1y = -lt*sin(etat);

% moments of inertia of leg bits about centers of mass
Izz2 = m(2)*rt^2;
Izz3 = m(3)*rs^2;
Izz1 = Izz2+m(2)*((pc1x-p1c2x)^2+(pc1y-p1c2y)^2)+Izz3+m(3)*...
((pc1x-pcsx)^2+(pc1y-pcsy)^2);

pc2lock(1)=(-pc1x+p12x)*cos(etat)+pc1y*sin(etat);
pc2lock(2)=(-pc1x+p12x)*sin(etat)-pc1y*cos(etat);

Izz = [Izz1 Izz2 Izz3]';
pc1 = [pc1x pc1y]';
pc2 = [pc2x pc2y]';
pc3 = [pc3x pc3y]';

tol = 1e-10;        % numerical tolerance; Newton-Raphson
%tsec = 1;        % Total simulation period; seconds
%tfinal = tsec/((g*(Ls+Lt))^1/2)        % Total simulation period;
dimensionless
```

```
tfinal = 0.1

global K KK
initializeK_not;
initializeKK;

[t,y,step]=int_walker_turbo(0,tfinal,...
y0,tol,m,g,R,sgam,cgam,Izz,p12x,p23x,pc1,pc2,pc3,pcs,p1k,...
lt,ls,etak,etat,etaf,pc2lock);

y(:,4)= y(:,4)./sqrt(g*(ls+lt));
y(:,5)= y(:,5)./sqrt(g*(ls+lt));
y(:,6)= y(:,6)./sqrt(g*(ls+lt));

% convert to mcgeer output
% y(:,7,8,9) are mcgeer angles and y(:,10,11,12) are corresp angular
velocities
y(:,7) = -y(:,1);
y(:,8) = pi-y(:,1)-y(:,2)-etat;
t(:,2) = t(:,1).*(g)^0.5/(ls+lt)^0.5;
y(:,9) =  y(:,8)-(y(:,3)-etak);
y(:,10) = -y(:,4);
y(:,11) = -y(:,4)-y(:,5);
y(:,12) = -y(:,4)-y(:,5)-y(:,6);

%Graph plots
%plot(t(:,1),y(:,4),t(:,1),y(:,5),t(:,1),y(:,6));
%plot(t(:,2),y(:,10),t(:,2),y(:,11),t(:,2),y(:,12));
plot(t(:,2),y(:,7),t(:,2),y(:,8),t(:,2),y(:,9));    %  McGeer Angles
%plot(t(:,1),y(:,1),t(:,1),y(:,2),t(:,1),y(:,3));

%Velocity of leg et al.
vcf1(:,1)=-R.*y(:,4);           %stance foot center, x-axis
vcf1(:,2)=0.*y(:,4)./y(:,4);
vhip(:,1)=vcf1(:,1)-p12x*y(:,4).*cos(y(:,1));           %velocity  of
hip; x-axis
vhip(:,2)=vcf1(:,2)+p12x*y(:,4).*sin(y(:,1));
```

```
vknee(:,1)=vhip(:,1)-lt*(-y(:,5)-y(:,4)).*sin(pi-y(:,1)-y(:,2));
%velocity of knee; x-axis
vknee(:,2)=vhip(:,2)-lt*(-y(:,5)-y(:,4)).*cos(pi-y(:,1)-y(:,2));
vcf2(:,1)=vknee(:,1)-(ls)*(-y(:,5)-y(:,4)-y(:,6))...
% swing velocity of foot; x-axis
.*sin(pi-y(:,1)-y(:,2)-y(:,3));
vcf2(:,2)=vknee(:,2)-(ls)*(-y(:,5)-y(:,4)-y(:,6))...
.*cos(pi-y(:,1)-y(:,2)-y(:,3));

%figure
%plot(t(:,2),vhip(:,1),t(:,2),vhip(:,2));      %velocity of hip; x-
axis
```

Appendix D

Design Drawings and Photos

D.1 **Full Assembly – 3D**

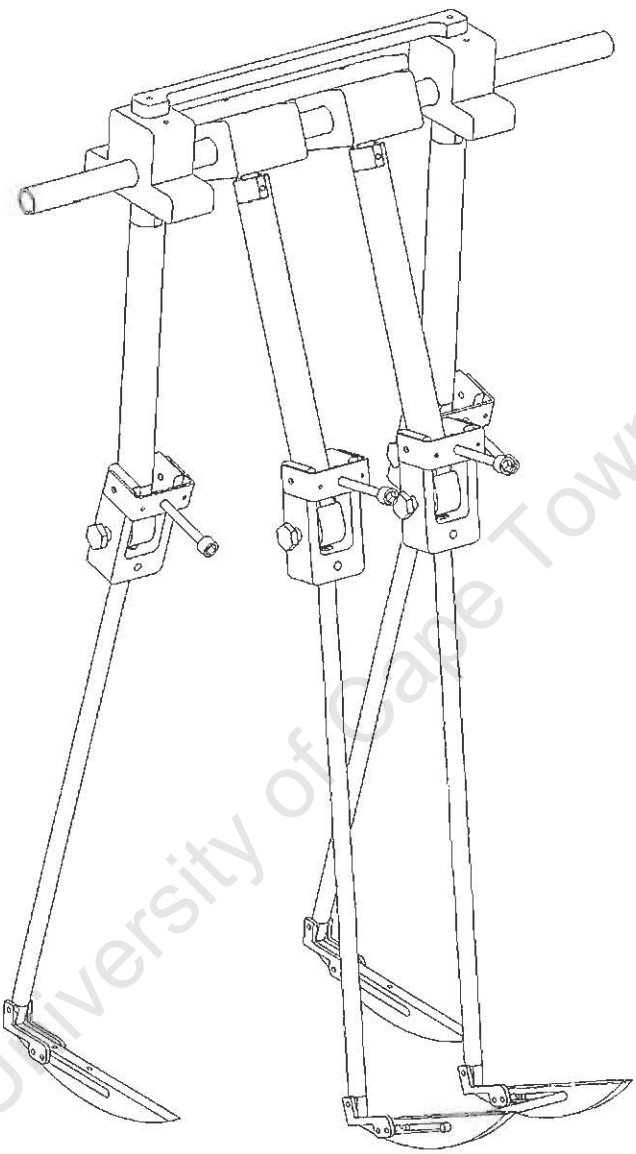

UNLESS OTHERWISE SPECIFIED DIMENSIONS ARE IN mm. TOLERANCES ARE:		UNIVERSITY OF CAPE TOWN Department of Human Biology BioMedical Engineering			
FRACTIONS DECIMALS ANGLES	DRAWN N.A Karbanee	Final Assembly - without suction-cups			
	CHECKED Prof. C.L Vaughan				
MATERIAL	ENGR. N.A Karbanee	SIZE A	CODE	DWG. NO.	REV
	DATE 11/2004				
DO NOT SCALE DRAWING		SCALE 1:4	WEIGHT	SHEET	

D.2 Single Leg Assembly – 3D Exploded

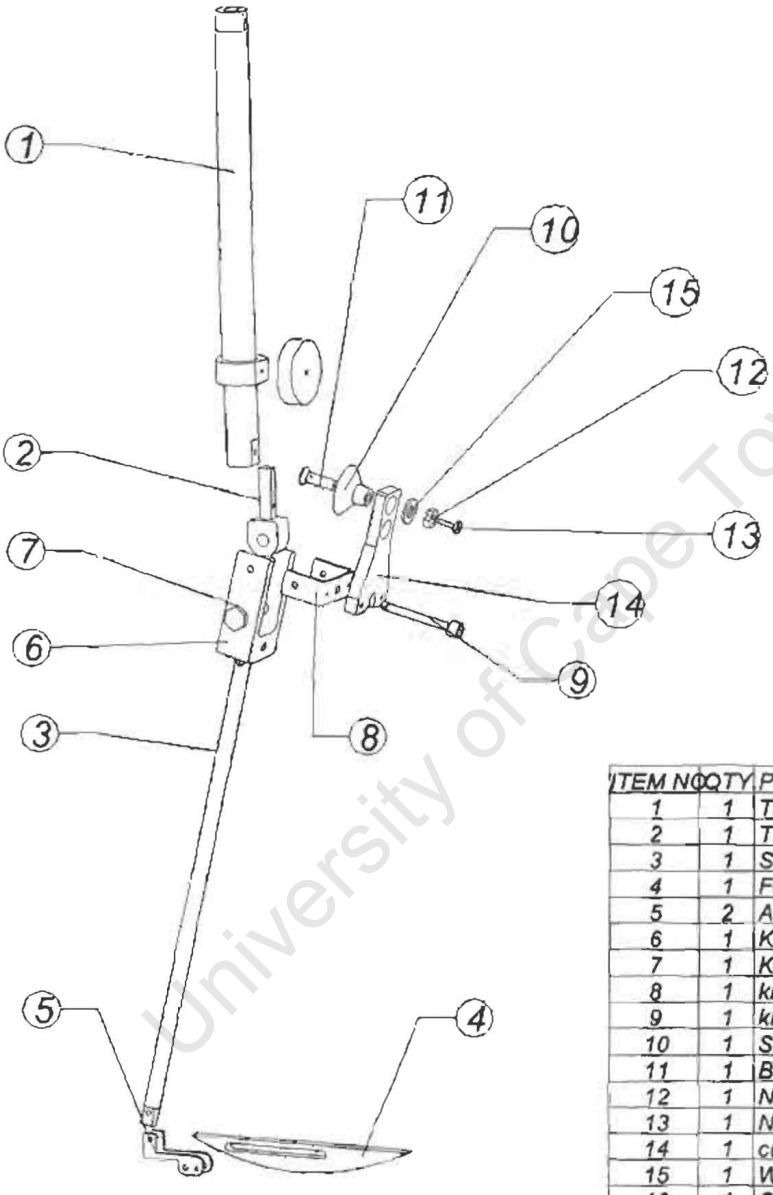

ITEM NO	QTY.	PART NO.	DESCRIPTIO
1	1	Thigh_2_simple	
2	1	Thigh_Knee_1	
3	1	Shank_1	
4	1	Foot_1	
5	2	Ankle_4	
6	1	Knee_1	
7	1	Knee_PIN	
8	1	knee_stop_plate	
9	1	knee_stop_pin	
10	1	Suction_cup	
11	1	Bolt	
12	1	Nut	
13	1	Needle_valve	
14	1	cup_mounting	
15	1	Washer	
16	1	Collar	
17	1	Plate	

UNLESS OTHERWISE SPECIFIED
DIMENSIONS ARE IN mm
TOLERANCES ARE:
FRACTIONS DECIMALS ANGLES

DRAWN	N.A Karbanee	
CHECKED	Prof C.L Vaughan	
ENGR.	N.A Karbanee	
Date	11/2004	

DO NOT SCALE DRAWING

University of Cape Town
Biomedical Engineering

Single Leg Assembly - Exploded View

SIZE	CODE	DWG. NO.	REV.
A			

SCALE 1:4.5 SHEET

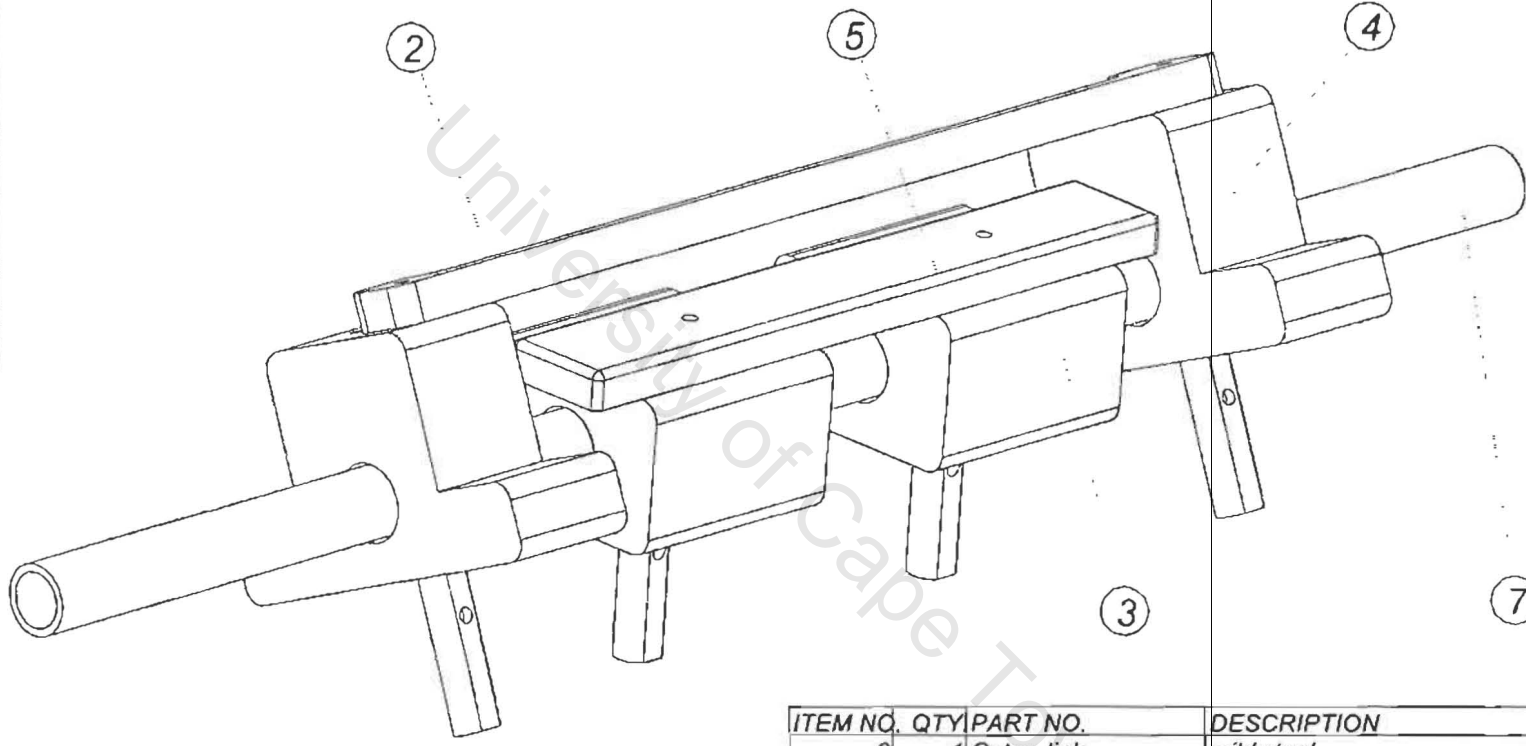

ITEM NO.	QTY	PART NO.	DESCRIPTION
2	1	Outer_link	mild steel
3	2	Inner_hip	mild steel
4	2	Outer_hip	mild steel
5	1	Inner_link_new	mild steel
7	1	Main_HIP_Pin	

UNLESS OTHERWISE SPECIFIED
DIMENSIONS ARE IN mm
TOLERANCES ARE:
FRACTIONS DECIMALS ANGLES
± .XX± .XX ±
.XXX±.XXX

MATERIAL: Mild steel

DO NOT SCALE DRAWING

CAD GENERATED DRAWING.
DO NOT MANUALLY UPDATE

APPROVALS	DATE
DRAWN N.A.Karbanee	2003/4
CHECKED Prof. C.L Vaughan	2003/4
RESP ENG	
MFG ENG Mr G. Newins, Mr K. Hall, Mr C.	2003/4

UNIVERSITY OF CAPE TOWN,
Department of Human Biology,
BioMedical Engineering

Final Hip Assembly

SIZE A | DWG. NO. Appendix D - Drawing D#

SCALE 1:1.5 CAD FILE: Hip_only_assem | SHEET | OF

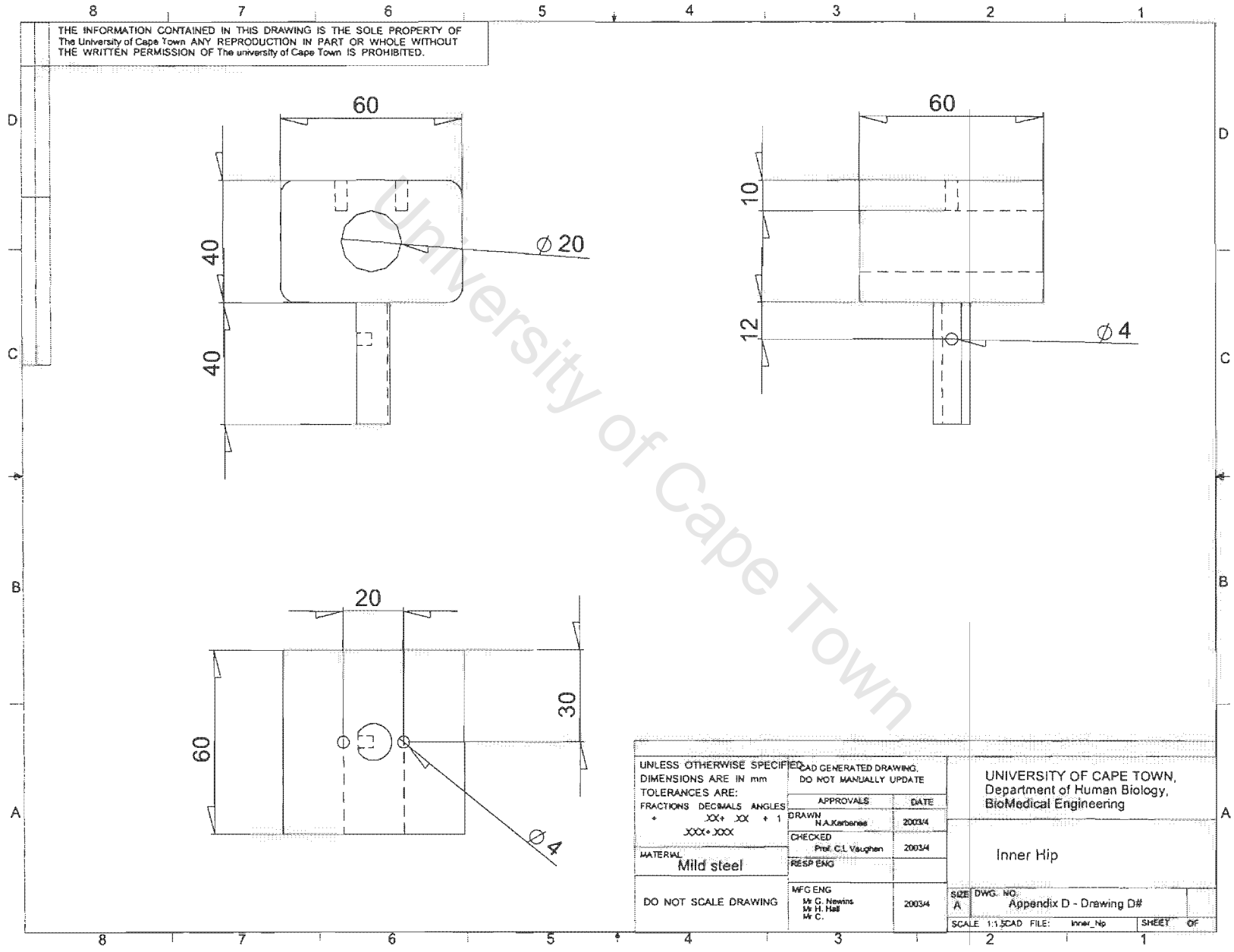

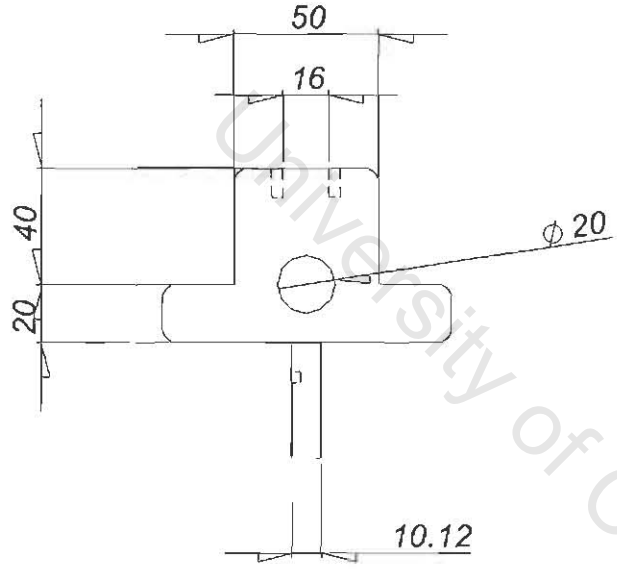

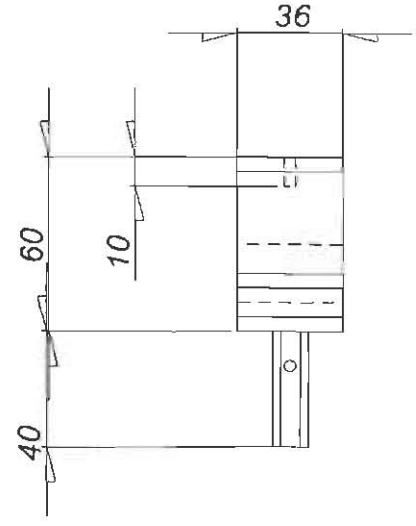

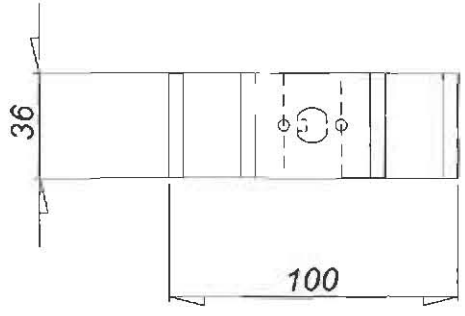

UNLESS OTHERWISE SPECIFIED DIMENSIONS ARE IN mm TOLERANCES ARE: FRACTIONS DECIMALS ANGLES ± XX ± .XX ± XXX ± .XXX	CAD GENERATED DRAWING. DO NOT MANUALLY UPDATE	UNIVERSITY OF CAPE TOWN, Department of Human Biology, BioMedical Engineering
	APPROVALS / DATE	
	DRAWN N.A.Karbanee 2003/4	
	CHECKED Prof C.L Vaughan 2003/4	Outer Hip
MATERIAL Mild steel	RESP ENG	
DO NOT SCALE DRAWING	MFG ENG Mr G. Newton, Mr H. Hall, Mr C. 2003/4	SIZE A DWG. NO. Appendix D - Drawing D#
		SCALE - 1 : CAD FILE: Outer_hip SHEET OF

D.5 Hip – Outer

D.6 Knee Full Assembly – 3D

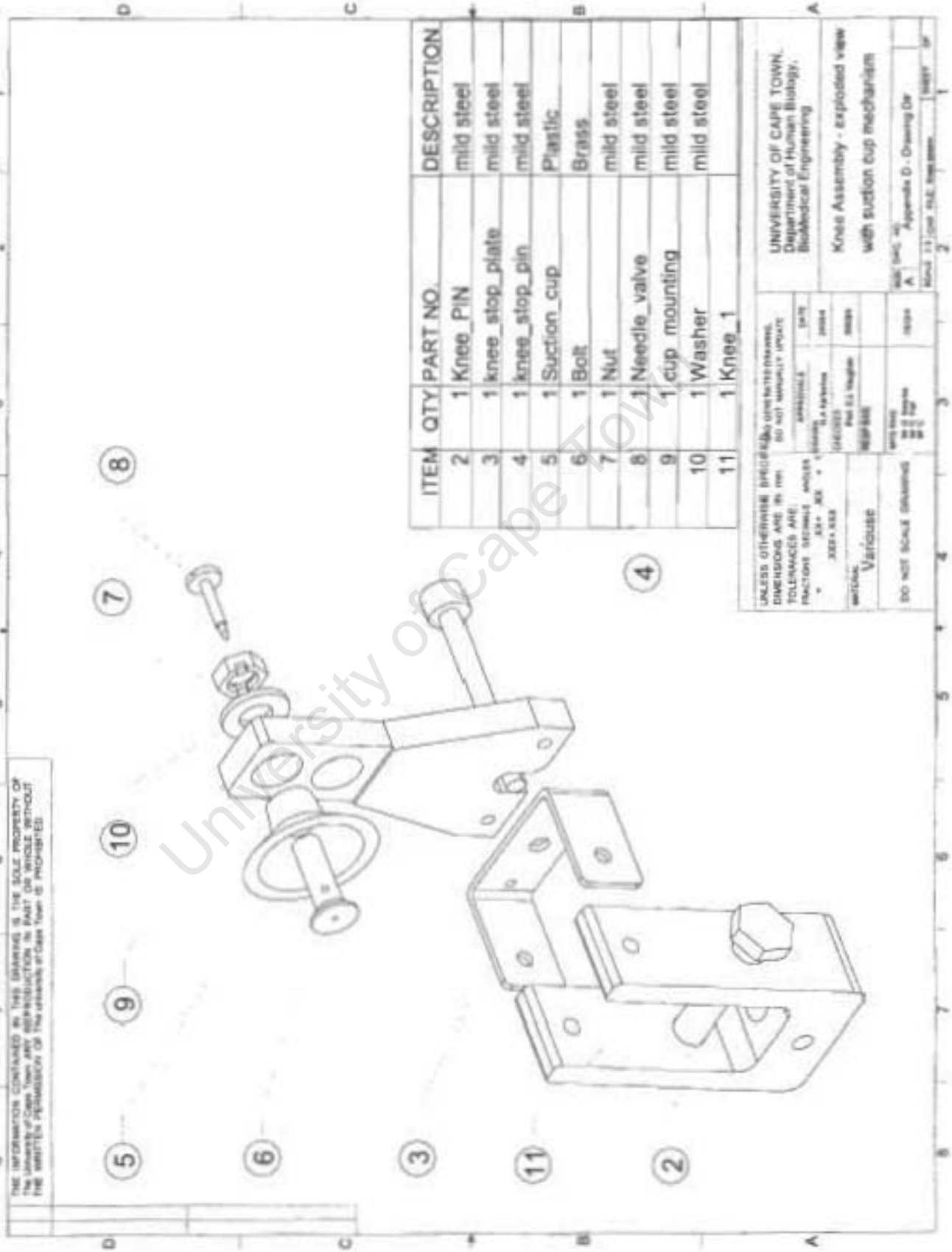

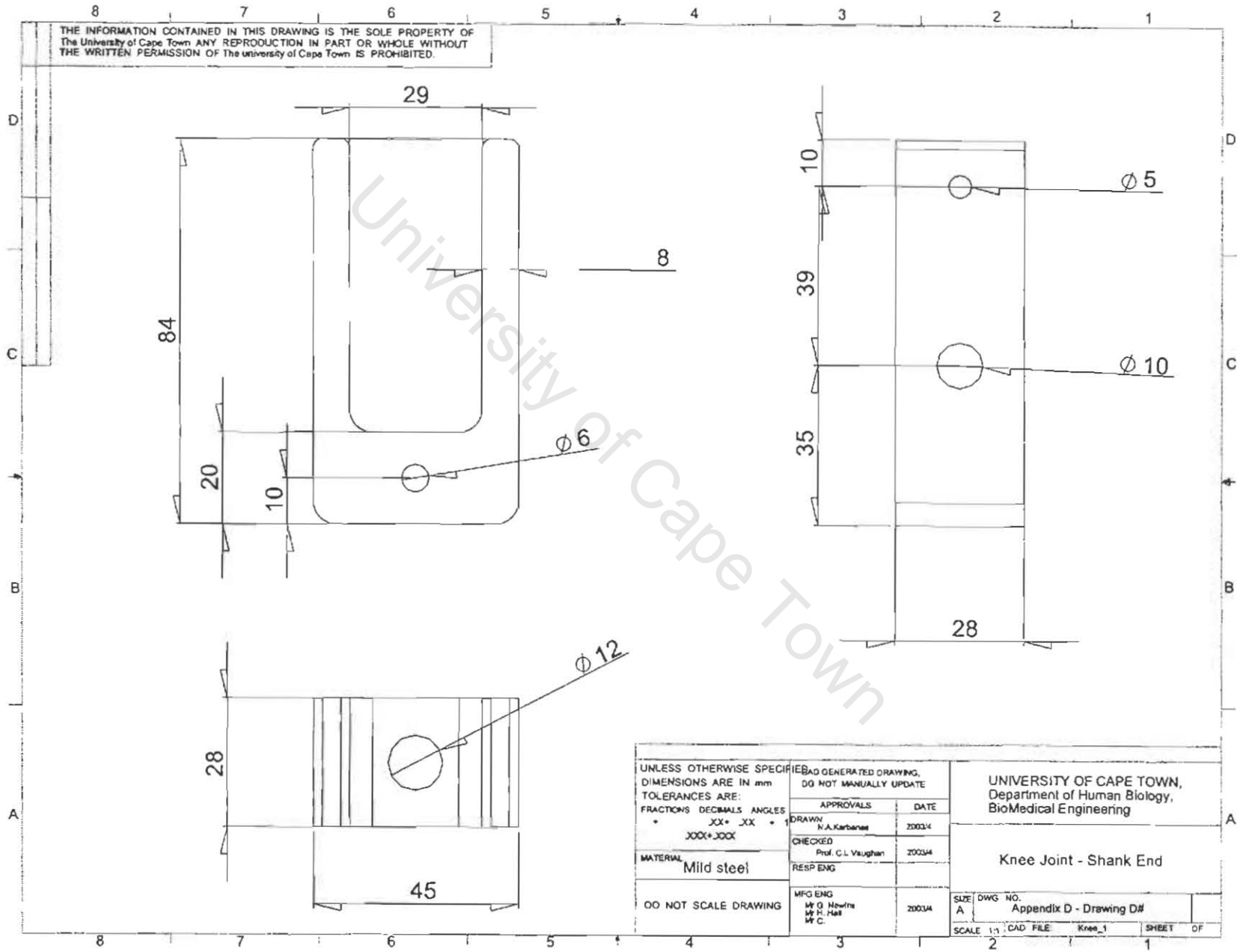

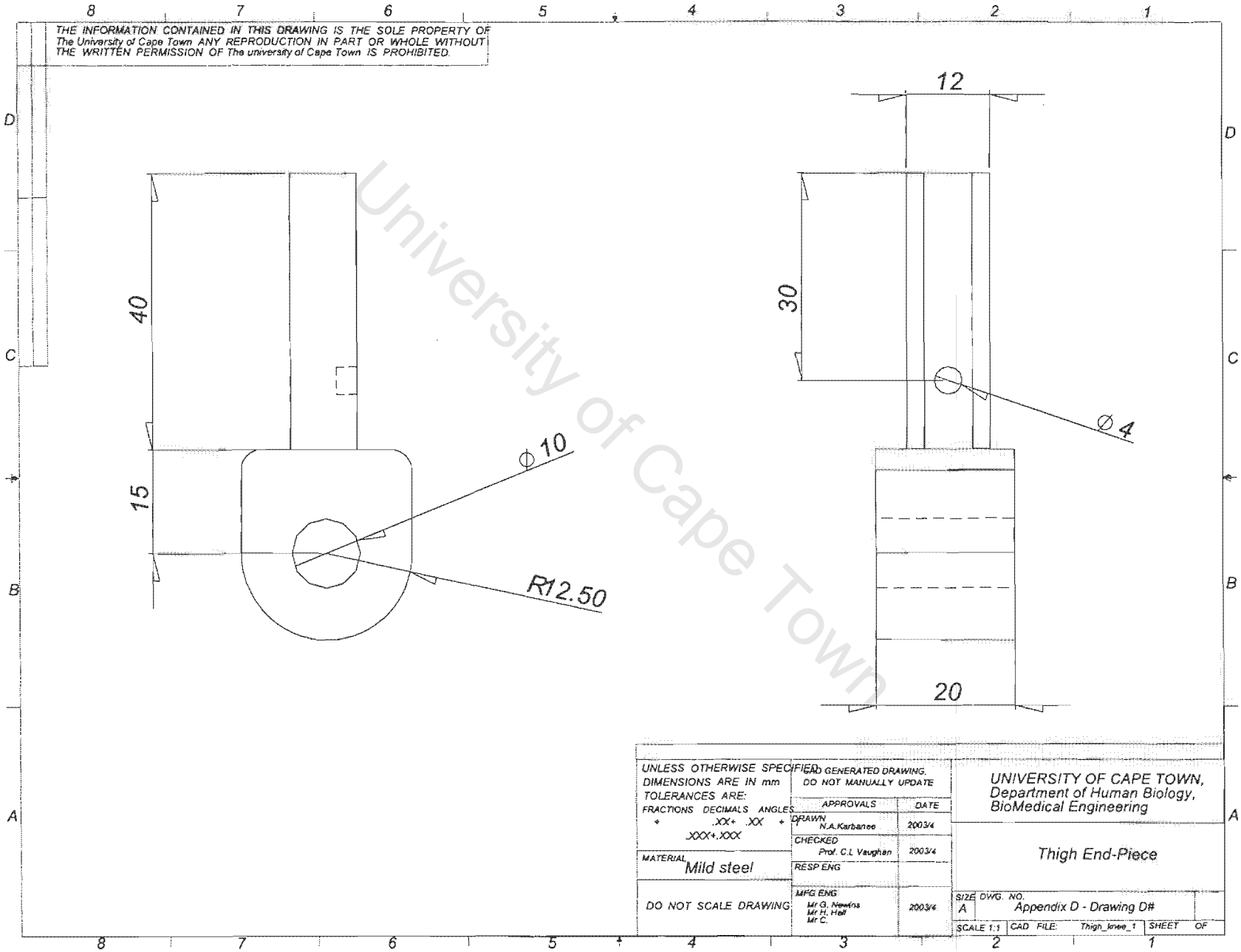

UNLESS OTHERWISE SPECIFIED DIMENSIONS ARE IN mm TOLERANCES ARE: FRACTIONS DECIMALS ANGLES ± .XX± .XX ± .XXX±.XXX	CAD GENERATED DRAWING. DO NOT MANUALLY UPDATE	UNIVERSITY OF CAPE TOWN, Department of Human Biology, BioMedical Engineering
	APPROVALS / DATE	
	DRAWN N.A.Karbanee 2003/4	
	CHECKED Prof. C.L Vaughan 2003/4	Thigh End-Piece
MATERIAL Mild steel	RESP ENG	
DO NOT SCALE DRAWING	MFG ENG Mr G. Newkins Mr H. Hall Mr C. 2003/4	SIZE A DWG. NO. Appendix D - Drawing D#
		SCALE 1:1 CAD FILE: Thigh_knee_1 SHEET OF

D.8 Knee – Thigh End Slider

D.9 Knee Stop Assembly – Exploded View

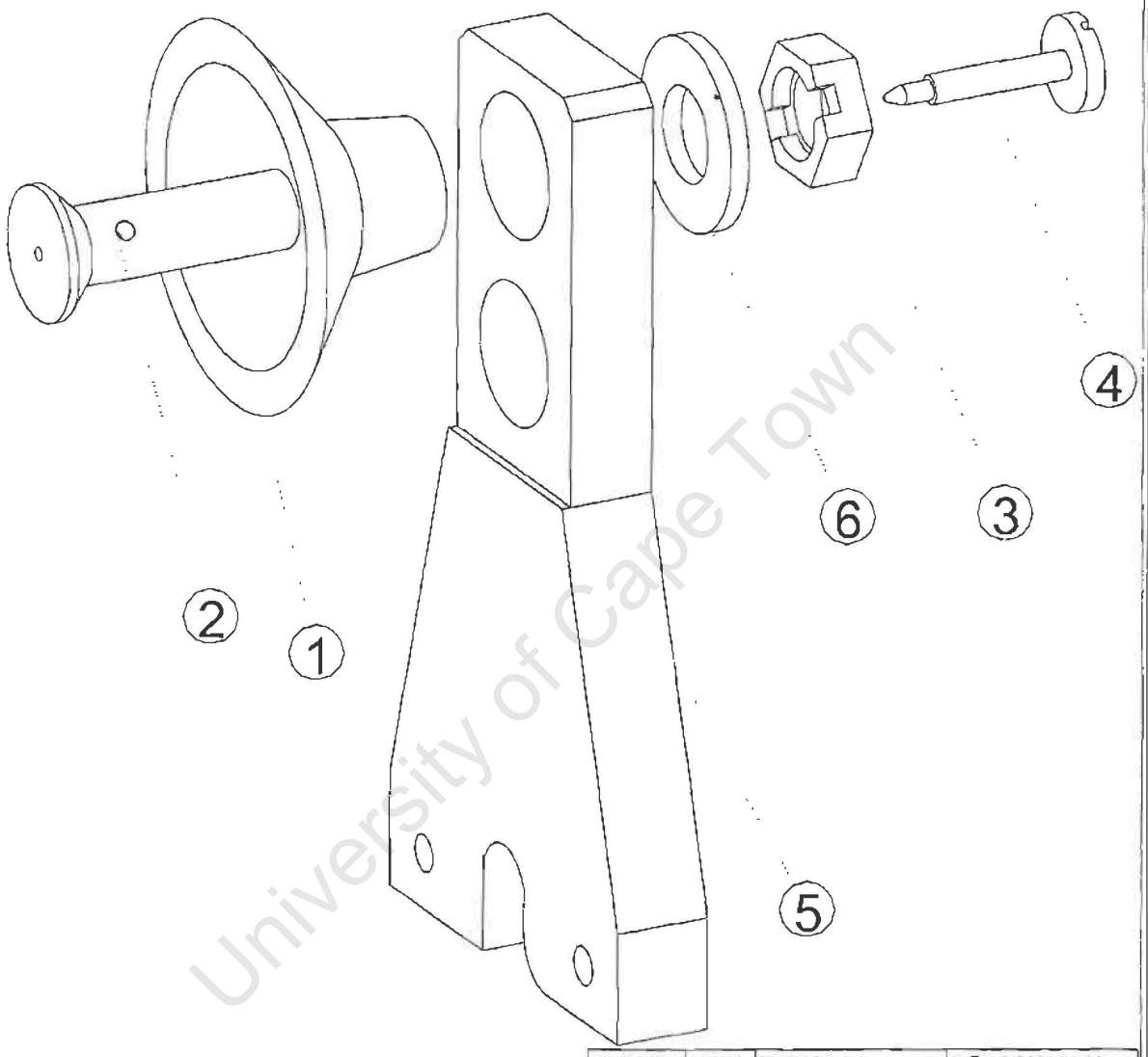

ITEM NO	QTY.	PART NO.	DESCRIPTION
1	1	Suction cup	
2	1	Bolt	
3	1	Nut	
4	1	Needle valve	
5	1	cup mounting	
6	1	Washer	

UNLESS OTHERWISE SPECIFIED DIMENSIONS ARE IN mm. TOLERANCES ARE: FRACTIONS %%d X/X DECIMALS .XX %%p .XX .XXX %%p .XXX ANGLES	DATE: June 2004		UCT, BME : 2D Passive Dynamic Walk			
	DRAWN	N.A Karbanee	Knee-Lock Suction-Cup Mechanism: Exploded View			
	CHECKED	Prof.C.L Vaughan				
MATERIAL	ENGR.	N.A Karbanee	SIZE A	CODE	DWG. NO.	REV.
DO NOT SCALE DRAWING			SCALE		SHEET	

D.10 Knee Stop Part – Mounting

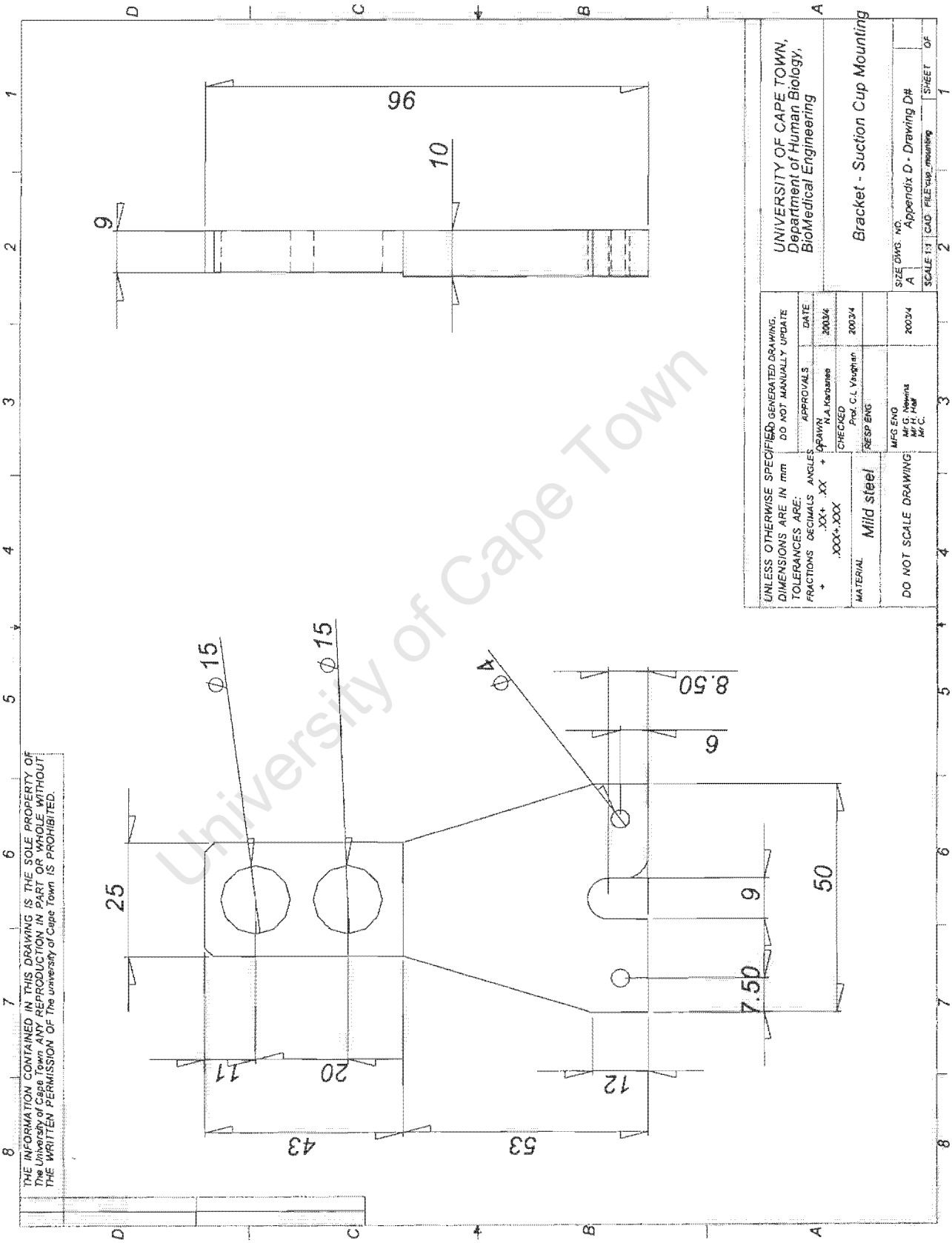

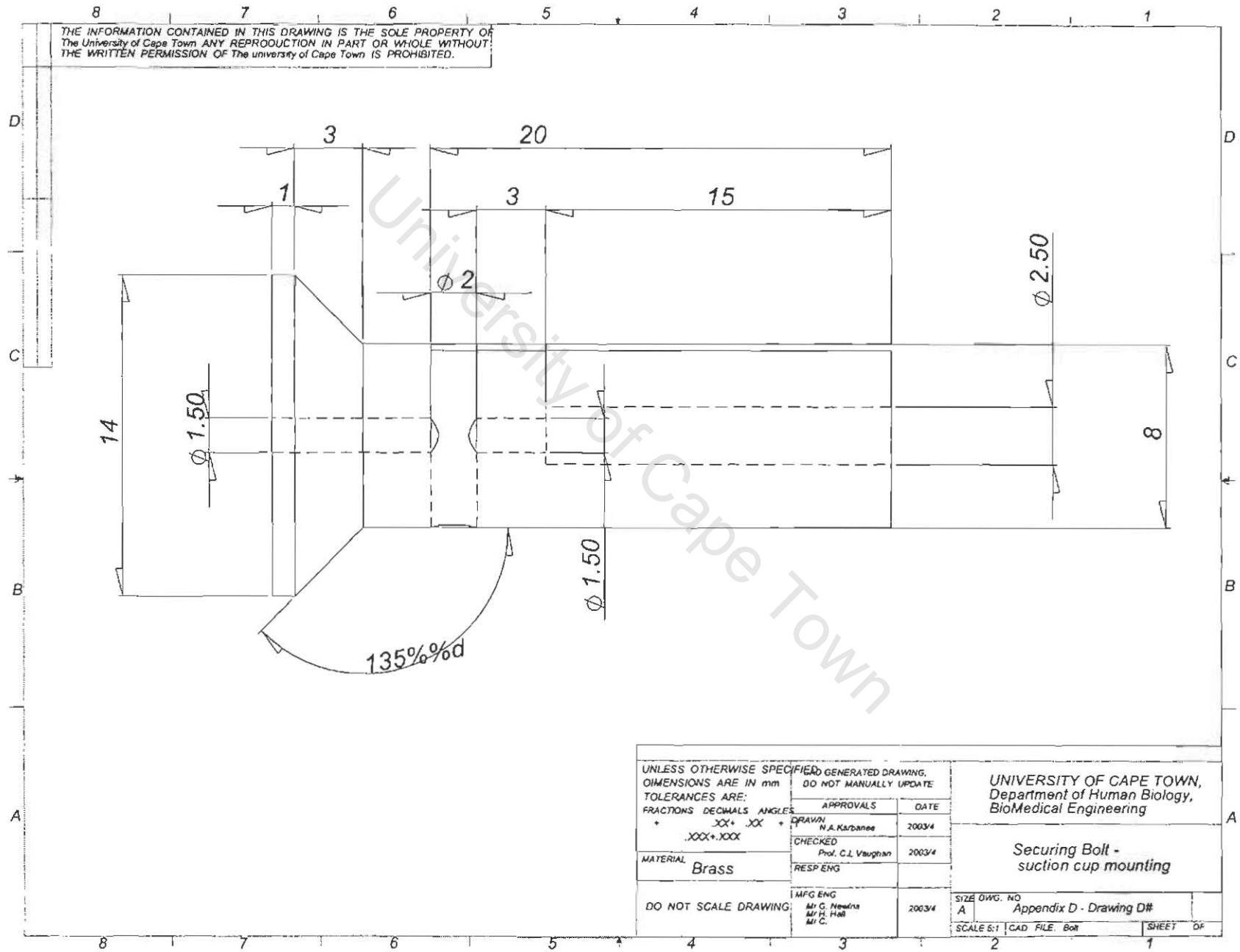

D.12 Knee Stop Part – Needle Valve Pin

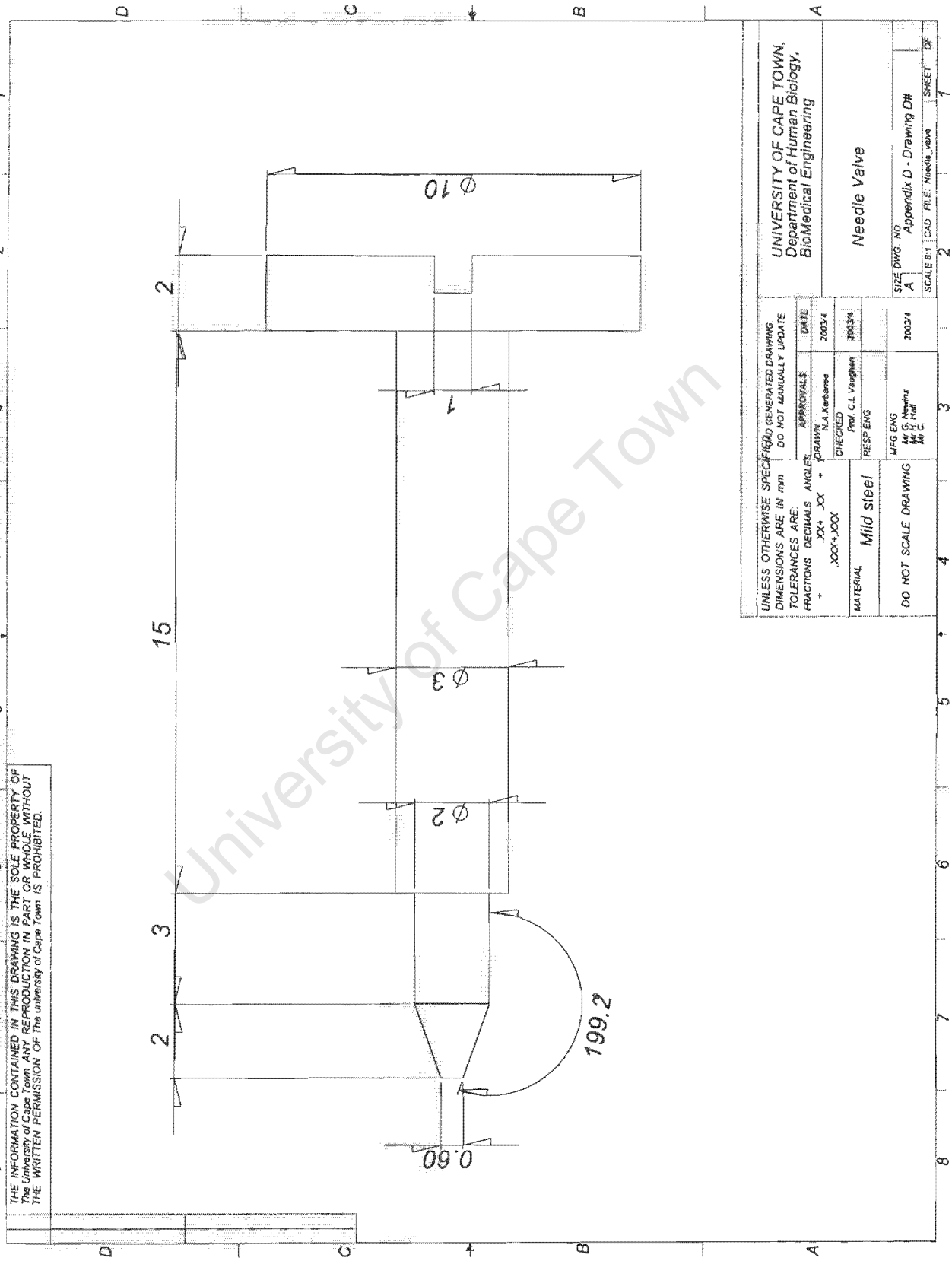

D.13 Ankle Assembly

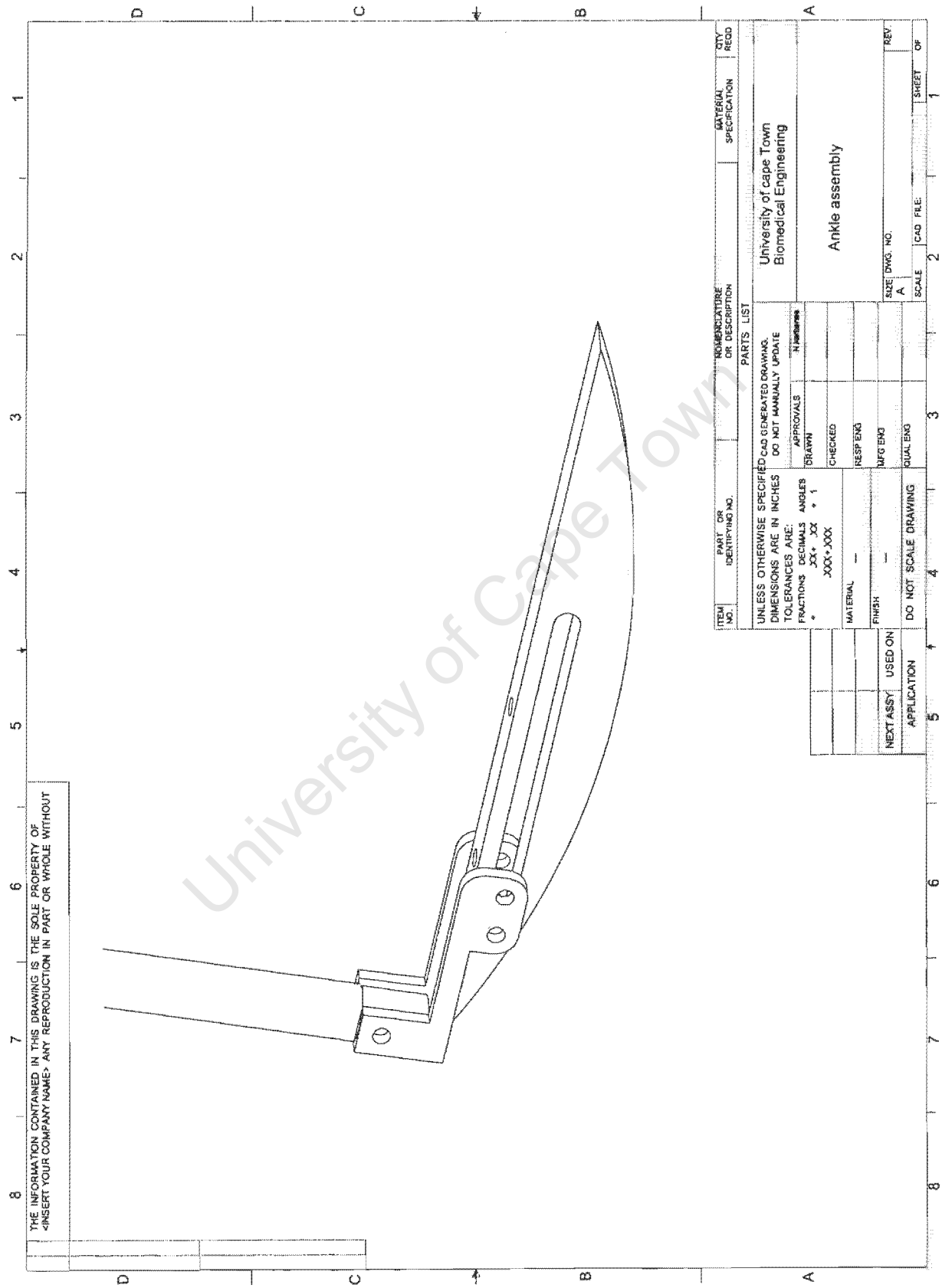

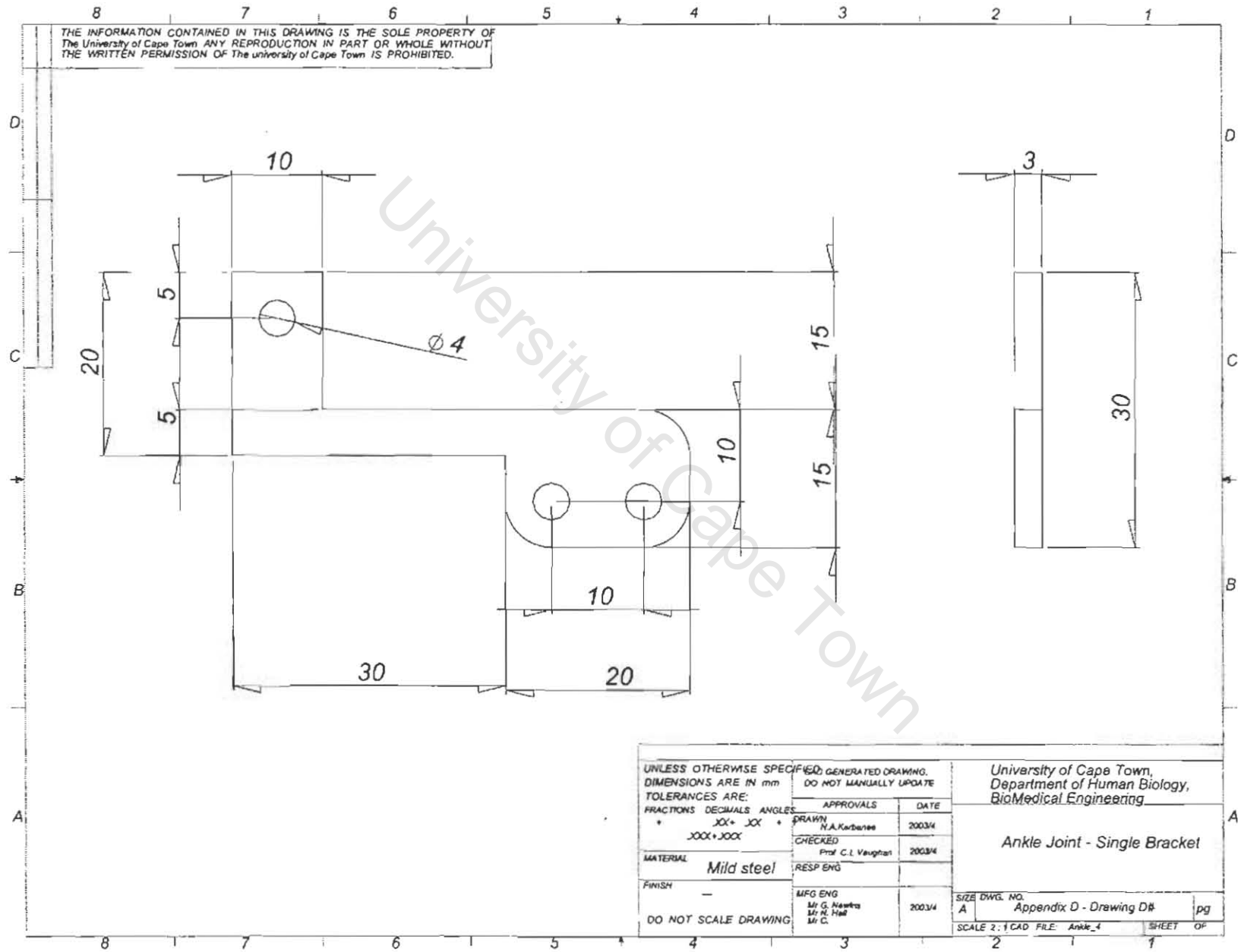

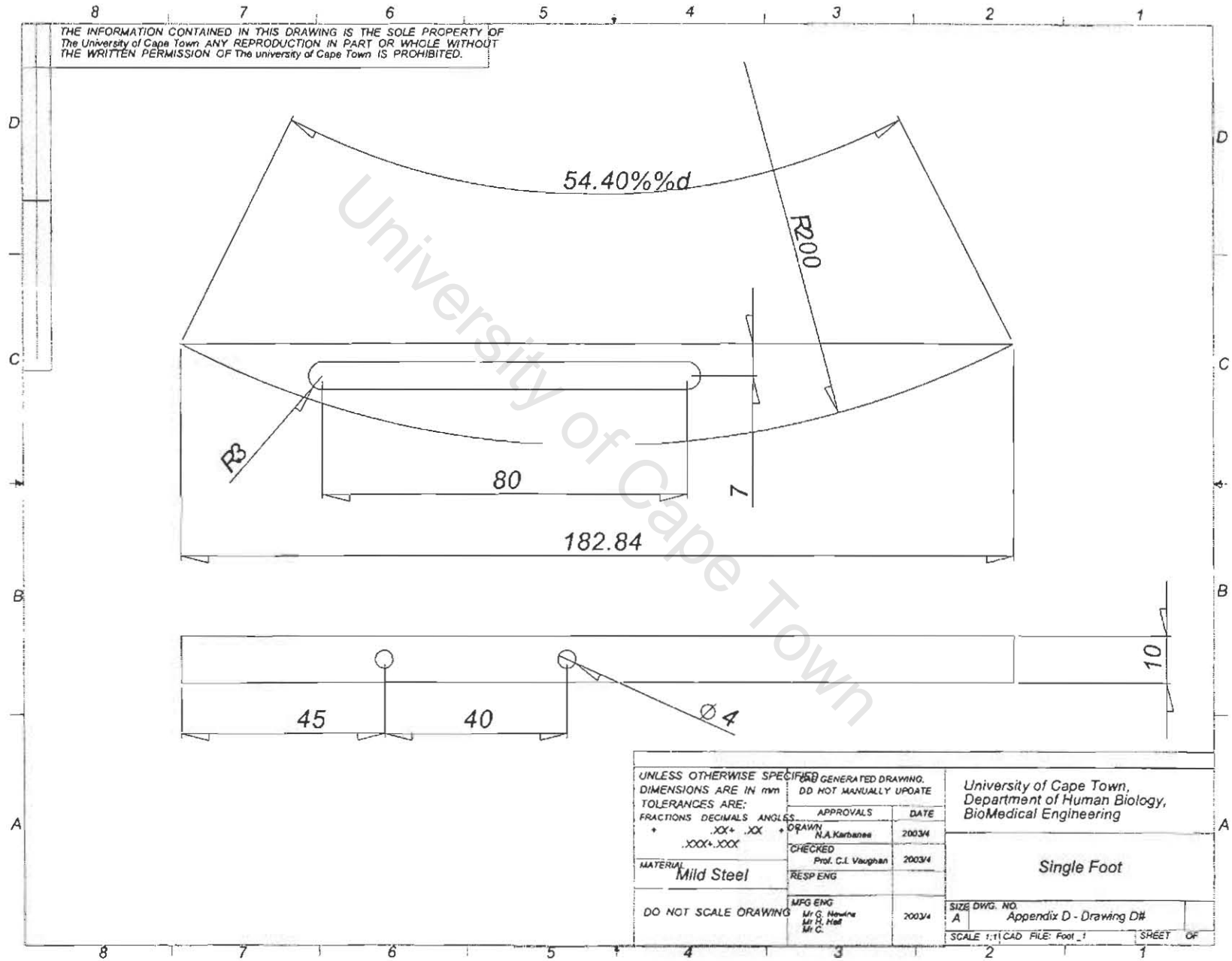

References

Alexander RM (1976) "Estimates of speeds of dinosaurs", *Nature* 261, 129–130.

Alexander RM (1977) "Scale effects in animal locomotion", edited by Pedley TJ, Academic Press.

Alexander RM (1984) "Stride length and speed for adults, children and fossil hominids", *American Journal of Physical Anthropology,* 63: 23-27.

Alexander RM (1984) 'The gaits of bipedal and quadrupedal animals", *International Journal of Robotics Research*, 3(2): 49-59.

Alexander RM (1989) "Optimisation and gaits in the locomotion of vertebrates", *Physiological Reviews,* 69(4): 1199-1227,

Alexander RM (1991) "Energy-saving mechanisms in walking and running", *Journal of Experimental Biology,* 160: 55-69, Review,(Outstanding).

Alexander RM (1991) "How dinosaurs ran", *Scientific American,* 264 (4): 62-68.

Alexander RM (1992) "The human machine", Colombian University Press.

Alexander RM (2004) "Bipedal animals and their differences from humans", *Journal of Anatomy,* 204: 321-330.

Atkins (2004) "Galileo's Finger, ten great ideas of science", Oxford University Press.

Azevedo C, Andreff N, Ariias S (2004) "Bipedal walking: from gait design to experimental analysis", *Mechatronics* 14 (6): 639–665.

Bailey DW (1995) 'Transfer of Support in a Dynamic Walking Robot", MSc-thesis, Massachusetts Institute of Technology, USA.

Basmajian JV (1980) "Electromyography–dynamic gross anatomy: a review", *American Journal of Anatomy*, 159(3): 245-260.

Basmajim JV, De Luca C (1985) "Muscles, alive: Their function revealed by electromyography", Williams and Wilkins Baltimore.

Basmajian JV (1973) "Electromyographic analyses of basic movement patterns", *Excersise and Sport Science Reviews*, 1: 259-284.

Borzova E, Hurmuzlu Y, (2004) "Passively walking 5-link robot" *Automatica* 40: 621 – 629.

Bullimore SR, Burns JF (2004) "Distorting limb design for dynamically similar locomotion", Proceedings of Biological Science, February. 271(1536):285-9.

Burton AW, Davies WE (1996) "Ecological task analysis: Utilizing intrinsic measures in research and practise", *Human Movement Science,* 15: 285-314.

Cavagna GA, Heglund NC, Taylor CR. (1977) "Mechanical work in terrestrial locomotion: two basic mechanisms for minimizing energy expenditure", *American Journal of Physiology*, 233(5):R 243-61.

Cavagna GA, Kaneko M.(1977) "Mechanical work and efficiency in level walking and runnin", *Journal of Physiology*, 268(2): 467--81

Cavagna GA, Willems PA and Heglund NC (1998) "Walking on Mars", *Nature*, 393:636.

Cavagna GA, Willems PA and Heglund NC (2000) 'The role of gravity in human walking: pendular energy exchange, external work and optimal speed', *Journal of Physiology*, 528 (3): 657-668.

Chang YH, Bertram JE, Lee DV (2000) "External forces and torques generated by the brachiating white-handed gibbon (Hylobateslar)", *American Journal of Physical Anthropology*, 113(2): 201-216.

Coleman M.J, Chatterjee A and Ruina A (1997) "Motions of a rimless spoked wheel: a simple 3D system with impacts", *Dynamics and Stability of Systems*, 12(3): 139 - 160.

Coleman MJ, Garcia M, Mombaur K and Ruina A (2001) "Prediction of stable walking for a toy that cannot stand", *Physical Review (Statistical, Nonlinear, and Soft Matter Physics)*, 64.

Collins AH, Wisse M and Ruina A, (2001) "A three-dimensional passive-dynamic walking robot with two legs and knees", *The International Journal of Robotics Research*, 20(7): 607-615.

Cottalorda J (1999) "Gait analysis: matching the method to the goal", *Review Rheumatism English Edition* 66 (7-9): 367-369.

Crane JR. (1989) "Realization of Dynamic Gait on a Robot Biped", MSc-thesis, Clemson University, USA.

Dankowicz H, Adolfsson J and Nordmark AB (2001) "Repetitive gait of passive bipedal mechanisms in a three-dimensional environment", *Journal of Biomechanical Engineering*, 123(1): 40-46.

Day MK, Ryan JM, Vallence K, McGuan S, Roy RR and Reggie V (2000) "Modelling the neuromechanical events of locomotion at varying gravitational levels", *Journal of Gravitational Physiology*, 7(2): 35-37.

DeJaeger D, Willems, PA, Heglund, NC (2001) 'The energy cost of walking in children', *European. Journal of Physiology*, 441:538-543.

Diedrich FJ, Warren WH (1995) 'Why change gaits? Dynamics of the walk-run transition', *Journal of Experimental Psychology: Human Perception and Performance*, 21(1): 183-202 and 21(3): 450

Donelan JM, Kram R (1997) "The effect of reduced gravity on the kinematics of human walking: a test of the dynamic similarity hypothesis for locomotion." *Journal of Experimental. Biology*, 200(24): 3193-201

Donelan JM, Kram R (2000) "Exploring dynamic similarity in human running using simulated reduced gravity", *Journal of Experimental. Biology*, 203 (16): 2405-15.

Drucker EG, Jensen JS (1996) "Pectoral fin locomotion in the striped surfperch-scaling swimming kinematics and performance at a gait transition", *Journal of Experimental Biology*, 199: 2243-2252.

Farley CT, Glasheen J, McMahon TA, (1993), "Running springs: speed and animal size" *Journal of Experimental Biology*. 185: 71-86.

Garcia, M., Chatterjee A and Ruina, A. (1997) "Speed, efficiency and stability of small slope 2-D passive-dynamic bipedal walking", *Proceedings of the 1998 International Conference on Robotics and Automation.*

Garcia M, Ruina A, Coleman M (1998) "Some results in passive-dynamic walking", *Proceedings of the European Mechanics colloquium on Biology and Technology of Walking.*

Garcia M, Chatterjee A, Ruina A, Coleman M (1998), "The simplest walking model: Stability, complexity, and scaling", ASME *Journal of Biomechanical. Engineering*, 120(2): 281-288.

Garcia M. (1999) "Stability, scaling and chaos in passive-dynamic gait models" PhD thesis, Cornell University, Ithaca, NY.

Garcia M., Chatterjee A and Ruina A (2000), "Efficiency, speed and scaling of 2-D passive-dynamic walking", *Dynamics and Stability of Systems*, 15: 75–100.

Garcia M, Kuo A, Peattie A, Wang P and Full R (2000) "Damping and size: Insights and biological inspiration" *Second International Symposium on Impact and Friction of Solids, Structures and Intelligent Machines*, Montreal, Quebec, Canada.

Goswami A., Thuilot B and Espiau, B (1998) "A study of the passive gait of a compass-like biped robot: symmetry and chaos", *International Journal of Robotics Research,* 17(12): 1282-1301.

Greene PR (1985) "Running on flat turns: experiments, theory, and applications". *Journal of Biomechanical Engineering*, 107(2): 96-103.

He J, Kram R and McMahon TA (1991) 'Mechanics of running under simulated low gravity', *Journal of Applied. Physiology*, 71(3): 863-870.

Hof At.L (1996) "Scaling gait data to body size", *Gait & Posture*, 4:222-223.

Hreljac A (1995) "Effects of physical characteristics on the gait transition speed during human locomotion", *Human Movement Science*, 14: 205-216.

Hurmuzlu Y and Moskowitz GD (1986) "Role of impact in the stability of bipedal locomotion", *International Journal of Dynamics and Stability of Systems*, (Oxford Press), 1 (3): 217-234.

Hurmuzlu Y and Moskowitz GD (1987) "Bipedal locomotion stabilized by impact and switching: i. two and three dimensional, three element models", *International Journal of Dynamics and Stability of Systems* (Oxford Press), 2 (2): 73-96.

Hurmuzlu Y and Moskowitz GD (1987) "Bipedal locomotion stabilized by impact and switching: ii. structural stability analysis of a four-element model", *International Journal of Dynamics and Stability of Systems* (Oxford Press), 2 (2): 97-112.

Hurmuzlu Y (1993) "Dynamics and control of bipedal robots", Invited Chapter, *Control Problems in Robotics and Automation*, Series of Lecture Notes in Control and Information Science, Sprintger-Verlag 230: 105-118.

Hurmuzlu Y (1993) "Dynamics of bipedal gait; Part i: Objective functions and the contact event of a planar five-link biped.", *ASME Journal of Applied Mechanics*, 60(2): 331-336.

Hurmuzlu Y (1993) "Dynamics of bipedal gait: Part ii: Stability analysis of a planar five-link biped", *ASME Journal of Applied Mechanics*, 60(2): 337-343.

Hutchinson JR, Garcia M (2002) "Tyrannosaurus was not a fast runner" Letter; *Nature* 415; 1018-1021.

Inman. VT, Ralston HJ and Todd F (1994) "*Human locomotion, Chapter: Human Walking", (2nd ai.),* Rose J and Gamble J.C (editors), Baltimore, MD: Williams & Wilkins, pp. 2-22.

Ivanenko YP, Dominici N, Cappellini G, Dan B, Cheron G, Lacquaniti F (2004) "Development of pendulum mechanism and kinematic coordination from the first unsupported steps in toddlers" Journal of Experimental Biology, 207(Pt 22):4011.

Khraief N, M'Sirdi N.K, Spong M.W (2003) "Nearly passive dynamic walking of a biped robot", *Proceedings of the European Control Conference,* University of Cambridge, UK.

Knight R, Nehmzow U (2002) "Walking robots – a survey and a research proposal", Technical Report CSM-375, Department of Computer Science, University of Essex.

Kram R, Domingo A and Ferris DP (1997) "Effect of reduced gravity on the preferred walk-run transition speed", *Journal of Experimental. Biology*, 200: 821-826.

Kuo AD (1999) "Stabilization of lateral motion in passive dynamic walking", *International Journal of Robotics Research,* 18 (9): 917-930.

Kuo AD (2001) "A simple model of bipedal walking predicts the preferred speed-step length relationship", *Journal of Biomechanical. Engineering,* 123: 264-269.

Kuo AD (2002) "Energetics of actively powered locomotion using the simplest walking model", *Journal of Biomechanical Engineering*, 124(1): 113-20.

McGeer T (1990) "Passive dynamic walking", *International Journal of Robotics Research,* 9(2):62-82.

McGeer T (1990) "Passive walking with knees", *Proceedings of the International Electrical Engineering E Robotics & Automation Conference,* Cincinnati, Ohio, 1640-1645.

McGeer T (1993) "Dynamics and control of bipedal locomotion", *Journal of Theoretical Biology,* 163(3): 277-314.

McMahon TA (1973) "Size and shape in biology", *Science* (Washington), 179: 1201-1204.

McMahon TA, Bonner J, Bonner JT (1983) "On size and life", *Scientific American Library*, W. H. Freeman, New York.

McMahon TA and Cheng GC (1990) "The mechanics of running: how does stiffness couple with speed?", *Journal of Biomechanics*, 23 (1): 65-78.

Mansour JM and Audu ML (1986) "The passive elastic moment at the knee and its influence on human gait", *Journal of Biomechanics,* 19 (5): 369-73.

Martinez MM, Full RJ and Koehl MAR (1998) "Underwater punting by an inter-tidal crab: A novel gait revealed by the kinematics of pedestrian locomotion in air versus water", *Journal of Experimental Biology*, 201: 2609-2623.

Minetti AE, Saibene F, Ardigo LP, Atchou G, Schena F and Ferretti G (1994) "Pygmy locomotion", *European Journal of Applied Physiology and Occupational Physiology,* 68(4): 285-90.

Minetti AE, Ardrigo L, Saibene F, Ferrero S and Sartorio A (2000) "Mechanical and metabolic profile of locomotion in adults with childhood-onset GH deficiency", *European Journal of Endocrinology,* 142: 35-41.

Minetti AE (2001) 'Walking on other planets', *Nature*, 409:467-469.

Minetti AE (2001) "Invariant aspects of human locomotion in different gravitational environments", *Acta Astronaut*, Aug-Nov, 49(3-10): 191-8.

Mochon S and McMahon TA (1980), "Ballistic walking", *Journal of Biomechanics*, 13: 49-57.

Montgomery H, Fifer F, (2001) "How fast did dinosaurs run?", *The Texas Science Teacher*, 30(1): 16-19.

Okamoto T, Okamoto K and Andrew PD (2003) "Electromyographic developmental changes in one individual from newborn stepping to mature walking", *Gait and Posture*, 17: 18-27.

Pierrynowski MR and Galea V (2001) "Enhancing the ability of gait analyses to differentiate between groups: scaling gait data to body size", *Gait and Posture,* 13: 193–201.

Russell S, Granata KP and Sheth P (2004) "Virtual slope control of a forward dynamic bipedal walker", *to appear in the Journal of Biomechanical Engineering*, under revision.

Sellers WI, Dennis LA, Wang WJ and Crompton RH (2004) "Evaluating alternative gait strategies using evolutionary robotics", *Journal of Anatomy*, 204 (5): 343-352.

Thompson DW (1961) "On Growth and Form", Abbreviated Edition, University Press, Cambridge.

Tuttle R, Basmajian JV, Regenos E and Shine G (1972) "Electromyography of knuckle-walking: results of four experiments on the forearm of Pan gorilla" *American Journal of Physical Anthropology*, 37(2): 255-265.

Van der Linde RQ (1998) "Active leg compliance for passive walking", *Proceedings of the IEEE International Conference on Robotics and Automation*, Leuven, Belgium: 2339-2344

Van der Linde RQ (2000) "Actively controlled ballistic walking", *Proceedings of the IASTED International Conference on Robotics and Applications*, Honolulu, Hawaii, USA.

Vaughan CL (2003) "Theories of bipedal gait: an odyssey", *Journal of Biomechanics*, 36: 513-523.

Vaughan CL and Verrijzer F (2002) "Exploring dynamic similarity in the gait of children and bipedal robots by means of the Froude Number", *Proceedings of the 7th Annual Meeting of the Gait and Clinical Movement Analysis Society*, Chattanooga, USA.

Vaughan CL and O'Malley MJ (2004) "Froude and the contribution of naval architecture to our understanding of bipedal locomotion", *Gait and Posture* in press

Winter DA (1987) *The Biomechanics and Motor Control of Human Gait*, University of Waterloo Press.

Witte H, Hoffmann H, Hackert R, Schilling C, Fischer M.S, and Preuschoft H (2004) "Biomimetic robotics should be based on functional morphology" *Journal of Anatomy*, 204 (5): 331-341.

Zamparo P, Pendergast DR, Termin B and Minetti AE (2002) "How fins affect the economy and efficiency of human swimming", *Journal of Experimental Biology* 205 (17): 2665-76.

Zatsiorky VM, Werner SL, Kaimin MA, (1994) "Basic kinematics of walking. Step length and step frequency. A review" *Journal of Sports Medicine and Physical Fitness*, 34(2): 109-34.

Web Based References

Boccuzzo S, Steiner D (2002) "Artificial and natural walking machines: Rapid locomotion", *Seminar on Artificial and Natural Walking Machines* http://www.ifi.unizh.ch/ailab/teaching/ANWM_Seminar/StudentMaterials/rapidloc.pdf [Last accessed 01/11/2004]

Donelan JM, Kram R (1996), "The influence of size, speed and gravity on the kinematics of human walking: a test of the dynamic similarity hypothesis for locomotion." *American Society of Biomechanics Annual Meeting* Atlanta, GA. http://www.ualberta.ca/~mdonelan/Pubs/DKASB96ab.pdf Last accessed 01/11/2004]

Donelan JM, Kram R and Park JY (1998) "A new dynamic similarity hypothesis for running animals", *Proceedings of the North American Congress on Biomechanics*. Waterloo, ON. http://www.asb-biomech.org/onlineabs/NACOB98/196/ [Last accessed 01/11/2004]

Farley CT, Ferris DP, (1998) Chapter 10: "*Biomechanics of walking and running. Center of mass movements to muscle action*", http://www.kines.umich.edu/facstaff/journals/FarleyFerris1998.pdf [Last accessed 08/11/2004]

Garcia M. Homepage http://tam.cornell.edu/students/garcia/msghomepage.html [Last accessed 01/11/2004]

Honda, Japan, 'Aisimo', www.world.honda.com/robot [Last accessed 01/11/2004]

Human Power and Robotics Lab, Theoretical and Applied Mechanics, Cornell Univ. (lab of Andy Ruina), http://www.tam.cornell.edu/%7Eruina/hplab/pdw.html [last accessed 01/11/2004]

Kubat R, (2000) "Moving on Mars: An overview" www.koobs.org/other/mars.pdf [Last accessed 29/10/2004]

Leg Lab at the Massachusetts Institute of Technology, (MIT), USA, http://www.ai.mit.edu/projects/leglab/ [Last accessed 01/11/2004]

Pratt, J.E., Pratt, G.A., (1998), "Exploiting natural dynamics in the control of a Planar bipedal walking robot", *Proceedings of the 36th Annual Allerton Conference on Communication, Control, and Computing,* Illinois 739-748. http://citeseer.ist.psu.edu/101027.html [last accessed 01/11/2004]

Robotstore, USA, Drunken sailor, www.walkingrobots.com: [Last accessed 01/11/2004]

Selles RW (2003), "Predicting the effect of prosthetic mass properties on the gait of transtibial amputees" Onderzoek en Publicaties, available at http://www.revalidatiegeneeskunde.nl/Onderzoek/R114/selles.htm#2 [last accessed 12/11/2004]

Shadow Projects, UK, 'Shadow Walker', www.shadow.org.uk/projects/biped.shtml : [Last accessed 01/11/2004]

University of Reading, UK, 'Tweekie', www.cyber.rdg.ac.uk/W.Harwin/WWW/tweekie, [Last accessed 29/10/2004]

Walking Machines Catalogue http://www.walking-machines.org/ [Last accessed 01/11/2004]

Directory of Attached CD

A. Design EXCEL Spread Sheets
   i. Joint Equations
   ii. Froude Number
   iii. Limb Design

B. Drawing Files
   i. Parts, Assemblies, and Drawings (Solid Works)
   ii. Pictures
   iii. Photographs

C. MATLAB Simulation Code
   i. Core Directory..... .....2D Passive Biped 4 Public
   ii. Original Garcia Execution File..... Run_walker_turbo
   iii. Modified UCT Version..... Run_walker_turbo_Change

D. Thesis Write Up